

AD-A102 625

TECHNICAL
LIBRARY

AD E430659

CONTRACT REPORT ARBRL-CR-00459

THE ROLE OF CARBURIZATION IN GUN
BARREL EROSION AND CRACKING

Prepared by

Calspan Corporation
P. O. Box 400
Buffalo, NY 14225

July 1981



US ARMY ARMAMENT RESEARCH AND DEVELOPMENT COMMAND
BALLISTIC RESEARCH LABORATORY
ABERDEEN PROVING GROUND MARYLAND

Approved for public release; distribution unlimited

Destroy this report when it is no longer needed.
Do not return it to the originator.

Secondary distribution of this report by originating
or sponsoring activity is prohibited.

Additional copies of this report may be obtained
from the National Technical Information Service,
U.S. Department of Commerce, Springfield, Virginia
22161.

The findings in this report are not to be construed as
an official Department of the Army position, unless
so designated by other authorized documents.

*The use of trade names or manufacturers' names in this report
does not constitute endorsement of any commercial product.*

UNCLASSIFIED

SECURITY CLASSIFICATION OF THIS PAGE (When Data Entered)

UNCLASSIFIED

SECURITY CLASSIFICATION OF THIS PAGE(When Data Entered)

20. (Cont.)

Tests were conducted with a mixture of argon and nitrogen to delineate the threshold of simple melting erosion which served as a chemically inert baseline. Progressive substitution of carbon monoxide for nitrogen in the mix quantified the carburizing effect as a function of CO concentration. Subsequent tests were conducted with a gas mixture containing carbon monoxide, argon and helium to measure the carburizing effect as a function of cycle time.

The basic carburizing effect was observed to be a shift in the erosion threshold to less severe convective heating conditions in response to surface chemistry. The magnitude of the shift appeared to be directly proportional to heating cycle time. Presence of carbon monoxide also resulted in enhanced downstream erosion of barrel steel test samples and distinct changes in their surface characteristics. Further, the carburizing effect was observed to be nearly independent of carbon monoxide concentration in the range of CO concentrations used in the program tests, and found in nitramine propellant gas.

UNCLASSIFIED

SECURITY CLASSIFICATION OF THIS PAGE(When Data Entered)

TABLE OF CONTENTS		Page
LIST OF FIGURES		5
LIST OF TABLES		7
I INTRODUCTION		9
II SHOCK TUBE GUN FACILITY		10
2.1 STG Concept		10
2.2 Construction		10
III TEST PREPARATIONS		14
3.1 Specimen Selection		14
3.2 Heat Transfer Instrumentation		15
3.3 Selection of Test Conditions		17
IV TEST PROCEDURE AND RESULTS		18
4.1 Test Procedures		18
4.2 Test Matrix		20
4.3 Test Gas Mixture Isentropes		22
V CORRELATION OF RESULTS		25
5.1 Erosion and Flow Conditions		25
5.1.1 Pressure, Temperature and Carburization Effects		25
5.1.2 Convective and Chemical Heating Effects		28
5.2 Erosion Distribution		33
5.3 Surface Characterization		37
5.4 Summary of Results		38
VI CONCLUSIONS		57
VII REFERENCES		58
APPENDIX I: SHOCK TUBE GUN COMPUTER SIMULATION		59
APPENDIX II: ISENTROPIC EQUILIBRIUM COMBUSTION CODES		81
DISTRIBUTION LIST		87

LIST OF FIGURES

<u>Figure</u>	<u>Title</u>	<u>Page</u>
1	Projectile Launch and Capture Components of the Shock Tube Gun	12
2	Piston, Chamber and Toggle Restraint Components of the Shock Tube Gun	13
3	Shock Tube Gun Test Sample	14
4	In-Wall Thermocouple Installation	16
5	Isentropes for Test Gas Mixtures Undergoing Adiabatic Compression	23
6	Mass Loss Vs. Peak Test Gas Pressure for Various Test Gas Mixtures	26
7	Mass Loss Vs. Peak Test Gas Temperatures for Various Test Gas Mixtures	27
8	Mass Loss Vs. Total Heat Input for Test Gas Mixtures	29
9	Mass Loss Vs. Total Heat Input Corrected for Local Heat Lost By Material Removal	31
10	Influence of Convective Heating and Carburizing-Type Reactions on Erosion of 4340 Steel	34
11	Influence of Test Gas Constituents on Surface Recession of 4340 Steel	36
12	4340 Steel Sample Surface Tested in an "Inert" Atmosphere To 223 MPa, 3422°K	40
13	4340 Steel Sample Surface Tested in an "Inert" Atmosphere To 248 MPa, 3531°K	41
14	4340 Steel Sample Surface Tested in an "Inert" Atmosphere To 285 MPa, 3678°K	42
15	4340 Steel Sample Surface Tested in an "Inert" Atmosphere To 335 MPa, 3865°K	43

LIST OF FIGURES (CONT.)

<u>Figure</u>	<u>Title</u>	<u>Page</u>
16	4340 Steel Sample Surface Tested in a 45.5 Percent Carbon Monoxide Atmosphere to 213 MPa, 3322°K	44
17	4340 Steel Sample Surface Tested in a 45.5 Percent Carbon Monoxide Atmosphere to 216 MPa, 3338°K	45
18	4340 Steel Sample Surface Tested in a 45.5 Percent Carbon Monoxide Atmosphere to 277 MPa, 3588°K and 256 MPa, 3507°K	46
19	4340 Steel Sample Surface Tested in a 45.5 Percent Carbon Monoxide Atmosphere to 245 MPa, 3462°K	47
20	4340 Steel Sample Surface Tested in a 40.5 Percent Carbon Monoxide Atmosphere to 299 MPa, 3690°F	48
21	4340 Steel Sample Surface Tested in a 25.5 Percent Carbon Monoxide Atmosphere to 281 MPa, 3637°K	49
22	4340 Steel Sample Surface Tested in a 20.5 Percent Carbon Monoxide Atmosphere to 287 MPa, 3665°K	50
23	4340 Steel Sample Surface Tested in a 15.5 Percent Carbon Monoxide Atmosphere to 288 MPa, 3673°K	51
24	4340 Steel Sample Surface Tested in a 45.5 Percent Carbon Monoxide Atmosphere to 250 MPa, 3479°K	52
25	4340 Steel Sample Surface Tested in a 45.5 Percent Carbon Monoxide Atmosphere to 236 MPa, 3422°K	53
26	4340 Steel Sample Surface Tested in a 45.5 Percent Carbon Monoxide Atmosphere to 219 MPa, 3351°K	54
27	4340 Steel Sample Surface Tested in a 45.5 Percent Carbon Monoxide Atmosphere to 201 MPa, 3268°K	55
28	Iron-Carbon Equilibrium Diagram	56

LIST OF TABLES

<u>Table</u>	<u>Title</u>	<u>Page</u>
1	Shock Tube Gun Characteristics	11
2	Test Results	21
3	Test Gas Mixture Composition	24

I. INTRODUCTION

The objective of this study is to determine the relative importance of carburization to the overall degradation of a gun barrel by propellant gases. Carbon monoxide, the pre-eminent carburizing atmosphere, is present in all existing gun propellants, in quantities large enough to suggest a significant contribution to the thermochemical history of a ballistic system. Carburization is normally thought of as a steady-state diffusion process which enhances a steel's compressive strength, surface hardness and wear resistance. But as a possible internal ballistic process, carburization can only be present as a transient, on-the-surface phenomenon, since high propellant gas temperatures cannot increase the rate of carbon diffusion to a level where subsurface microstructure is noticeably altered in the span of several milliseconds. Furthermore, there is no regenerative medium present in a ballistic system to dissociate the CO₂ produced in the Fe-CO reaction. Any CO₂ produced by CO induced Fe₃C formation is either expelled by forced convection or, more importantly, reverses the carburizing process as barrel temperature decreases. It is this cyclical history of carburizing and decarburizing of the gun tube surface during a ballistic event that is believed to be responsible for any erosion potential exhibited by the presence of carbon monoxide. It is further postulated that in high performance guns, where barrel surface temperatures already hover near the steel's normal solidus temperature, an increase in carbon concentration, even for a few milliseconds, will artificially lower the melting point to where the barrel's surface shear strength is lowered or lost. This program has been designed to ascertain the significance of these processes and quantify their contribution to gun barrel erosion and cracking.

Research is being performed by utilizing Calspan's Shock Tube Gun (STG) facility, which duplicates the thermodynamics of gun chamber combustion with a tube chamber incorporating a moving wall, i.e., the leading face of a gas driven piston. The gases compressed in the tube chamber by piston motion vent in a conventional manner by forcing a projectile down the adjoining gun barrel. During the venting cycle, the gases must pass through the nozzleled flow channel of a gun-steel sample positioned in front of the barrel entrance. As a result, the channel wall of the sample experiences histories of pressure, temperature and forced convective heating, similar to those of a gun barrel. Unlike the combustion system where propellant formulation dictates a set flame temperature and impetus, the STG permits independent variation of any or all conditions affecting ballistic histories.

Several computer programs provide analytic support for the STG tests. One code models the STG gas compression cycle using a van der Waals equation of state. It computes gas pressure and temperature, convective heating, total heat input and in-wall temperatures of the test sample surface. This program is used mainly in a predictive mode to select gas composition and peak pressure for an actual test. Another code accepts gas mixture and pressure data from tests conducted and computes equilibrium temperature and species concentration values along the correct isentropes. This information can then be returned to the preceding program to improve its prediction of barrel heating and wear. STG testing and computer analysis, as performed in this program, are intended to expand present knowledge of wear and erosion phenomenology.

II. SHOCK TUBE GUN FACILITY

2.1 STG Concept

The Shock Tube Gun, as designed and developed by Calspan applies shock tube principles to the study of interior ballistics. The facility consists of a driver gas chamber, a driven tube containing a latchable flying piston, an instrumented gas collection chamber and an instrumented gun tube containing a projectile.

One unique design feature of the STG is the driven piston which, by its presence, affords physical isolation of the driver gas, normally nitrogen, and the chamber or test gas, which varies in composition with test objectives. The driven piston, by virtue of its mass in conjunction with the projectile's mass, also controls the compression history of the test gas, enabling the facility to duplicate the interior ballistic environment of various large caliber guns, up to and including an 8" howitzer.

Another key design feature of the STG is the test section contained within the gas collection chamber. It accepts specimens of various physical configurations equipped with in-wall thermocouples and/or surface heat flux meters, and holds them in place adjacent to the attached barrel. In effect, this design offers a replaceable, highly instrumented bore entrance to an otherwise conventional gun tube.

With suitable variation in test parameters, made possible by the design of the STG, including driver pressure, piston mass, test gas composition, specimen configuration, shot start capability and projectile mass, one may investigate any or all of the internal factors affecting ballistic phenomena, such as the gun barrel erosion and cracking, which the present study addresses.

2.2 Construction

Table 1 lists the present structural dimensions of the STG as used in this study, and dictated by adiabatic compression modeling and material availability.

As shown in Figure 1, the projectile launch components consist of the 191 millimeter driven tube, the instrumented, high pressure, test gas collection chamber and a 30mm smooth-bore barrel. These are supported on a shock table which is free to move on tracks in the direction of piston motion, during the severe impulse loading caused by unbalanced chamber pressure due to test gas compression by the decelerating piston. This floating mount system minimizes shearing forces to the supporting base structure, but requires an adjustable pneumatic brake on the driven tube to absorb the axial loading on the launch components, primarily the driven tube itself.

Table 1. Shock Tube Gun Characteristics

Configuration Data:

Driven Tube I.D.	0.191m	(7.5 in.)
Driven Tube Length	24.6m	(970 in.)
Piston Area	0.0285m ²	(44.179 sq. in.)
Piston Mass	Up to 91 kg.	(200 lb.)
Projectile Diameter	30mm	(1.181 in.)
Projectile Area	706mm ²	(1.095 sq. in.)
Projectile Mass	Up to .91 kg.	(2 lb.)
Driver Volume	0.885m ³	(54,000 cu. in.)
Chamber Volume	2140mm ³	(130.8 cu. in.)
Pressure - at release of projectile	Variable	
Barrel Length	4.57m	(180 in.)

The projectile capture components consist of a telescoping tube coupled to the barrel muzzle, a projectile blast chamber, and a sand filled tube to decelerate and catch the projectile. The telescoping tube, the purpose of which is to permit independent motion of the shock table and blast chamber, contains replaceable screens for measuring projectile velocity. The blast chamber reduces the noise and pressure levels as the projectile exits the barrel.

Figure 2 shows the chamber and toggle restraint system needed to contain the high chamber pressures and associated axial loads. Chamber pressures are sensed using piezoelectric transducers. The entrance region of the launch tube can accommodate pressure, heat flux, and erosion sensing devices.

The piston, which is used to compress the test gas, is made from 4340 steel and weighs 68 kg. including the latching block on its rear face which secures it at the upstream end of the driven tube, prior to release or "firing." Gas seal is maintained using "T" rings at the front and rear of the piston. Three brass wear rings or "bore riders" are used to prevent steel-to-steel contact between piston and tube. A buffer projection on the face of the piston and a complementary piston stop ring at the downstream end of the driven tube prevent direct impact of the piston into the test gas collection chamber in the event that the compressed test gas develops insufficient pressure or loses pressure prematurely due to chamber seal failure.

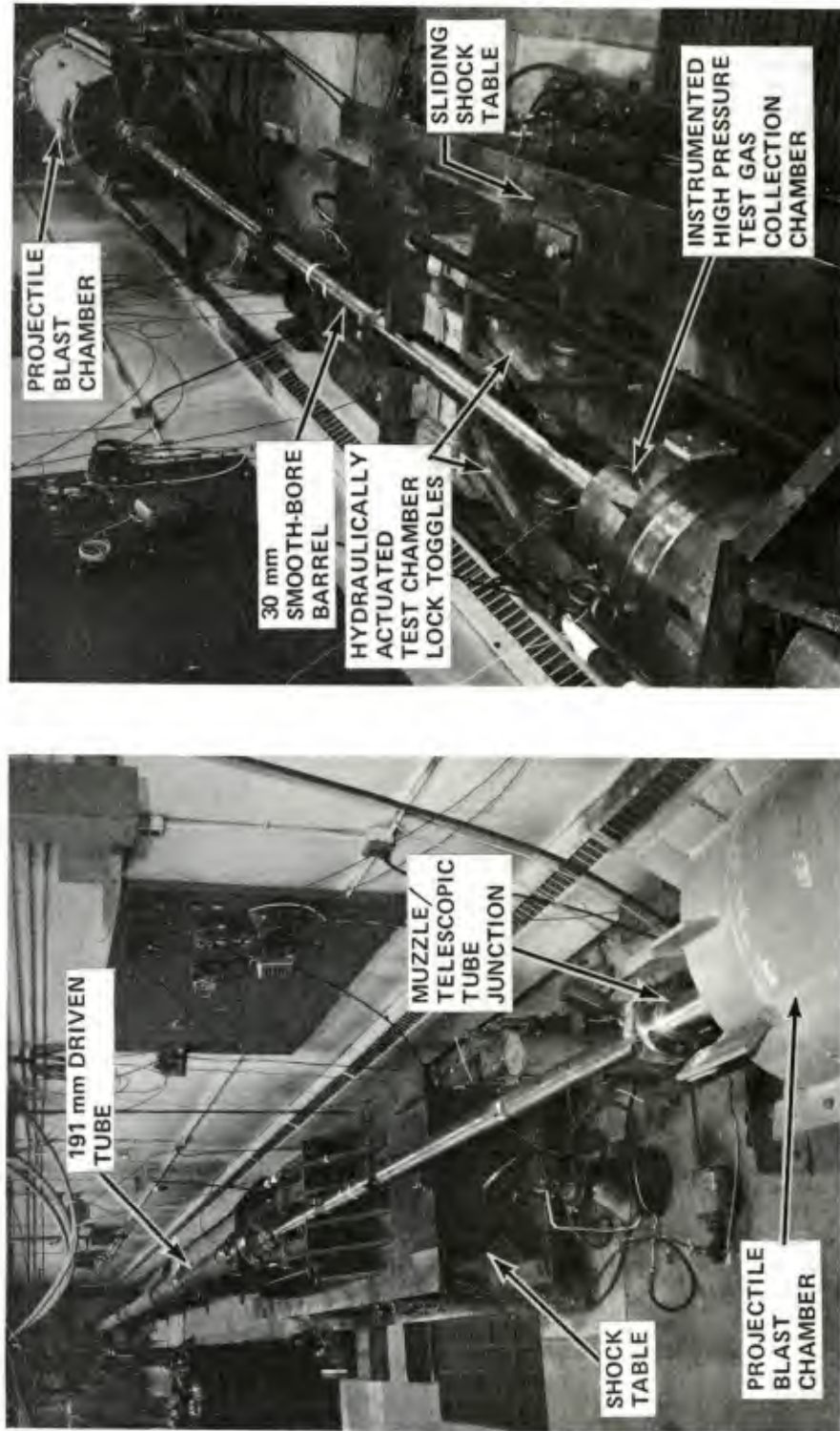


Figure 1 PROJECTILE LAUNCH AND CAPTURE COMPONENTS OF THE SHOCK TUBE GUN

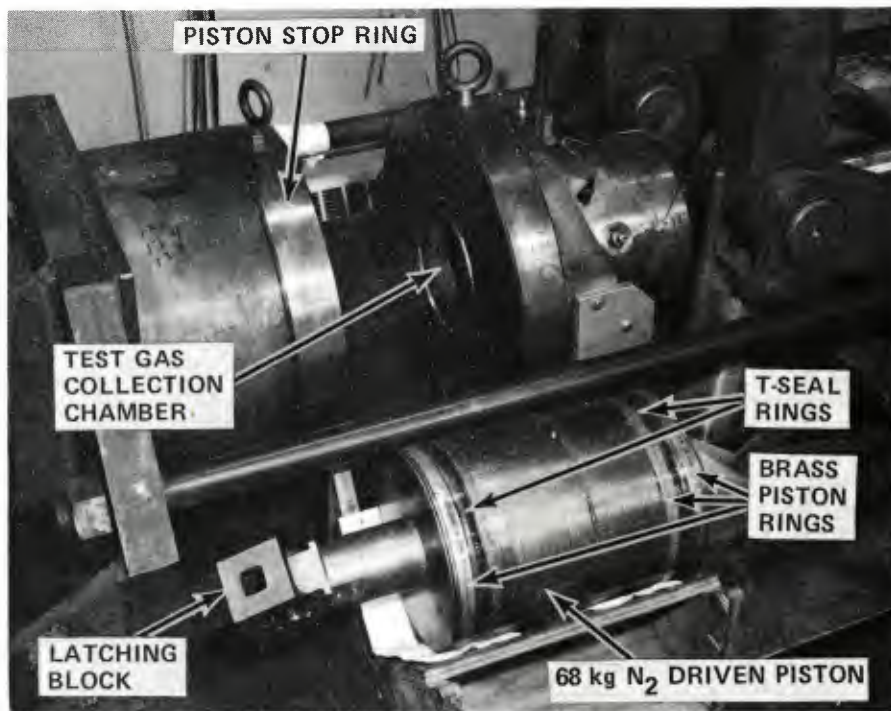
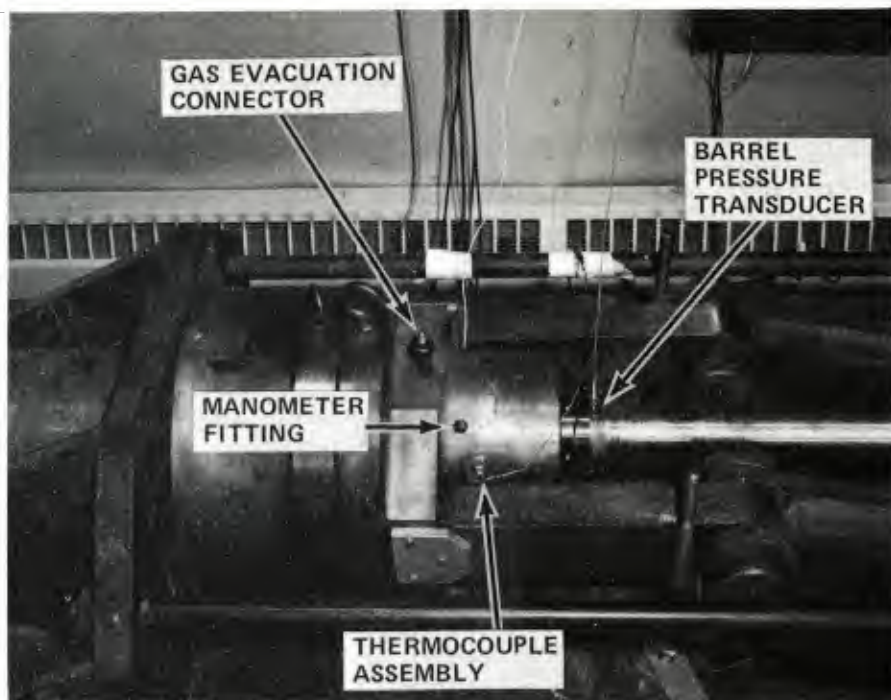


Figure 2 PISTON CHAMBER AND TOGGLE RESTRAINT COMPONENTS OF THE SHOCK TUBE GUN

III. TEST PREPARATIONS

3.1 Specimen Selection

The primary objective of this study was to determine if certain propellant gas conditions enhance barrel erosion and cracking. To correlate the test data, the specimens used were made nearly identical in shape and composition, i.e., a 4340 steel cylinder, 38.1mm in length, 31.75mm in diameter, and bored concentrically to 12.7mm, to create a sonic flow condition during the tests. The flow channel inlet was radiused to reduce turbulence and to increase heat flux over a larger portion of the flow channel surface. The samples were small enough to fit in the specimen stage of Calspan's Scanning Electron Microscope (SEM) such that bore surface examinations could be conducted without using replicas. Conversely, the samples were large enough to register finite changes in weight and bore diameter, resulting from test conditions. Mass changes were measured in tenths of a milligram on an analytical balance. Diametral recession was measured to within 10^{-4} mm at four specific axial locations, as shown in Figure 3. Also shown in the figure are the ports for in-wall thermocouples which are used to determine the integrated heat input.

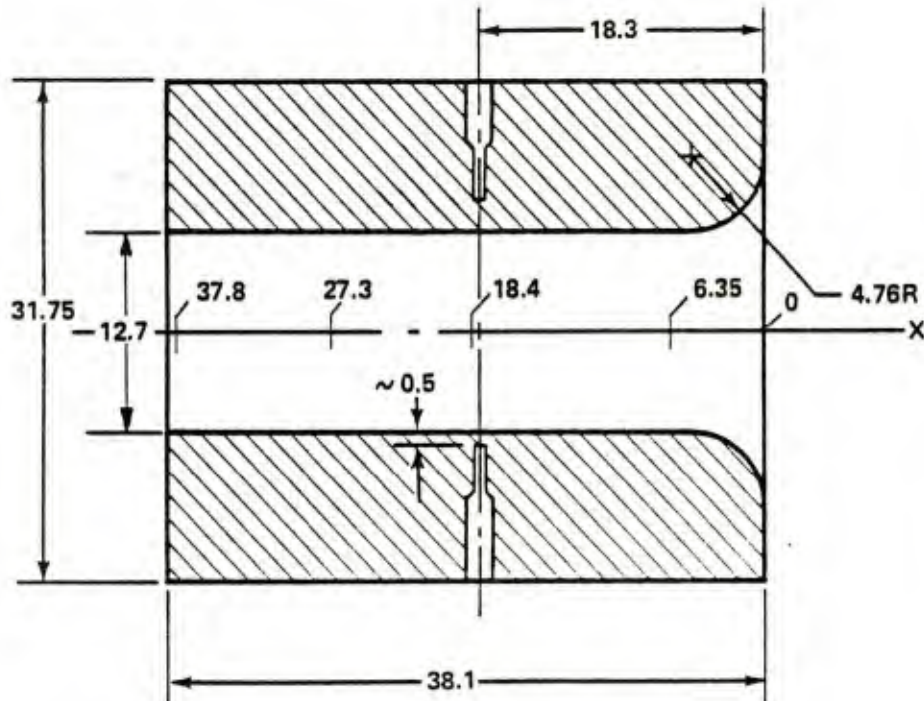


Figure 3 SHOCK TUBE GUN TEST SAMPLE

3.2 Heat Transfer Instrumentation

A primary measurement of the study is the amount of bore heating associated with each test. For this measurement, two in-wall thermocouples were installed in each sample, at distances approximately 0.5mm from the bore surface. The method of installation is shown in Figure 4. Each of these thermocouples independently may be used to determine net heating to the bore. Total heat input is calculated from the in-wall thermocouple's output by use of methods developed and reported by Calspan.¹ Briefly, conversion of thermocouple output (millivolts vs. time) to total net heat input per unit area is made by use of the relation

$$Q(t) = \Delta T(t) \sqrt{\pi k c_p t} \quad (1)$$

where $Q(t)$ is the net bore heat input

$\Delta T(t)$ is the indicated change in in-wall temperature as a function of time

k is the thermal conductivity

c_p is the heat capacity per unit volume

t is the time after start of heating.

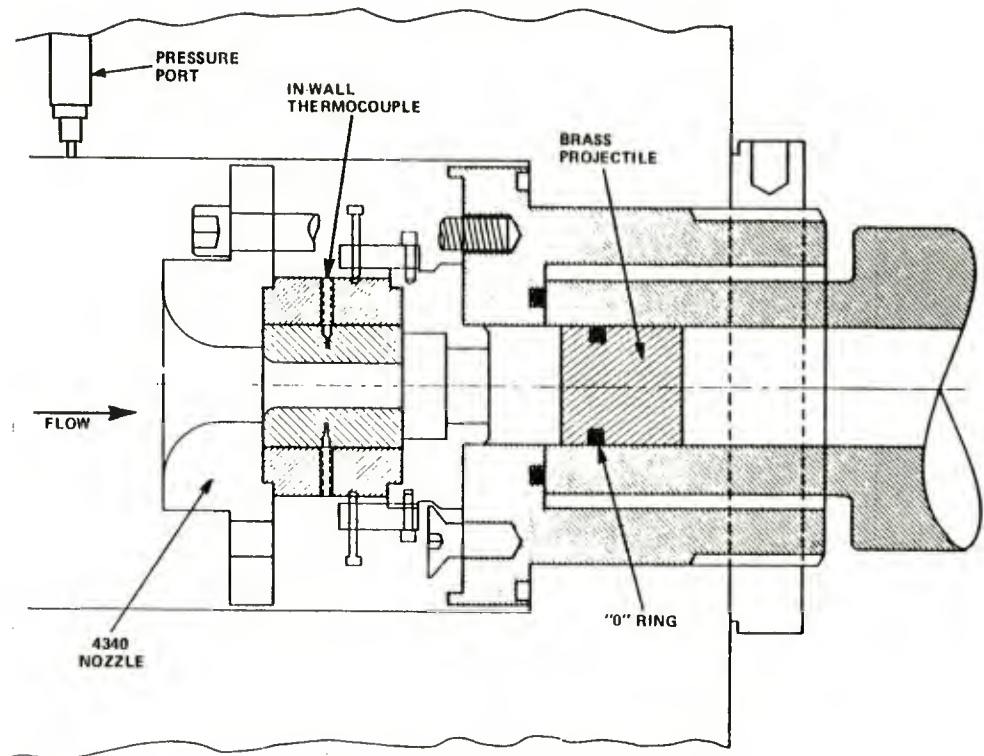
Data reduction procedure consists of calculating $Q(t)$ using Equation (1) at successive time intervals to produce a curve of $Q(t)$ vs. t which becomes asymptotic to the true heat input. To compute the correct asymptote, time zero for the start of heating must be established accurately on the thermocouple trace. It was concluded in the previous STG study², that correctly shaped asymptotes were most consistently produced by placing time zero at the intersection of the trace baseline and the average slope of the initial heat pulse's leading edge.

The Table 2 values for Heat Input are taken from end points on the $Q(t)$ vs. t curves that have been divided by a correction factor to account for the heat flux being dispersed over an increasing surface area as it passes through the test specimen's radial wall. This correction factor, $\eta(r)$, based on geometric considerations,¹ is calculated from the relation

$$\eta(r) = 1 - 0.32e^{-3.71r}$$

For the test specimen bore radius of 6.35mm, $\eta(r) = .87$

1. F.A. Vassallo, "Mathematical Models and Computer Routines Used in Evaluation of Caseless Ammunition Heat Transfer," Calspan Report No. GM-2948-Z-1, June 1971.
2. E.B. Fisher, C.C. Morphy, "The Role of Oxygen in Gun Barrel Erosion and Cracking--A Shock Tube Gun Investigation," U.S. Army Ballistic Research Laboratory, ARRADCOM, Contract Report No. ARBRL-CR-00427, April 1980.



SHOCK TUBE GUN TEST SECTION

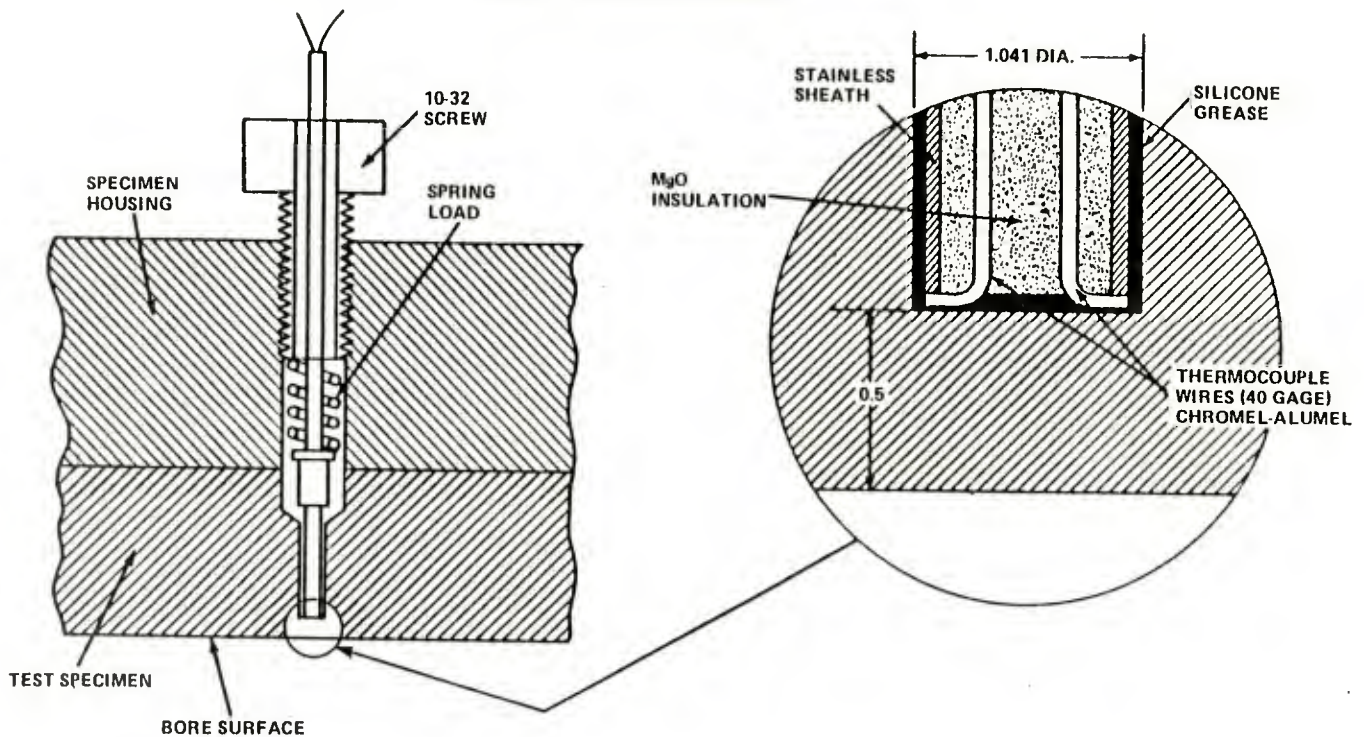


Figure 4 IN-WALL THERMOCOUPLE INSTALLATION

3.3 Selection of Test Conditions

The program objective was to experimentally characterize the role of carburization in gun barrel erosion. To insure meaningful results, the selection of test conditions had to meet three basic criteria. First, all but the "inert" test gas mixtures contained carbon monoxide to duplicate the reducing species in propellant gas atmospheres, particularly those with low flame temperatures, such as nitramines which have relatively high CO concentrations. Test concentrations of carbon monoxide were on the average higher than any found in actual propellant gas, but were deemed appropriate for this initial study of the gross effects of carburization in relation to other ballistic phenomena such as oxidation or pure melting which were previously shown to influence barrel erosion and cracking.^{2,3} The logical extension of this present study would be an investigation of quantitative propellant gas chemistry, incorporating all of the phenomena reported on to date.

The second criterion to be met was the selection of thermodynamic conditions indigenous to large caliber guns. To a large extent the interior conditions were dictated by the STG's present physical configuration, including the mass of the driven piston which transfers energy from the compressed gas to the test mixture. However, the mass of the test mixture often varied from run to run and appropriate calculations were made with the use of the STG computer code to determine the correct driver pressure that would produce the desired real gun conditions, namely pressures in the neighborhood of 300 MPa and temperatures near the melting point of the test specimen alloy, 4340 steel.

A third criterion for the selection of test conditions was concerned with event time variation. Since carburization is dependent upon time in addition to concentration gradient and temperature, an effort was made to alter the profile of the heat and pressure pulse while maintaining its peak amplitude at a constant value through several tests. It was felt that if carburization affected gun barrel wear within a period of several milliseconds, then a variation in time of several fractions of a millisecond would also effect barrel wear.

In meeting the above criteria, the test conditions selected were able to separate the contributions of chemistry, pressure, temperature and time to carburization potential and, in turn, its effect upon barrel erosion.

3. F.A. Vassallo, W.R. Brown, "Shock Tube Gun Melting Erosion Study," USA Ballistic Research Laboratory, ARRADCOM, Contract Report ARBRL-CR-00406, January 1979. (AD #A076219)

IV. TEST PROCEDURE AND RESULTS

4.1 Test Procedures

Operation of the STG to collect test data regarding ballistics, heating and erosion followed a fixed experimental pattern. Prior to a run being conducted, the facility was inspected for damage from the preceding test and needed repairs were performed. Components such as the driven tube, piston, and gas collection chamber which contact the test gas during a run were carefully cleaned to eliminate contaminants from their surfaces. All wearing surfaces, including piston "O" rings and bore riders, tube seals and stop ring buffers were replaced if their wear limits were reached. The piston was then inserted in the upstream end of the tube and latched to the driver release mechanism. A new projectile was inserted in the barrel.

The numbered specimen was weighed prior to testing using an analytical balance for initial mass, given a final cleaning with freon, and then installed in the sample holder within the gas collection chamber. M-11 mechanical pressure gauges were also installed in the chamber. Thermocouples were inserted through the chamber wall, positioned in the sample wall and then the chamber/barrel assembly was lowered into position and sealed to the downstream end of the driven tube with hydraulic toggles.

After installation of the projectile and specimen, the entire tube/chamber cavity was evacuated to a pressure of 2.0mm Hg or less. If vacuum was maintained for a reasonable time, indicating seal integrity, the cavity was purged with argon, re-evacuated, again purged with argon, and evacuated for a third time. The cavity was then charged to the local atmospheric condition with the required partial pressures of the gases selected for the test mixture. These partial pressures are dependent upon the mix ratio desired.

Equations for establishing partial pressure settings were derived from the Dalton model of ideal gas mixtures, which assumes the following:

1. The moles of mixture, n , equals the sum of the moles of the component gases, $n_A + n_N + n_{CO}$, where A, N and CO are subscripts referring to argon, nitrogen and carbon monoxide, respectively.
2. Each component gas in the mixture occupies the entire mixture volume, V , which in this case is the volume of the driven tube.
3. The temperature, T , of the components before and after mixing remains constant.
4. The mixture pressure, P , in this case, 1 atmospheric, is reasonably low, to assure near ideal gas behavior.

$$\text{For the components: } P_A V = n_A \bar{R}T$$

$$P_N V = n_N \bar{R}T$$

$$P_{CO} V = n_{CO} \bar{R}T$$

$$\text{For the mixture: } PV = n \bar{R}T$$

Since $V/\bar{R}T$ is a constant in all the equations:

$$\frac{P_A}{n_A} = \frac{P_N}{n_N} = \frac{P_{CO}}{n_{CO}} = \frac{P}{n}$$

Rewriting:

$$\frac{P_A}{P} = \frac{n_A}{n}$$

$$\frac{P_N}{P} = \frac{n_N}{n}$$

$$\frac{P_{CO}}{P} = \frac{n_{CO}}{n}$$

That is, for each component of a mixture of ideal gases, the mole fraction and the ratio of the partial pressure to the total pressure are equal.

Upon completion of test gas charging, the mixture was given time to equilibrate in the driven tube while the required instrumentation including pressure transducers, thermocouples and velocity screens were connected to suitable recording devices and checked for correct operation. The piezoelectric pressure output was stored for future playback at a tape speed of .76 mps (30 ips) on a Bell & Howell 7 channel recorder. The thermocouple output was recorded on a CEC oscilloscope at a paper speed of 5 ips. The projectile transit time between velocity screens was measured directly on a Tektronix oscilloscope with trace storage at 1 ms per division.

If the instrumentation checked out satisfactorily, the nitrogen tank farm valve was opened, the tube air brake was charged, the driver was pressurized to the desired level for the experiment, recording devices were activated and the piston was released.

After exhausting residual driver pressure, the air brake was bled, and the chamber/barrel assembly was decoupled from the tube. The specimen was carefully removed, inspected, weighed and measured diametrically at the aforementioned axial locations. Hard copy was made of all test data for further reduction and analysis.

4.2 Test Matrix

A total of 32 tests were conducted during this program. A summary of the test conditions, mass loss, the recession measurements along the length of the sample's flow channel and total heat input as measured by the in-wall thermocouples and corrected for radial dispersion, are presented in Table 2.

The test matrix was divided into essentially five groups. The first group, tests 63 through 68 established a wear curve for a 10 percent carbon monoxide mixture, at a fixed driver pressure. The remaining test gas constituents, nitrogen and argon were varied to alter the ratio of specific heats, which was the sole independent variable altering flow conditions between tests. Two subsequent tests, 69 and 70 adding 5 percent hydrogen to the first group's formula, were conducted to ascertain the peak flow conditions obtained with a "lighter" gas mixture with the same concentration of active constituents as tests 63 and 64. Test 71 was conducted as an "inert" comparison of tests 63 and 69, since the peak gas temperatures experienced with the first group were well above threshold of erosion values, in a temperature region where no previous STG data had been collected and where no baseline melting had been quantified.

The second group of runs, tests 72 through 75 and also 77, better defined the inert wear curve, begun in the previous program², near and above the erosion threshold for flow conditions experienced in existing large caliber guns, using hot double-base propellants.

The third group of runs, tests 78 through 82, established a wear curve for high CO concentration mixtures, by direct substitution of 45.5 percent carbon monoxide for an equal mole fraction of nitrogen used in the previous group of "inert" tests. Since CO and N₂ have the same molecular weight, peak conditions of tests performed at identical driver pressures varied little between the second and third groups. Direct comparison of test results of these two groups proved of primary importance in establishing the enhanced erosivity of propellant gases containing large quantities of CO.

A fourth group of runs, tests 83 through 88, attempted to establish any concentration threshold for CO that may exist between the "inert" no CO atmosphere of group 2 mixtures and the high CO concentration mixtures of group 3. The combined fractional percentage of CO and N₂ remained constant at 45.5. The mass of the mixture, as previously explained, also remained constant for all tests in this group.

A fifth and final group of runs, tests 89 through 94, were conducted for purposes of comparison with the results of group 3 (45.5% CO-no N₂) tests. 4% He was substituted for an equal mole fraction of argon, which "lightened" the gas mixture, but left its chemical "activity" unchanged. The purpose of these tests was to ascertain the contribution of heating time to the CO erosion mechanism, in terms of rise time and period of duration of the heat pulse above a critical bore temperature, i.e., the solidus temperature of 4340 steel with appropriate modification for local (bore surface) chemistry changes determined from comparison of group 3 results and STG code computations.

TABLE 2. TEST RESULTS

Test No.	Specimen No.	Active** Constituent	Peak Gas pressure (MPa)	Peak Gas Temperature (°K)	Mass Loss* (mg)	A (mm)	B (mm)	C (mm)	D (mm)	Heat Input (J/mm ²)
63	29	10%CO (0%N ₂)	222	5377	706	.112	.122	.094	.112	1.28
64	30	10%CO (5%N ₂)	224	5007	630	.135	.109	.076	.043	1.29
65	31	10%CO (10%N ₂)	245	4801	460	.089	.069	.053	.030	1.16
66	32	10%CO (15%N ₂)	264	4589	512	.132	.071	.061	.041	1.14
67	33	10%CO (20%N ₂)	242	4179	268	.066	.005	.041	.013	1.14
68	34	10%CO (20%N ₂)	299	4471	568	.109	.081	.084	.058	1.13
69	35	10%CO, 5%H ₂ (0%N ₂)	232	3352	694	.130	.114	.089	.099	1.17
70	36	10%CO, 5%H ₂ (5%N ₂)	244	3218	684	.157	.178	.091	.053	----
71	37	(10%N ₂)	225	5456	563	.112	.086	.069	.056	1.44
72	38	Inert (4.5%N ₂)	223	3422	0	0	(.010)	(.043)	(.013)	1.15
73	39	Inert (4.5.5%N ₂)	248	3531	8	(.010)	(.003)	0	(.023)	1.16
74	40	Inert (4.5.5%N ₂)	208	3355	(3)	0	(.018)	(.005)	(.018)	1.12
75	41	Inert (4.5.5%N ₂)	285	3678	112	.046	.020	(.013)	(.008)	1.26
76	48	10%CO (35.5%N ₂)	296	3711	123	.038	.015	0	.010	----
77	42	Inert (4.5.5%N ₂)	335	3865	267	.089	.025	.008	0	1.23
78	43	45.5%CO (0%N ₂)	277	3588	226	.038	.025	.020	0	1.31
79	43	45.5%CO (0%N ₂)	256	3507	158	.038	.018	.003	1.27	----
80	44	45.5%CO (0%N ₂)	245	3462	124	.025	.010	(.013)	0	----
81	45	45.5%CO (0%N ₂)	213	3322	2	0	0	(.003)	0	----
82	40	45.5%CO (0%N ₂)	216	3338	1	0	0	(.005)	0	----
83	46	40.5%CO (5%N ₂)	299	3690	246	.051	.030	.015	(.013)	----
84	47	35.5%CO (10%N ₂)	299	3695	254	.051	.030	.025	.013	----
85	39	30.5%CO (15%N ₂)	288	3660	166	.010	.041	.018	.010	1.05
86	49	25.5%CO (20%N ₂)	281	3637	184	.005	.025	.023	.036	1.10
87	50	20.5%CO (25%N ₂)	287	3665	244	.023	.030	.013	.069	1.12
88	51	15.5%CO (30%N ₂)	288	3673	215	.008	.025	.025	.025	1.19
89	52	45.5%CO (4%He)	250	3479	110	(.008)	.018	.008	.008	1.12
90	53	45.5%CO (4%He)	222	3363	194	.015	.038	.020	.018	1.12
91	54	45.5%CO (4%He)	236	3422	98	(.013)	.005	(.003)	(.010)	1.15
92	55	45.5%CO (4%He)	219	3351	97	(.005)	.008	.015	0	1.10
93	56	45.5%CO (4%He)	193	3227	1	(.008)	(.005)	(.003)	1.00	1.14
94	57	45.5%CO (4%He)	201	3268	20	(.008)	(.005)	(.010)	(.010)	1.14

*Parenthesis indicates mass gain due to surface deposition of material.

**The remaining percentage of the test gas mixture is argon.

--- Indicates lost data due to instrumentation malfunction.

4.3 Test Gas Mixture Isentropes

Adiabatic compression of the test gas in the STG generates the pressure and temperature profiles. The test gas composition alters the relationship between the gas temperature and pressure for a given compression ratio. This relationship is shown in Figure 5 for the major gas compositions used in this program. Test numbers indicate the peak position of each run on its respective isentrope. The isentropes were computed by an equilibrium combustion program. Appendix II contains a brief description of the code and a sample printout. This computer program was also used to determine the equilibrium composition of the gas mixture at peak flow conditions. In this way, with a specified gas mixture and measured pressure, the temperature and gas constituents generated as a result of the dissociation and chemical reactions were determined for the compression cycle.

It is important to note that the equilibrium code treats a given gas mixture as a closed system with no chemical or thermal interaction with its boundary. The code does not recognize the presence of a gun barrel wall that is removing heat from, and exchanging molecules, including C, with the compressed gas mixture. The significance of gas-boundary interaction is demonstrated by the isentropes of Figure 5. The 45.5% N₂ (inert) mixture reaches the solidus temperature of 4340 steel at a lower pressure than the 45.5% CO mixture, indicating a lower expected threshold of erosion for nitrogen. As will be shown in Section V, just the opposite effect resulted in actual STG testing.

Table 3 lists the active constituents by mole fraction of each test gas mixture, both at ambient, pre-test conditions and at the peak pressure and temperature conditions of each test. Nitrogen, though classified as "inert" when not in the presence of carbon monoxide, has been included in the table to illustrate its potential for forming oxides, acids and cyanides with active mixture components during a test. These nitrogen compounds, all gaseous byproducts, contribute little to direct barrel wear and erosion. The significant role they do play is in limiting the carburizing potential of the truly reactive components in the mixture. Argon and Helium have been excluded from the table since they truly are "inert". The ratio of specific heats, γ , has been included in the table at both ambient and peak temperature for each test gas mixture, to indicate the changing heat transfer capability of a gas mixture during adiabatic compression. The significance of convective heating to the overall results of this program will be discussed in Section V.

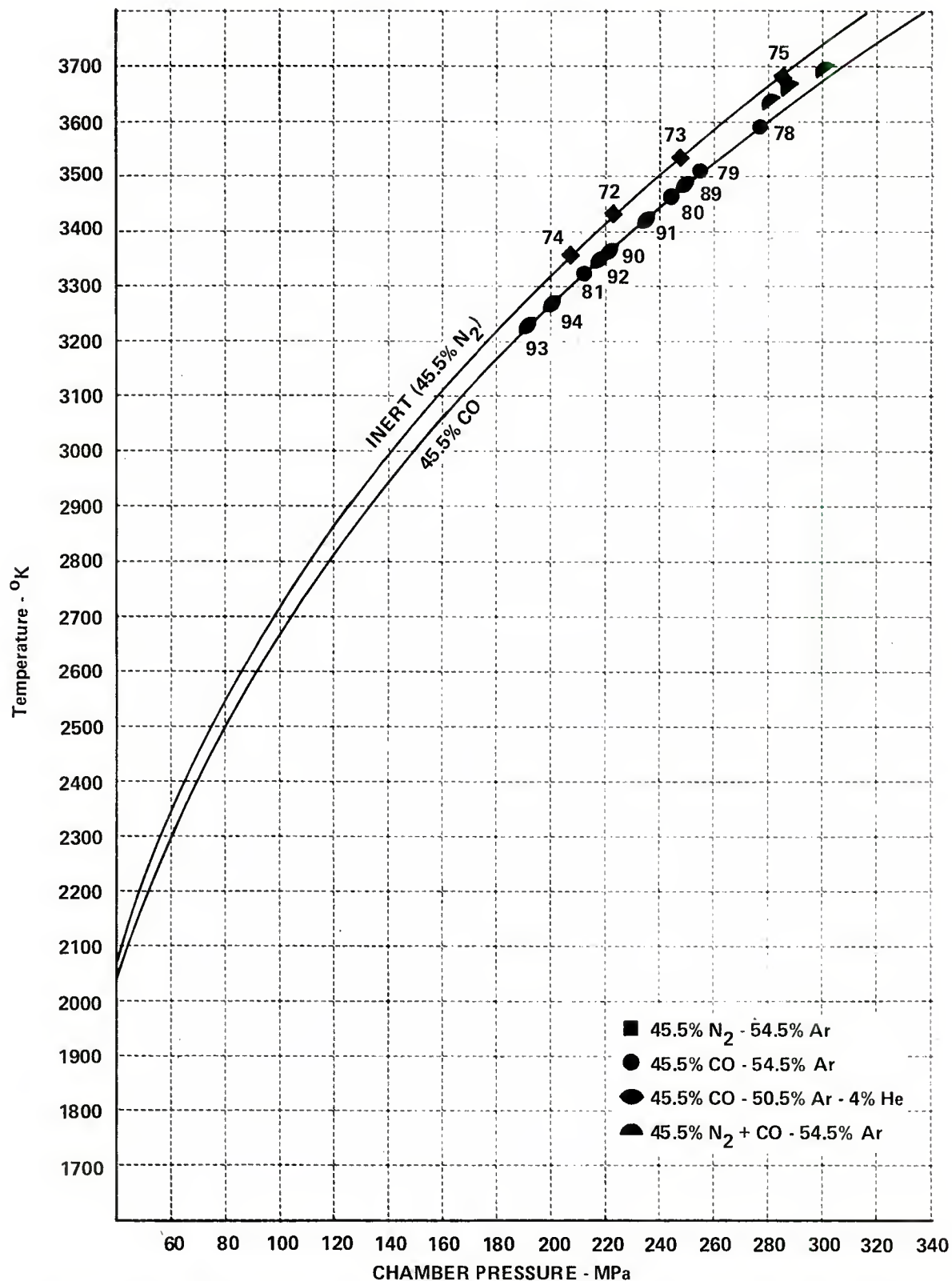


Figure 5 ISENTROPES FOR TEST GAS MIXTURES UNDERGOING ADIABATIC COMPRESSION

TABLE 3. TEST GAS MIXTURE COMPOSITION

Test No.	Ambient Conditions				Peak Test Conditions				Comments
	Y	CO	N ₂	H ₂	Y	CO	CO ₂	CN	
63	1.625	.1000			1.570	.0996	.0010		.0002 O, C(g)
64	1.606	.1000	.0500		1.533	.0994	.0002	.0003	.0002 N; .0001 NO, 0; Trace** C(g)
65	1.588	.1000	.1000		1.508	.0995	.0002	.0003	.0001 N, NO, 0; Trace C(g)
66	1.571	.1000	.1500		1.486	.0995	.0002	.0003	.0001 N, NO; Trace C(g), 0
67	1.555	.1000	.2000		1.470	.0997	.0002	.0002	.0001 N, NO, 0
68	1.555	.1000	.2000		1.476	.0999	.0001	.0002	Trace CN, N, NO, 0
69	1.483	.1000		.0500				.2000	No Equilibrium Code Output
70	1.474	.1000	.0500		1.506	.0986	.0003		.0013 H, .0478 H ₂
71	1.625		.1000		1.570				.0006 N
72	1.511		.4550		1.416				.4550
73	1.511		.4550		1.416				.4550
74	1.511		.4550		1.417				.4550
75	1.511		.4550		1.415				.4550
76	1.511	.1000	.3550		1.413	.0997	.0002	.0001	.3549 Trace N, NO, 0
77	1.511		.4550		1.414				.4550 Trace N
78	1.511	.4550			1.412	.4546	.0002		.0001 C ₂ O
79	1.511	.4550			1.413	.4546	.0002		.0001 C ₂ O
80	1.511	.4550			1.413	.4547	.0002		
81	1.511	.4550			1.414	.4547	.0002		
82	1.511	.4550			1.414	.4547	.0002		
83	1.511		.0500		1.410	.4042	.0005	.0002	.0498 C ₂ N, C ₂ N ₂
84	1.511		.1000		1.410	.3541	.0005	.0002	.0998 C ₂ N, C ₂ N ₂
85	1.511		.1500		1.410	.3042	.0004	.0002	.1498 C ₂ N, C ₂ N ₂ ; Trace NO
86	1.511		.2000		1.411	.2543	.0004	.0002	.1999 C ₂ N, C ₂ N ₂ ; Trace NO
87	1.511		.2500		1.412	.2045	.0003	.0002	.2499 C ₂ N, C ₂ N ₂ ; Trace NO
88	1.511		.3000		1.412	.1546	.0002	.0001	.2999 C ₂ N, C ₂ N ₂ ; Trace NO
89	1.511	.4550			1.413	.4547	.0002		.0001 C ₂ O
90	1.511	.4550			1.414	.4547	.0001		
91	1.511	.4550			1.413	.4547	.0002		.0001 C ₂ O
92	1.511	.4550			1.414	.4547	.0001		
93	1.511	.4550			1.414	.4548	.0001		
94	1.511	.4550			1.414	.4548	.0001		

* Y - Ratio of specific heats
 ** .00005 > Trace > .000005

V. CORRELATION OF RESULTS

5.1 Erosion and Flow Conditions

5.1.1 Pressure, Temperature and Carburization Effects

Five groups of tests were conducted to quantify erosion due to carburization of 4340 steel as described previously in Section 4.2. The primary variable among groups, the fourth group being an exception, was carbon monoxide concentration. The primary variable among group members was compression ratio which determined pressure and temperature. A baseline test mixture, labeled "inert", comprised of 45.5 percent nitrogen and 54.5 percent argon was selected and utilized during the previous two programs.^{2,3} This baseline mixture was modified in this program to include carbon monoxide by replacing nitrogen with CO. With the exception of the first group of tests, runs 63 through 71, the total concentration of carbon monoxide and nitrogen remained constant to maintain comparable gas temperature and pressure conditions throughout the program. In carbon monoxide tests, CO concentration was kept relatively high, from 10 to 45.5 percent, to simulate the expected CO levels in gas evolved from burning low flame temperature propellants, particularly nitramines. Pressure levels ranged from 193 to 335 MPa with the majority of tests recording peak pressures from 220 to 300 MPa.

The variation of mass loss with flow conditions, as specified by peak pressure and by peak temperature are shown in Figures 6 and 7, respectively. The threshold at which sample mass loss is first observed occurs at 248 MPa, 3530°K for an inert (45.5% N₂) gas mixture, 216 MPa, 3340°K for a mixture containing 45.5 percent carbon monoxide, and 193 MPa, 3230°K for this same 45.5 percent CO mixture when 4% of the argon is replaced with helium. The mass loss curve for this last mixture is indicated by two dashed lines since it is unclear from the point scatter on this group of tests, what the true shape of the curve should be. (Correlation of heating data implies that the right hand curve is more nearly correct.) However the offset in erosion threshold between 45.5 percent carbon monoxide mixtures that differ only in total gas mass, produced by substituting helium for part of the argon, implies that the carbon monoxide surface reaction is dependent more on diffusion time, than on the surface concentration gradient of the diffusing species, the predominant control in the case with oxygen.² Mixtures containing less than 45.5 percent CO, namely runs 83 through 88, do fall between the 45.5 percent CO and inert gas curves which would indicate some diffusion control at above threshold conditions, but since the measured erosion of these mixtures does not approach the inert value with decreasing CO concentration in any logical fashion, no true implication of diffusion controlled erosion can be made.

Erosion curves for 1 and 2.5 percent oxygen mixtures from the previous program² have been included on Figures 6 and 7 for comparison with the new curves representing neutral and carburizing activity. As was previously noted² for the 2.5 percent oxygen curve, the shift in the erosion

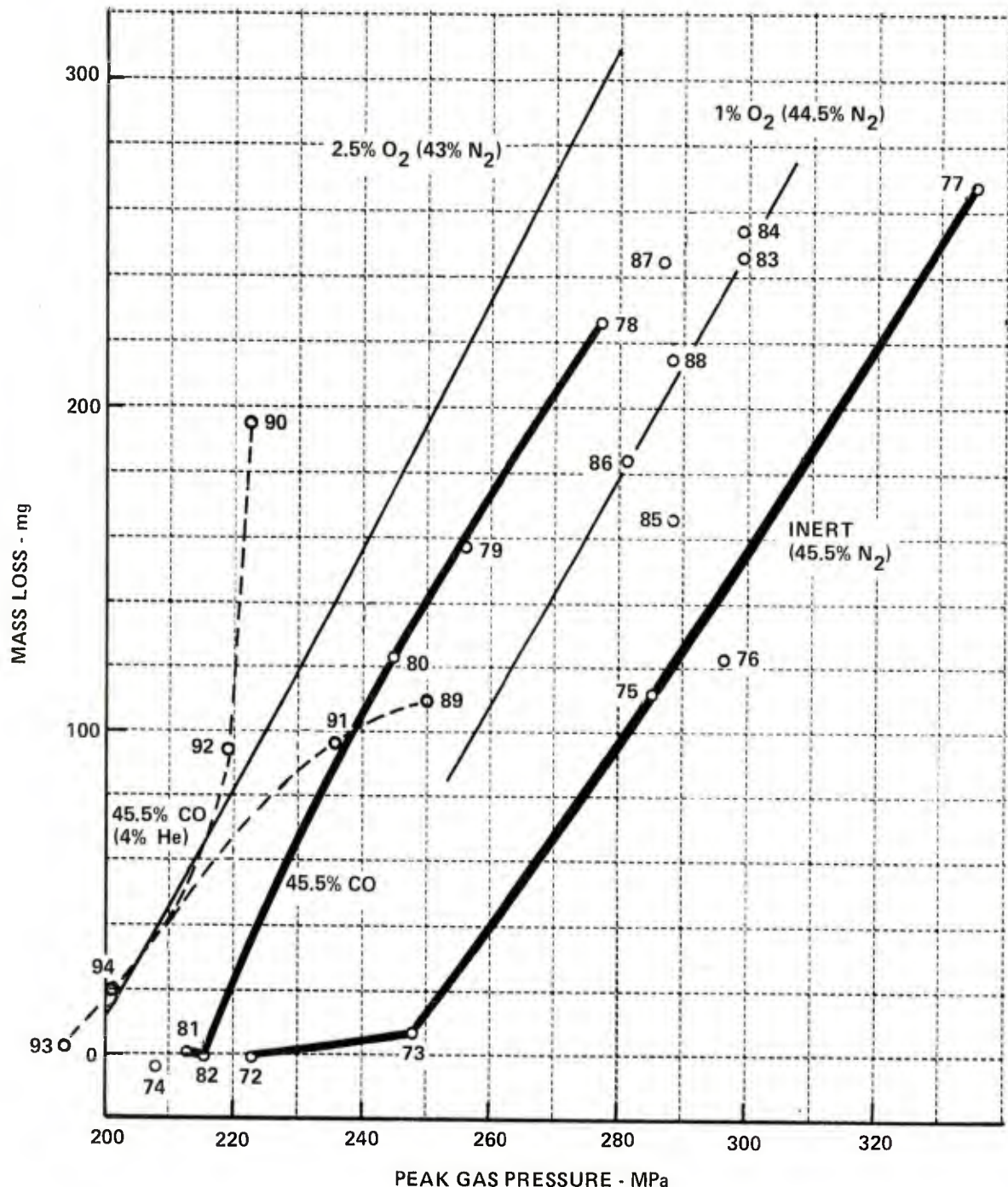


Figure 6 MASS LOSS vs PEAK TEST GAS PRESSURE FOR VARIOUS TEST GAS MIXTURES

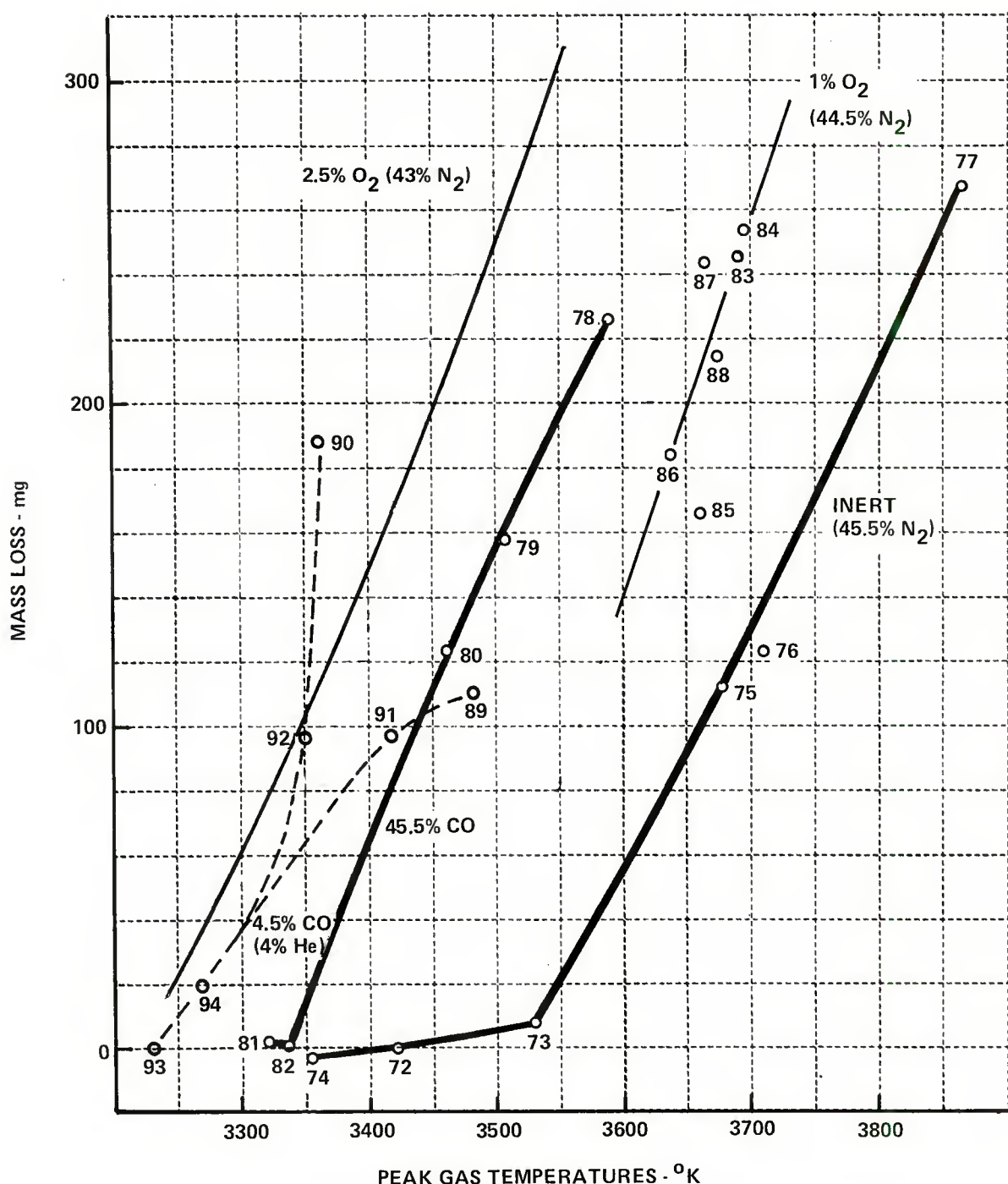


Figure 7 MASS LOSS vs PEAK TEST GAS TEMPERATURES FOR VARIOUS TEST GAS MIXTURES

threshold for the 45.5 percent carbon monoxide mixture from the inert threshold conditions is an indication that melting is not a prerequisite for the onset of a surface reaction, which is the mechanism by which carburization of steel enhances material loss. The parallel nature of the CO and inert curves above their respective erosion thresholds further indicates that the effects of carburization represent a nearly constant increment to the erosion caused by convective heating of 4340 steel by propellant gas flow conditions found in large caliber guns.

5.1.2 Convective and Chemical Heating Effects

Part of the enhanced CO erosion indicated by Figures 6 and 7 may be attributed to differences in the ballistic cycle. The amount of material removal is basically a function of the steel sample's entire heating history. Both the time at a high heating rate and the dynamic heat conduction processes are important. The measured total heat input represents the integrated convective and chemical heat flux to the sample and is an indicator of differences in ballistic cycle time between tests with similar heat flux levels and chemical environments.

The measured total heat input, with the correction for radial heat dispersion, as given in Table 2, is plotted against mass loss in Figure 8. A gross comparison of test results for mixtures experiencing similar peak flow conditions reveals that a mixture containing CO produces higher specimen mass loss at a lower experimental total heat input than a comparable inert gas mixture. However, there appears to be no quantitative correlation between mass loss and experimental heat input in Figure 8 because the act of material removal, which varies in magnitude from test to test, removes a likewise varying amount of heat from the location of the in-wall thermocouple. Therefore, a correction factor was derived that when added to the heat input data used in Figure 8, would better correlate mass loss measurements. The factor is based on the assumptions that any material removed from a sample's surface was done so at 1720°K, the solidus temperature of 4340 steel, and that the material was removed before its latent heat was absorbed by the remaining steel. The correction factor is

$$\Delta Q = \rho c \Delta x \Delta T = 3.27 \Delta x \text{ J/mm}^2$$

where ρ is the density of 4340 steel (7840 kg/m^3); c is the steel's specific heat ($586 \text{ J/kg}^{-\circ}\text{K}$); Δx represents the diametral erosion in millimeters at the location of the heat sensor (column B of Table 2); and ΔT is the difference in ambient and solidus temperatures for the steel (1425°K). A factor of $1/2$ is included in the equation to convert diametral recession to an averaged radial recession. The calculated ΔQ for each test is simply added to the heat input given in Table 2 to form Q_{corr} . Thus, Q_{corr} represents an effective heat input consisting of convective and chemical components. This quantity treats a reduction in surface temperature required for melting as an equivalent increase in heating. Thus, differences in material loss caused by surface chemistry cause differences to appear in Q_{corr} between tests with similar convective heating, temperature, and pressure.

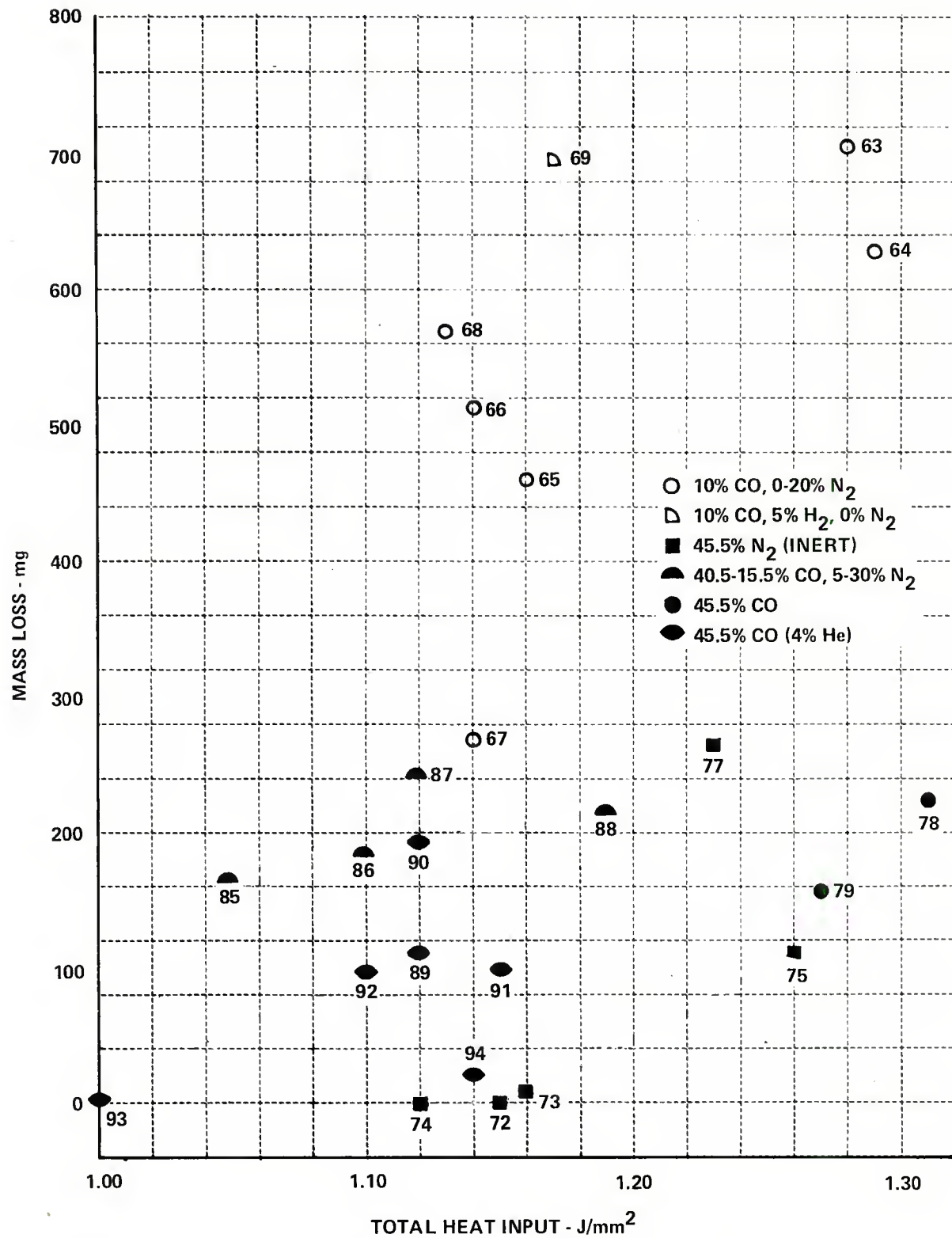


Figure 8 MASS LOSS vs TOTAL HEAT INPUT FOR TEST GAS MIXTURES

The correlation of mass loss with the total heat input, corrected for material loss is shown in Figure 9. The improved agreement among tests in each group is readily apparent as well as a noticeable erosion path for all the tests for which heating data was available. Instrumentation failure during the tests for 45.5 percent CO mixtures at threshold conditions prevents the illustration of a critical heat input for this mixture. However, the points representing the 45.5% CO-4% He-50.5% Ar test group with the same active chemistry as the 45.5% CO-54.5% Ar mixture, indicates that this carburizing mixture requires less total heat input, up to .15 J/mm² less in some cases, to affect the same material removal than the "inert" gas mixture requires. This variation in total heating to produce similar levels of erosion can be attributed to surface chemistry, convective heat transfer coefficient, heat required to remove material, and heat absorption characteristics. In order to delineate the contribution of each mechanism to the heating cycle of a particular gas mixture tested in the STG, a calculation of convective hot wall heat flux for each test was made.

Convective hot wall heat flux is the driving potential for melting erosion once the melting temperature is achieved. Similarity of heating cycles is important because the heat flux history determines the surface temperature. Therefore, if the relative difference in heating cycles is known, as is the case with 45.5 percent carbon monoxide mixtures (with and without a 4 percent substitution of helium for argon), the computed convective heat flux to the hot sample surface will quantify that difference in heating cycles since the heating due to chemistry remains constant. In the opposite case with test mixtures comprised of 54.5 percent argon and the remaining mole fraction being various ratios of carbon monoxide and nitrogen, convective hot wall heat flux calculations reflect the differences in chemical heating among tests, namely the fluctuation of critical surface temperature at which simple melting erosion may commence.

To perform the heat flux calculation, flow conditions for each test were computed, using a combination of two computer programs and the experimentally measured peak pressures. The STG cycle model (Appendix I) was used to create the proper pressure profile. Also included in this particular code is a representation of the flow through the test sample and calculation of the convective heat flux using the empirical equation for turbulent flow over a flat plate. The gas conditions of temperature, density and velocity are evaluated in this code. The local hot wall heat flux is computed and a running summation of the heat input to the wall is evaluated. The computed total heat input was compared with the experimentally determined value for the input gas mixture. A factor was applied to the heat flux calculation to bring the total heat input into agreement with the experimentally determined value. In this manner, the instantaneous value of convective heating, as determined by the flow conditions and exclusive of chemical heating, is believed to be reasonably correct for tests with inert and carbon monoxide gas mixtures.

The gas temperature, as determined by the STG model in its current state of development, is only an approximate calculation. A more accurate temperature calculation is provided by the equilibrium combustion code that is described briefly in Appendix II. The code computes an isentropic

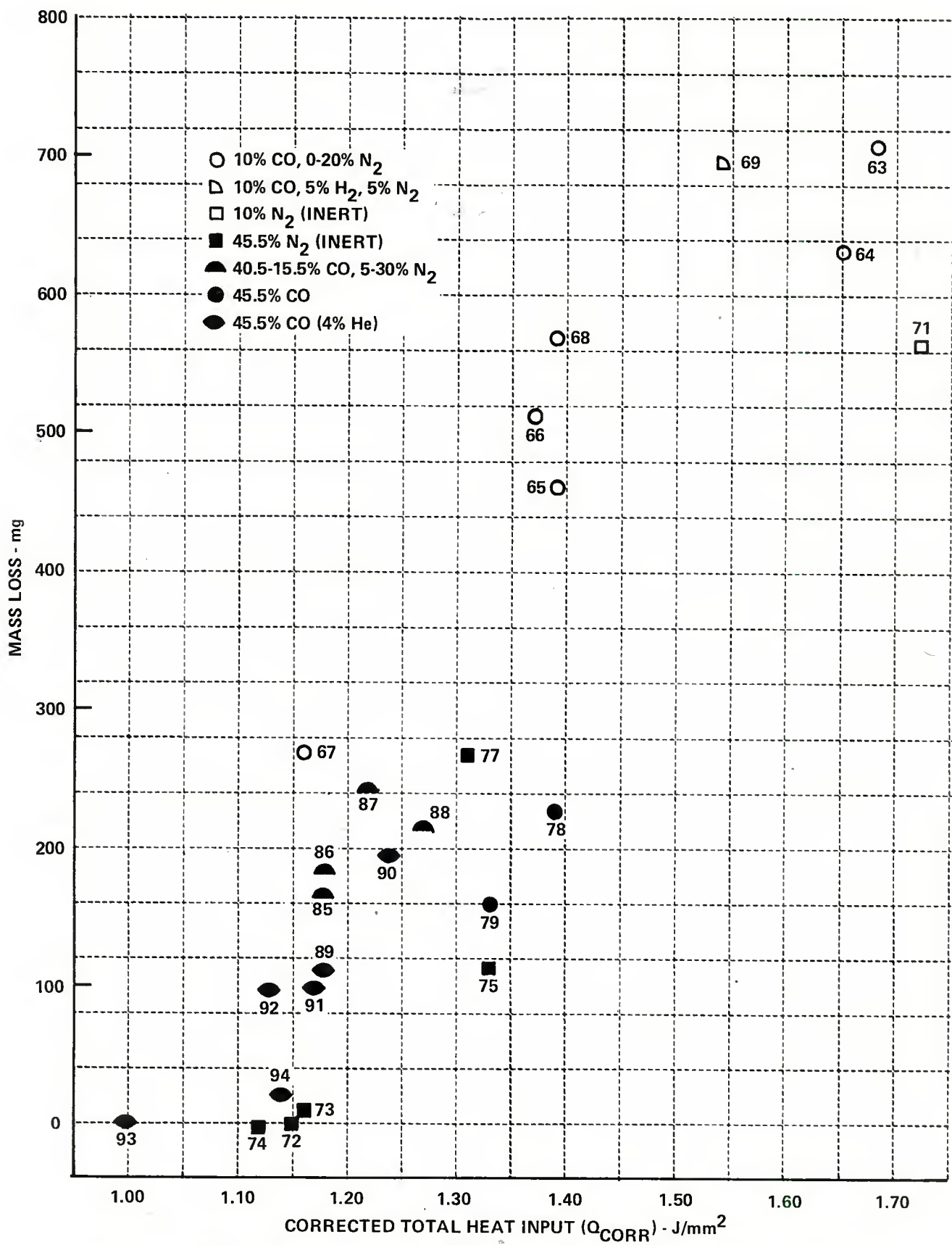


Figure 9 MASS LOSS vs TOTAL HEAT INPUT CORRECTED FOR LOCAL HEAT LOST BY MATERIAL REMOVAL

compression of gases beginning with an arbitrary mixture. In addition to determining the temperature and pressure, the concentration of the various chemical species formed during the equilibrium combustion process are also determined. For example, the mole fraction of cyanide formed by compression of gas mixtures containing nitrogen and carbon monoxide is evaluated.

An approximate technique was used to correct the heat flux calculated by the STG model to the more accurate temperature conditions of the equilibrium combustion code. The heat flux to a surface is equal to the product of a coefficient and the temperature difference between the gas and the surface,

$$q = h (T_o - T_w).$$

For the heat flux to a flat plate in turbulent flow, the coefficient is functionally proportional to the gas density, velocity and viscosity,

$$h \sim (\rho u)^{0.8} \mu^{0.2}$$

These gas parameters can be expressed in terms of temperature as follows:

$$\begin{aligned} \rho &\sim T^{-1} \text{ through the ideal gas equation of state} \\ u &\sim T^{0.5} \text{ through the energy equation,} \\ \text{and } \mu &\sim T^{0.5} \text{ from molecular transport theory.} \end{aligned}$$

Thus, the approximate dependence of h on the gas temperature is

$$h \sim (T^{-1} \cdot T^{0.5})^{0.8} (T^{0.5})^{0.2} = T^{-0.3}$$

The convective hot wall heat flux computed by the STG code is

$$q_s \sim T_{gs}^{-0.3} (T_{gs} - T_{ws})$$

where T_{gs} and T_{ws} are the respective peak values for gas and surface temperatures. Similarly, the convective heat flux to a melting steel surface is

$$q_{hw} \sim T_{ge}^{-0.3} (T_{ge} - T_{wm})$$

where T_{ge} is the gas temperature calculated by the equilibrium combustion code and T_{wm} is the solidus temperature of 4340 steel, 1720°K. The corrected value for the heat flux, q_{hw} , is

$$q_{hw} = q_s \left(\frac{T_{ge}}{T_{gs}} \right)^{-0.3} \left(\frac{T_{ge} - T_{wm}}{\frac{T_{gs}}{T_{ws}} - T_{ws}} \right)$$

This represents an approximate value of convective heat flux to a melting surface.

A graph showing the correlation of mass loss with convective hot wall heating is shown in Figure 10. The expected offset between flux curves for 45.5 percent CO mixtures both with and without a 4 percent substitution of helium for argon represents the difference in heat cycle histories for gas mixtures of equal chemical activity, but different total mass.

The test gas mixtures of 45.5 percent carbon monoxide and 45.5 percent nitrogen, both containing identical mole fractions of argon, have nearly identical masses, ratios of specific heat and, therefore, similar heating cycles. However the CO mixture was capable of producing similar erosion to the "inert" gas mixture at a heat flux rate nearly 100 J/mm²-sec lower than the "inert" mix, both at and well above erosion threshold conditions. To account for the difference in erosion threshold, the above convective heat flux equation was recalculated for a reduced hot wall melting temperature that would shift the CO erosion curve to coincide with the "inert" erosion curve. The computed solidus temperature, assuming all other properties of the steel remained the same, was lowered to 957°K. A reduction of over 750°K in melting temperature is unrealistic for simple diffusion of carbon into steel, according to the iron-carbon phase diagram (Figure 28). Therefore the shift in the CO erosion threshold suggests the strong influence of surface phenomena that alter the thermal properties of the materials, enhance the net heat input, or both.

5.2 Erosion Distribution

Measurements of diametral recession were made at the four axial locations identified in Figure 3 and are presented for each test sample in Table 2. While examining these measurements, it was observed that the distribution of material erosion was altered by the gas mixture. Several of these distributions, normalized to the most forward measurement, are shown plotted in Figure 11. In this figure, the averages for several runs in a group with similar characteristics are compared.

The typical inert distribution, as illustrated by averages of points from Run 75 and 77, shows the highest erosion near the leading edge of the sample which progressively decreases until very little or no erosion is observed by the third measuring point, which is labeled point C. Thus, with only argon and nitrogen in the gas mixture, negligible erosion is observed over the latter half of the sample.

The downstream level of erosion tends to increase when carbon monoxide is added to the gas mixture. Run Numbers 78 through 80 and 83 and 84 all have quite similar gas temperatures and pressures and all experience measurable mass loss during the test. The significance of the erosion distribution from these tests in comparison with that of the inert test, is that the erosion at Points B and C is substantially higher.

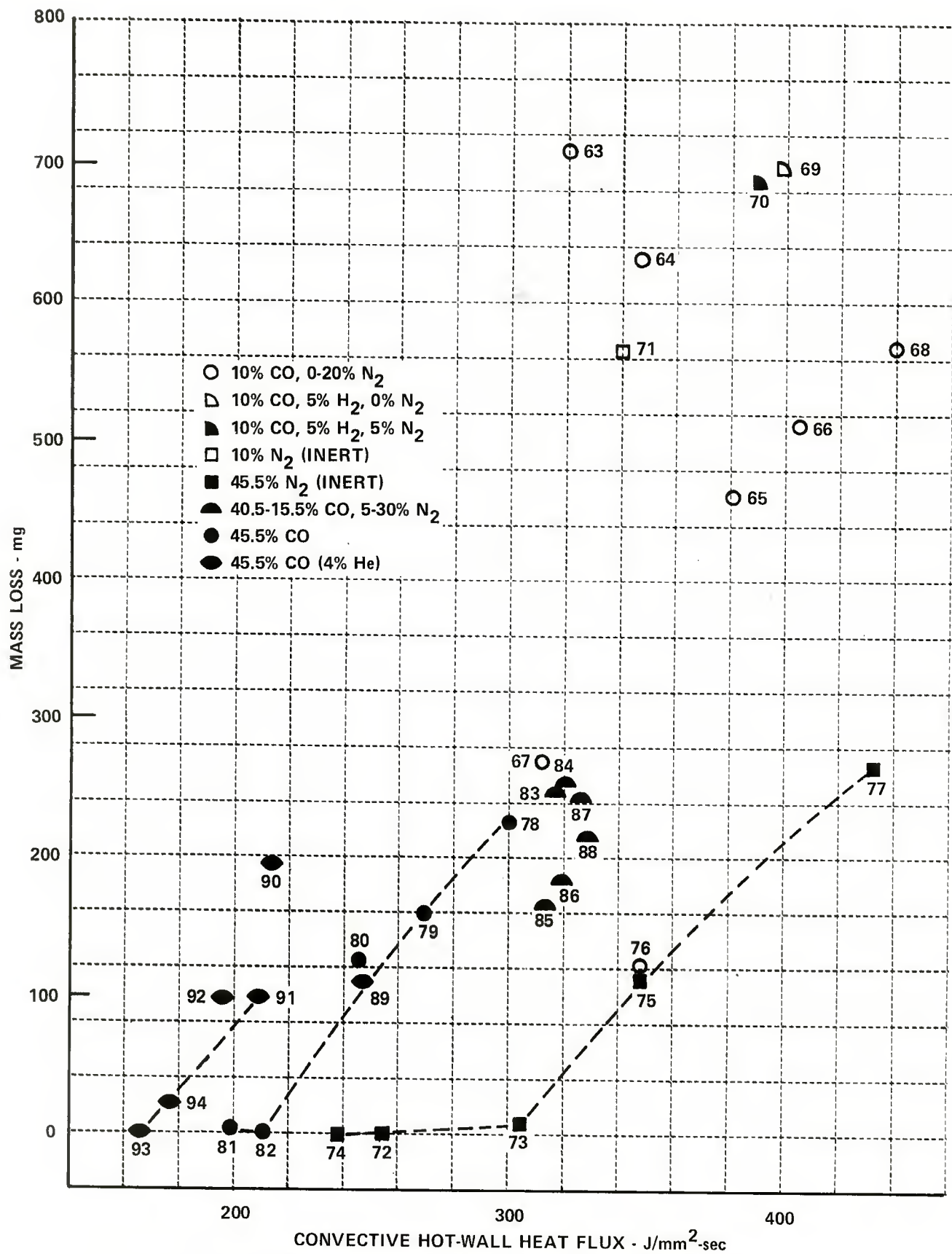


Figure 10 INFLUENCE OF CONVECTIVE HEATING AND CARBURIZING-TYPE REACTIONS ON EROSION OF 4340 STEEL

The average of Runs 85 through 88 show an overwhelming increase in erosion towards the downstream end of the test sample. The erosion of the downstream end of the sample in relation to that of the leading edge, which was used to normalize results, is likely not as dramatic as indicated in Figure 11 because the erosion at the leading edge appears to be unusually small. However, erosion at the downstream end of the samples is large in relation to that of the inert samples and, therefore, it appears as though carbon monoxide in the gas is contributing to a downstream erosion effect. This is similar to that observed when oxygen was introduced into the test gas as described in Reference 2.

Carbon monoxide and nitrogen have the same molecular weight. When one is exchanged for the other in the test gas, there is very little effect on STG test conditions. Carbon monoxide can be substituted for the nitrogen and the effects of carbon monoxide on the specimen can be observed with little change in convective heating and cycle time as long as the concentration of argon remains the same. Therefore, differences in these quantities are not responsible for the observed differences in erosion.

Rapid falloff of erosion was observed with no carbon monoxide in the test gas. When 45.5% carbon monoxide and no nitrogen was incorporated, the falloff was less rapid as shown in Figure 11, but very little or no erosion was observed again at the trailing edge. When carbon monoxide and nitrogen were approximately equal in concentration, that is, when 15 to 30% of the gas was carbon monoxide, the maximum enhancement of erosion distribution was observed. This suggests that the presence of nitrogen in the gas plays a role in the observed erosion pattern. Again it is noted that the low erosion at the leading edge of the sample during these tests caused the curve to exaggerate this effect, but enhanced downstream erosion does appear to be real.

This is also substantiated by the results of Runs 63 and 71 which are not shown in Figure 11. Run 63 was a test with 10% carbon monoxide and 90% argon. This test was very high in temperature and a great deal of material was lost. The diametral recession was nearly constant along the entire length of the sample with the measurements being equal at both the leading and trailing edges. Run 71 was a test with 10% nitrogen, no carbon monoxide, and 90% argon. The pressure and temperature of these two runs was almost identical. The erosion at the leading edge of Run 71 was the same as for Run 63. However, at the trailing edge, erosion was approximately half that of the forward measurement.

It is evident that surface chemistry plays an important role in material loss in a carbon monoxide atmosphere. The inert run indicates a falling off of erosion in much the way that one would expect heat transfer to fall off in turbulent flow over a flat plate. When carbon monoxide is present, the falloff in erosion is altered. The data show the observed effect to be independent of convective heating. The resemblance of this effect to that of oxygen cited earlier suggests the presence of an exothermic reaction.

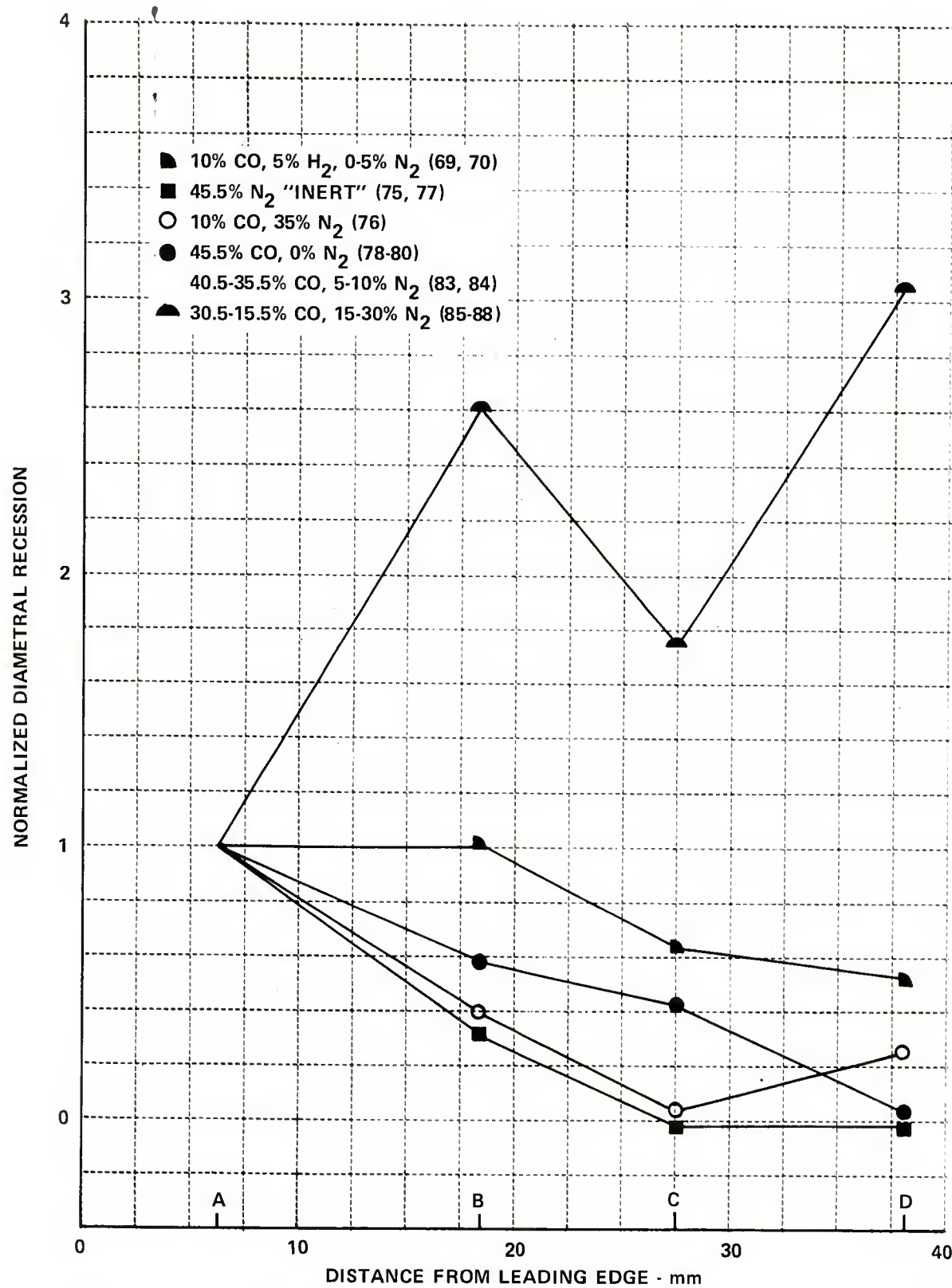


Figure 11 INFLUENCE OF TEST GAS CONSTITUENTS ON SURFACE RECESSION OF 4340 STEEL

5.3 Surface Characterization

The Scanning Electron Microscope was used to help characterize the surface features of each test sample. Selected photographs are shown in subsequent figures. The first four figures (12-15) illustrate the surface of an inert sample with increasingly severe test conditions. Figures 12 and 13 show the sample's surface at the inlet, center, and exit point for flow conditions at the onset of melting. That is, the point where weight loss is first observed. At this time, erosion is initiated at the leading edge of the sample. As conditions increase, the point at which erosion occurs moves farther downstream on the sample. These figures show the presence of small solidified droplets. There is also what appears to be a small crust of solidified material. The presence of a crust-like layer is more evident in Figures 14 and 15 which are representative of samples tested in an inert atmosphere above the erosion threshold. The surface of these samples displays a mottled characteristic that appears to be solidified melt or surface layer of some sort.

The next series of four figures (16-19) illustrates surface features of 4340 steel samples tested in an atmosphere consisting of 45.5% carbon monoxide and argon. The difference between these and the inert tests was that the nitrogen was exchanged for carbon monoxide. The molecular weight of these two gases is the same and test conditions and, most significantly, the convective heating are also approximately the same. The samples shown in Figures 16 and 17 were tested at approximately the same conditions and show what appear to be solidified droplets or perhaps molten protrusions that existed on the base metal surface. Otherwise, there is very little change to the initial surface. At more severe conditions (Figures 18 and 19) it is noticed that the surface appears to be quite clean although rough and exhibits what might be interpreted as a turbulent flow pattern. The surface does not have the crust-like layer that was observed for the inert shots. One might postulate that the presence of carbon monoxide facilitated removal of the crust-like layer that was observed in the inert shots and that this is also responsible for the increased erosion at farther downstream stations that was noted in the previous section.

Some cracking was also noted in the regions of high erosion. This is contrary to the observation made in Reference 2, concerning the effects of oxidation, where significant cracking was observed at the onset of erosion rather than in a region of high erosion.

The next series of four figures (20-23) illustrates the surface features of the 4340 carbon steel sample as influenced by decreasing percentage of carbon monoxide. For these runs, the test conditions are very much the same and nitrogen was exchanged for carbon monoxide in an attempt to fill in the region between inert and 45.5% carbon monoxide. The significant feature of these SEM photographs is the slight tendency of the surface features to approach those of an inert sample with decreasing carbon monoxide concentration. When the gas contains 15.5% carbon monoxide, the lowest concentration tested, the surface still tends to resemble more of the high concentration of

carbon monoxide rather than the inert sample. This seems to indicate that the process is only slightly diffusion limited for the concentration tested. An interesting aspect of the 40.5% carbon monoxide run is that it was tested at a higher pressure than any of the others and the flow patterns that were observed looked like eyes on a potato. This indicates a high interaction of the turbulent flow with the surface and the presence of a sluffing mechanism. At the lower concentrations of carbon monoxide, this feature was not apparent. At low to intermediate concentrations of carbon monoxide, the presence of solidified melt became more evident, whereas at the high concentrations all the melt appeared to be swept away.

The final set of four figures (24-27) illustrates surface features of a sample tested in a gas mixture containing 4% helium, where helium was exchanged for some of the argon. This series of four tests had gradually increasing pressures. Substantial erosion was observed at the three higher pressures where 201 MPa appears to be the threshold point. The surface features of all three appear to resemble each other with respect to the formation of a kind of a web. A dendrite feature on the surface could be solidification of a surface melt or a slushy layer. Flow turbulence near the surface and some cracking was observed under all conditions. The marbled crust that appeared with the inert shot was not present here.

5.4 Summary of Results

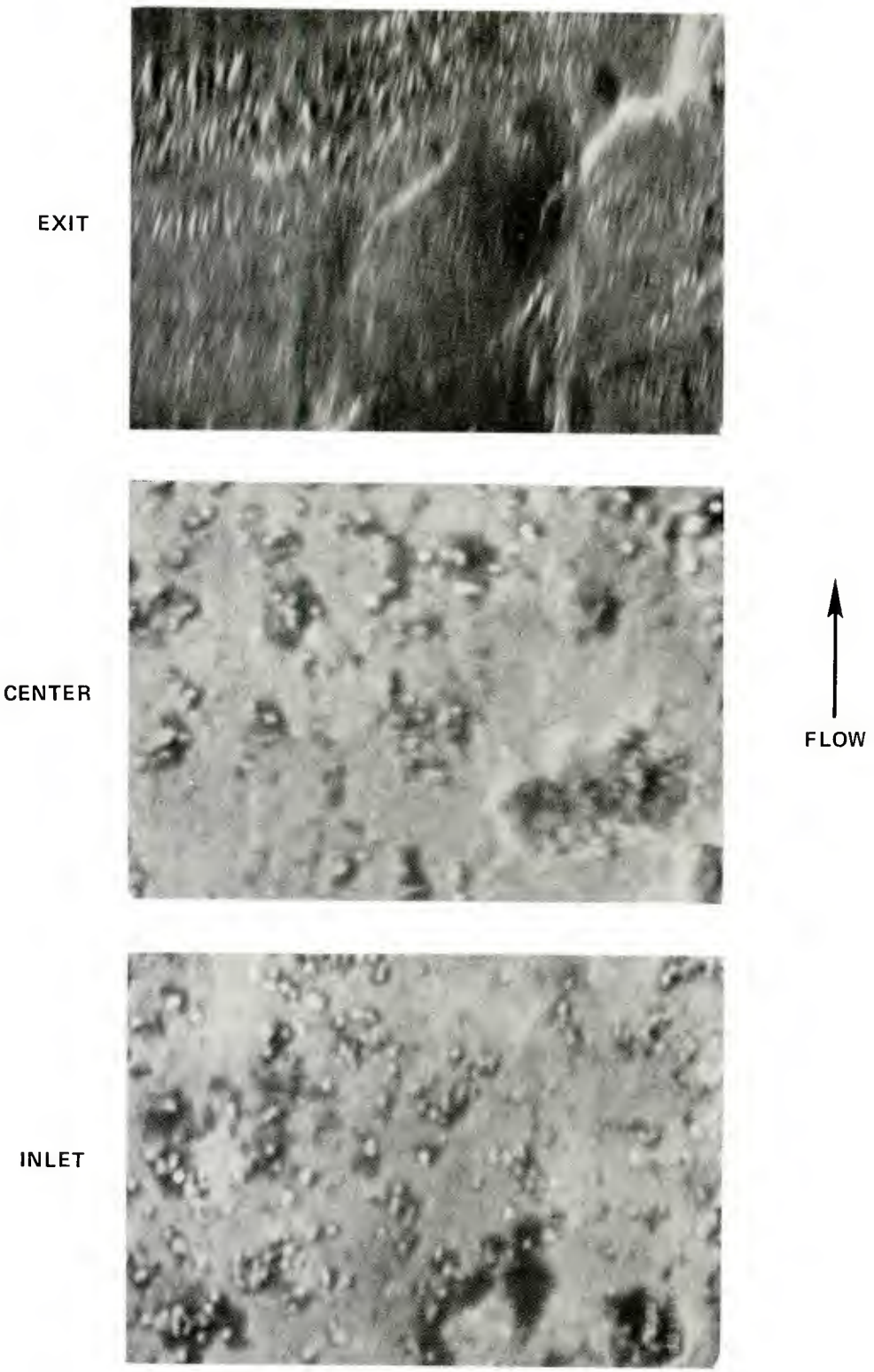
Carbon monoxide gas interacts chemically with a gun barrel wall within the time constraints of a ballistic cycle. Evidence of surface phenomena between CO and steel to support this statement are:

1. A shift in the onset of erosion due to the presence of carbon monoxide.
2. Enhancement of downstream erosion when carbon monoxide is a test gas constituent.
3. A change in surface characteristics of barrel steel when exposed to carbon monoxide rather than to nitrogen.

Several explanations for the short time CO-steel erosion mechanism are postulated. Simple carburization or diffusion of carbon atoms, into the steel surface would produce several effects. First, increased carbon concentration, present either as graphite or iron carbide, would reduce the solidus temperature of the steel as shown on the Iron-Carbon Equilibrium Diagram in Figure 28. Second, an increase in surface carbon concentration would reduce the thermal conductivity of the affected layer, causing it to experience an accelerated temperature rise. The elevated heat content of the affected layer would be further enhanced by the exothermic iron carbide (cementite) reaction between CO and iron, even when flow conditions started to become less severe.

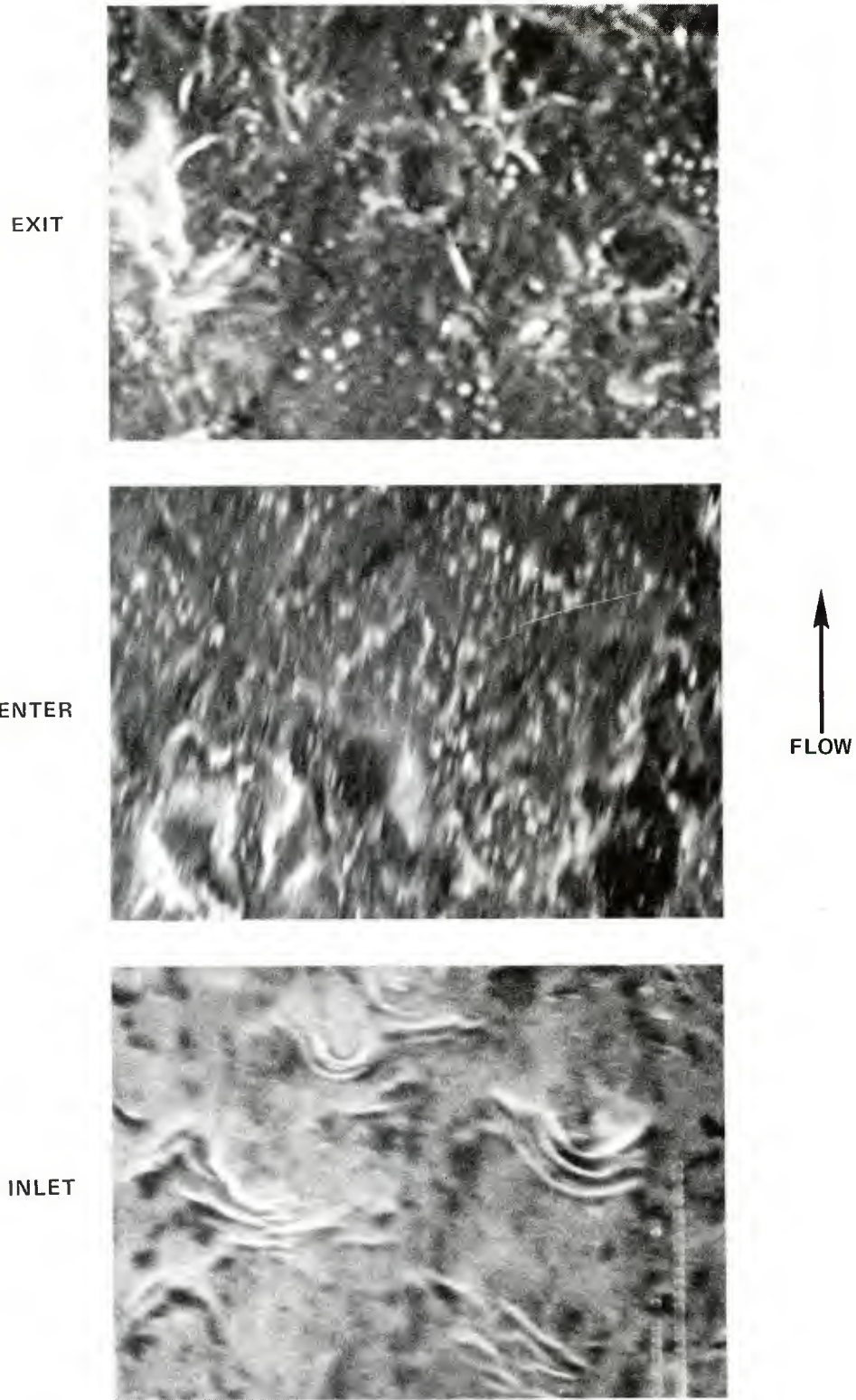
A second explanation of the CO-steel erosion mechanism, previously proposed,⁴ attributes increased heat input to the entire steel surface layer from the highly exothermic boundary layer reaction of carbon monoxide molecules and iron to form iron penta carbonyl, $\text{Fe}(\text{CO})_5$. To a lesser degree, carbon monoxide molecules may also be reacting with chromium and nickel, the chief alloying metals in barrel steel to produce equally volatile $\text{Cr}(\text{CO})_6$ and $\text{Ni}(\text{CO})_4$.

At the present time, metallographic examination of the 4340 steel samples, tested in this program, are being conducted at Government laboratories. It is anticipated that these additional examinations will shed light on the precise erosion mechanisms that can be linked to propellant gas atmospheres, rich in carbon monoxide.



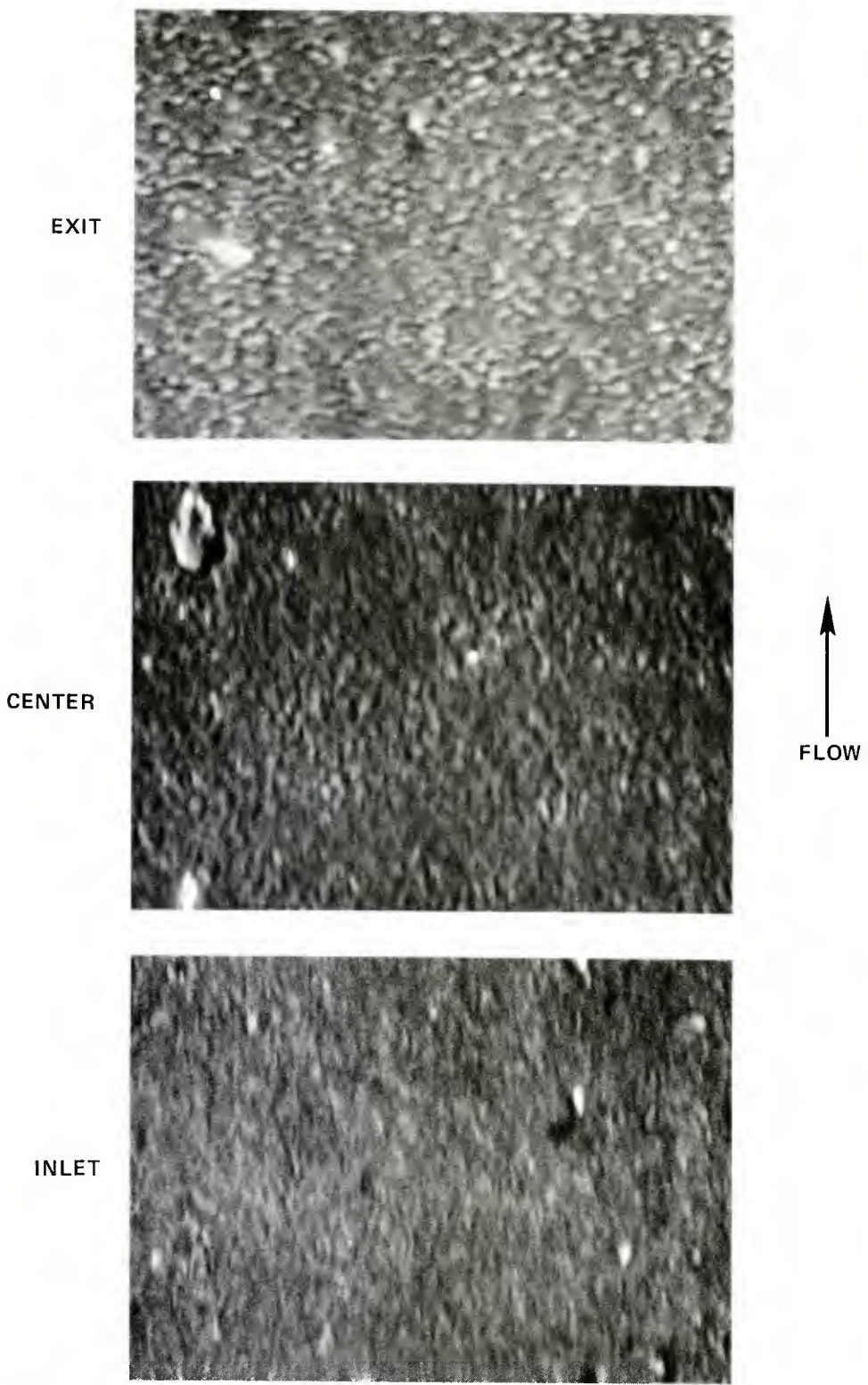
SAMPLE 38, RUN 72, 1000 MAGNIFICATION

Figure 12 4340 STEEL SAMPLE SURFACE TESTED IN AN
"INERT" ATMOSPHERE TO 223 MPa, 3422°K



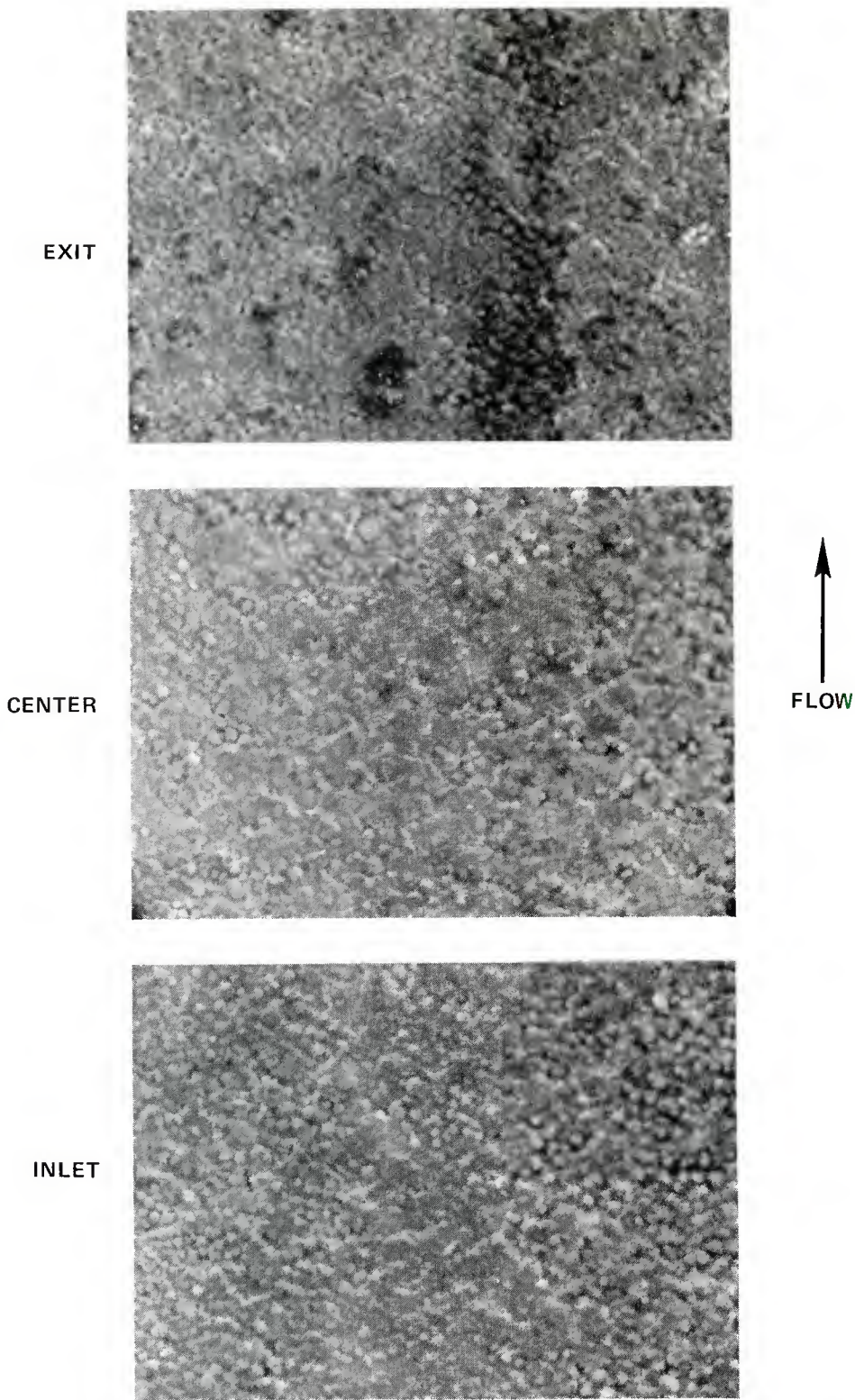
SAMPLE 39, RUN 73, 1000 MAGNIFICATION

Figure 13 4340 STEEL SAMPLE SURFACE TESTED IN AN
"INERT" ATMOSPHERE TO 248 MPa, 3531°K



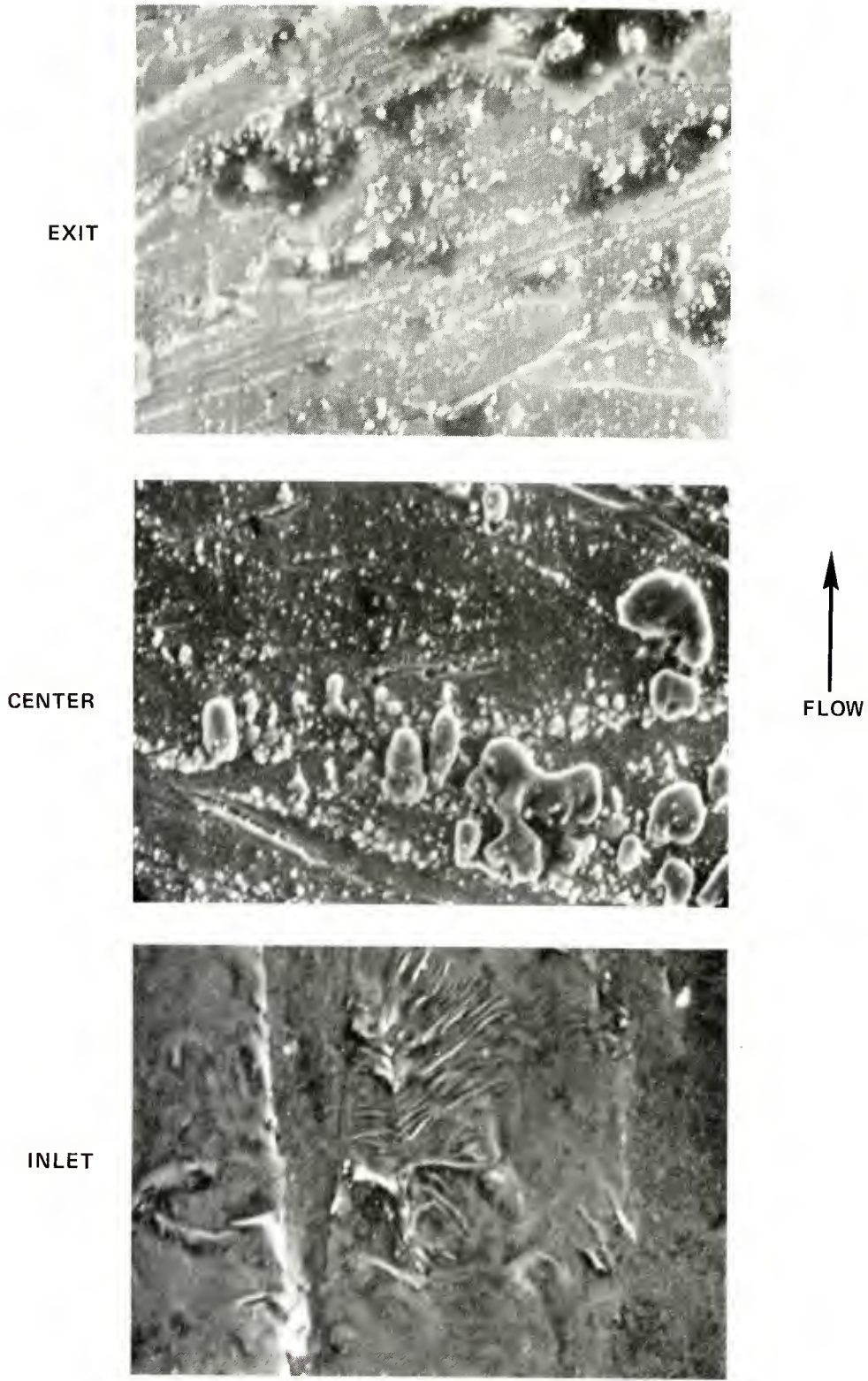
SAMPLE 41, RUN 75, 1000 MAGNIFICATION

Figure 14 4340 STEEL SAMPLE SURFACE TESTED IN AN
"INERT" ATMOSPHERE TO 285 MPa, 3678°K



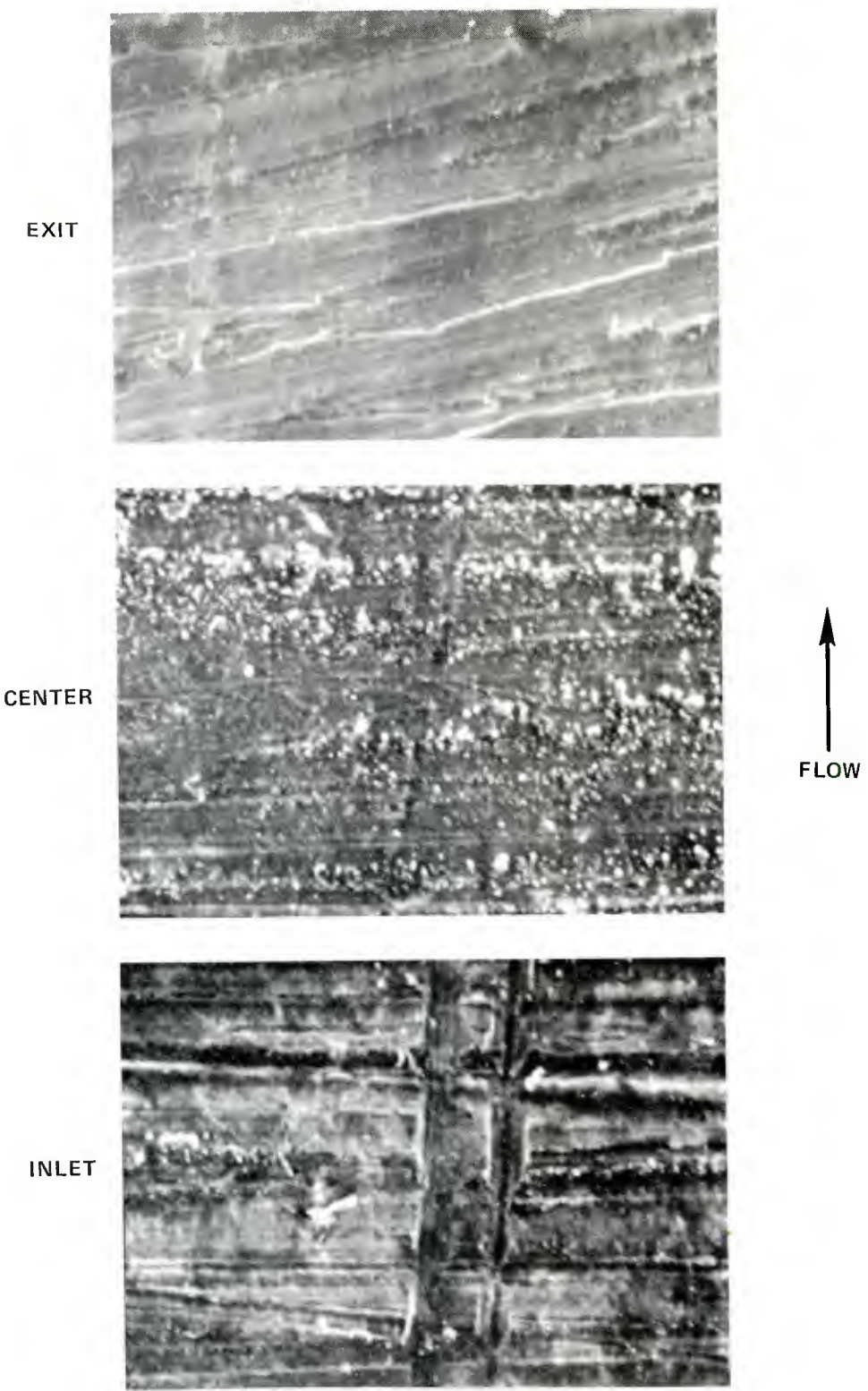
SAMPLE 42, RUN 77, 1000 MAGNIFICATION

Figure 15 4340 STEEL SAMPLE SURFACE TESTED IN AN
"INERT" ATMOSPHERE TO 335 MPa, 3865°K



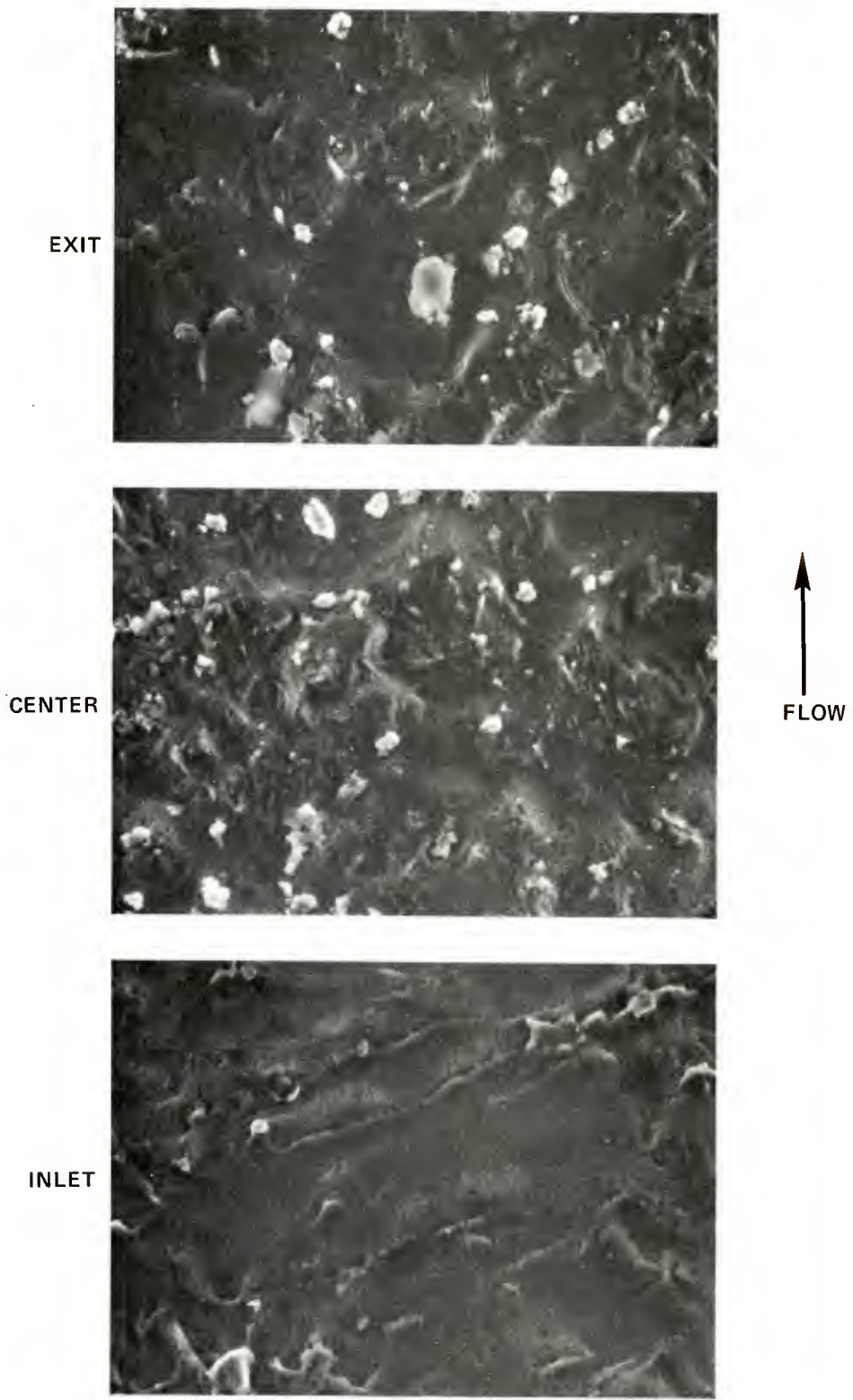
SAMPLE 45, RUN 81, 1000 MAGNIFICATION

Figure 16 4340 STEEL SAMPLE SURFACE TESTED IN A 45.5 PERCENT CARBON MONOXIDE ATMOSPHERE TO 213 MPa, 3322°K



SAMPLE 40A, RUN 82, 1000 MAGNIFICATION

Figure 17 4340 STEEL SAMPLE SURFACE TESTED IN A 45.5 PERCENT CARBON MONOXIDE ATMOSPHERE TO 216 MPa, 3338⁰K



SAMPLE 43, RUNS 78, 79, 1000 MAGNIFICATION

Figure 18 4340 STEEL SAMPLE SURFACE TESTED IN A 45.5 PERCENT CARBON MONOXIDE ATMOSPHERE TO 277 MPa, 3588⁰K AND 256 MPa, 3507⁰K

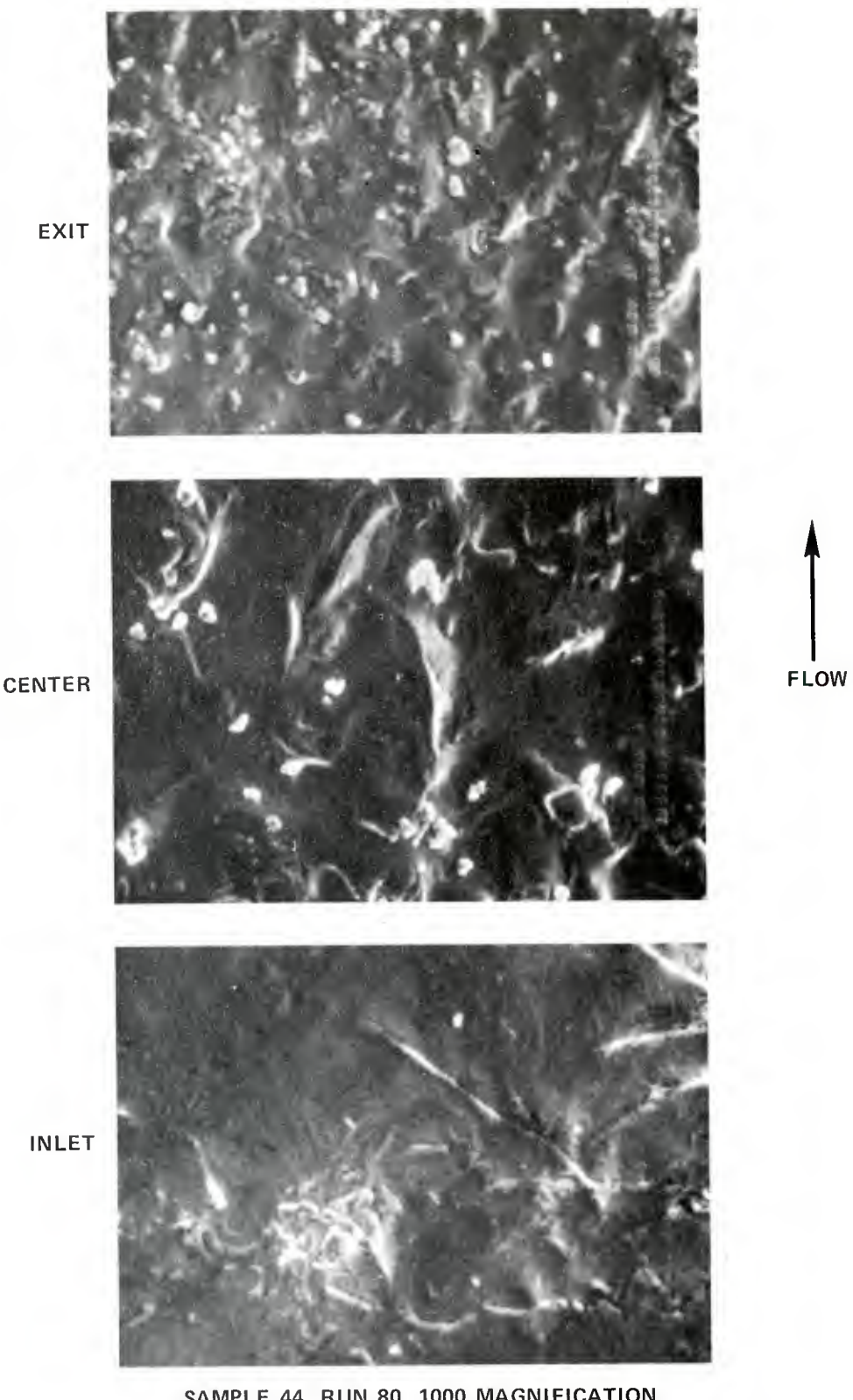
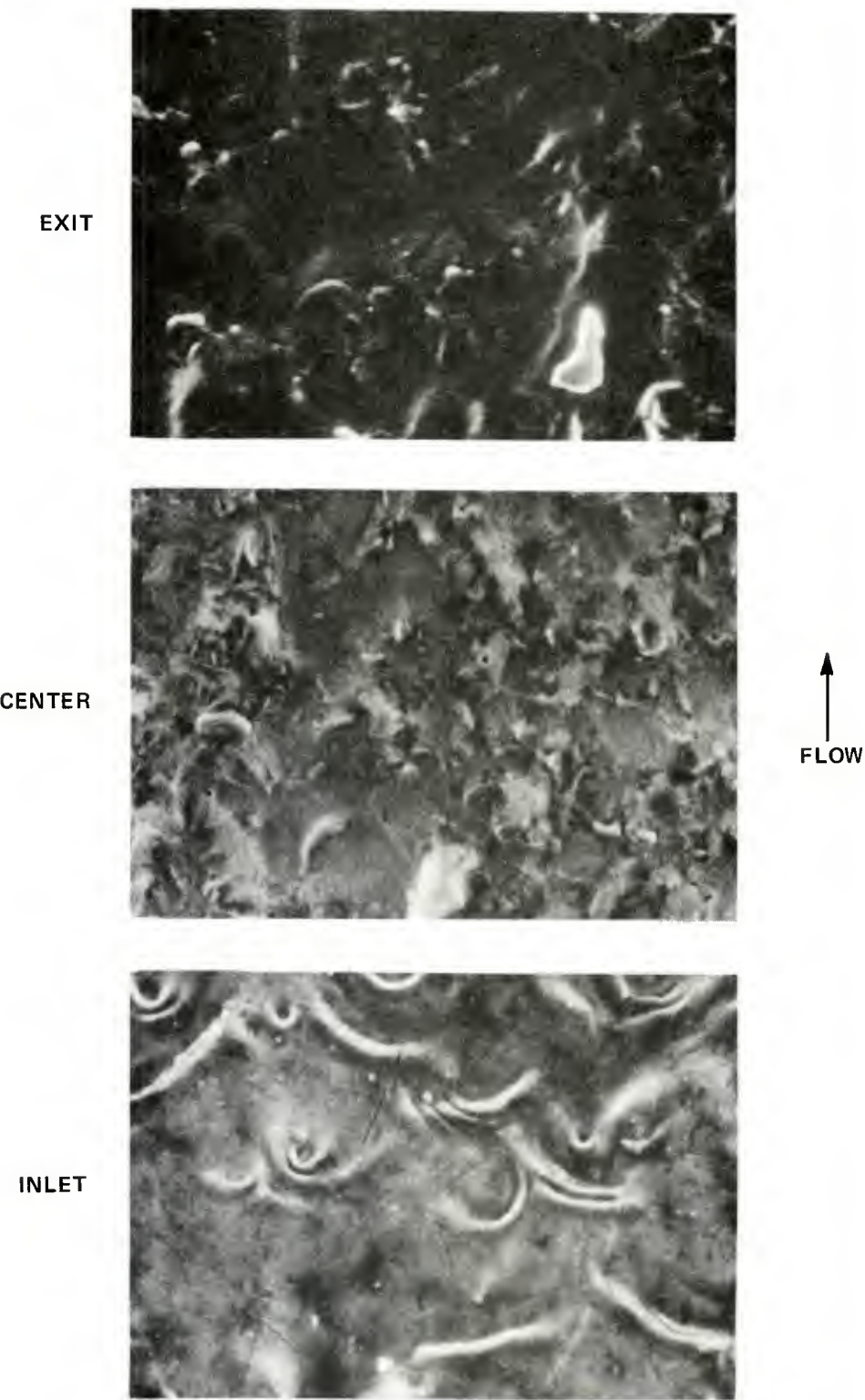
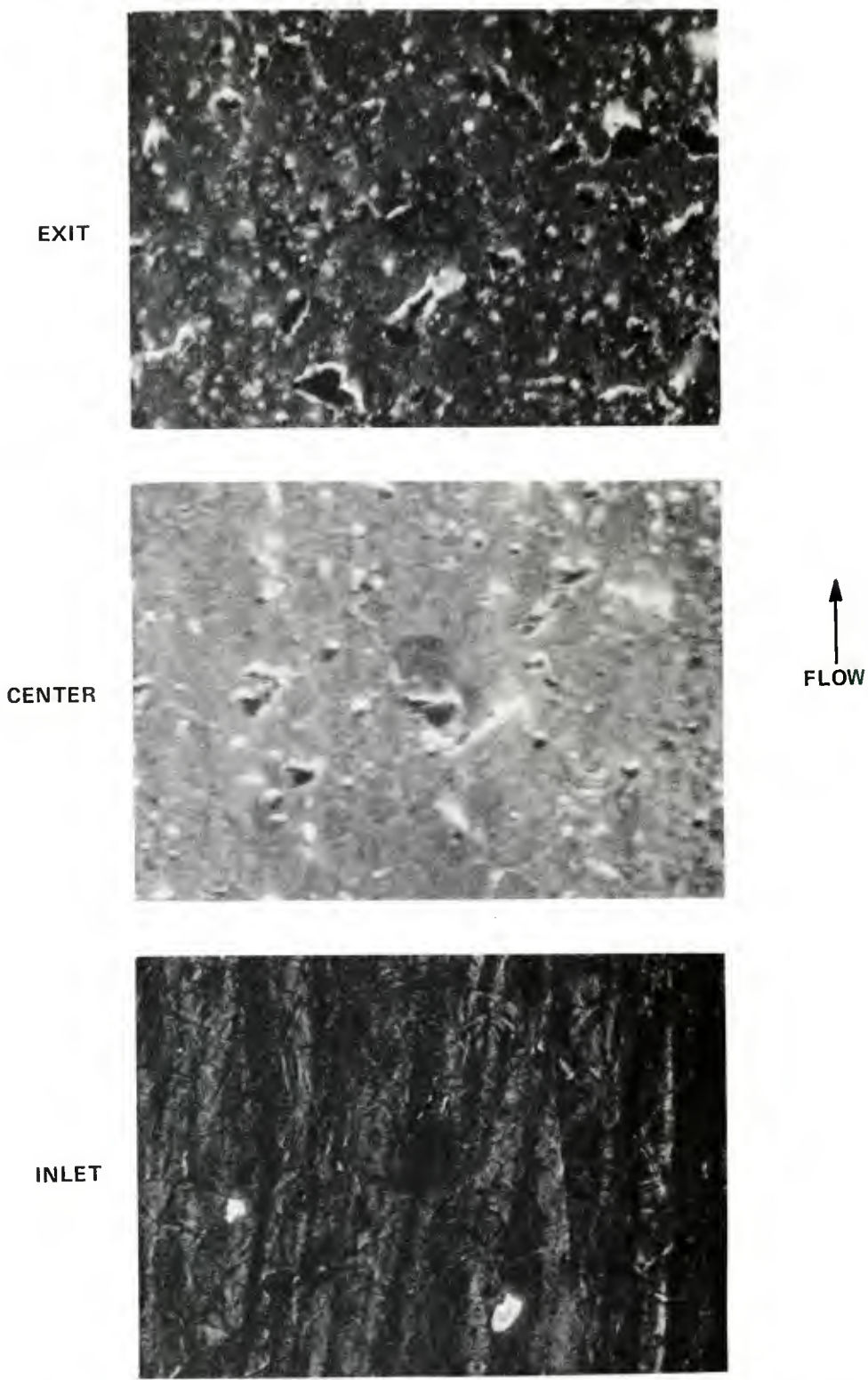


Figure 19 4340 STEEL SAMPLE SURFACE TESTED IN A 45.5 PERCENT CARBON MONOXIDE ATMOSPHERE TO 245 MPa, 3462°K



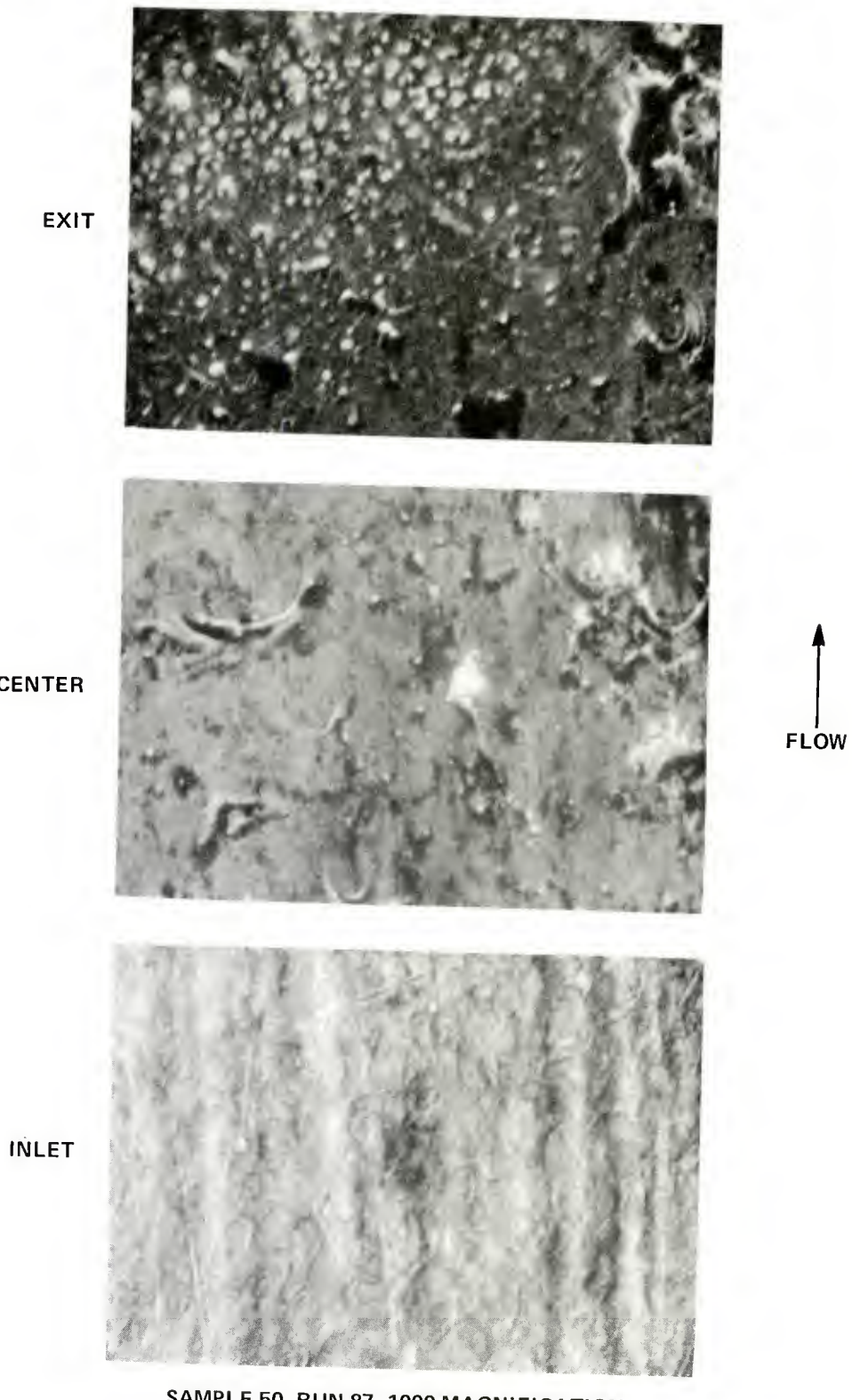
SAMPLE 46, RUN 83, 1000 MAGNIFICATION

Figure 20 4340 STEEL SAMPLE SURFACE TESTED IN A 40.5 PERCENT CARBON MONOXIDE ATMOSPHERE TO 299 MPa, 3690°K



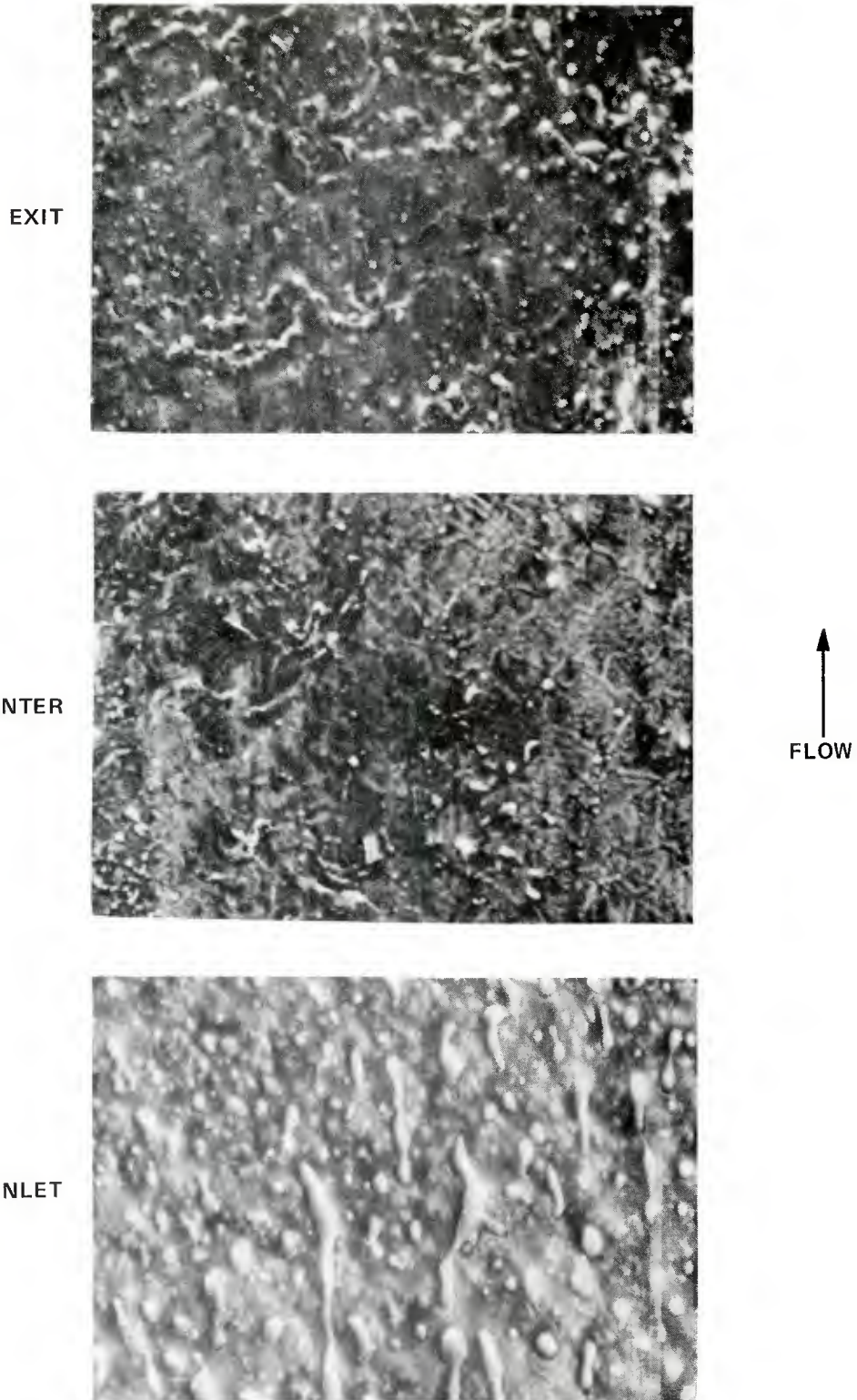
SAMPLE 49, RUN 86, 1000 MAGNIFICATION

Figure 21 4340 STEEL SAMPLE SURFACE TESTED IN A 25.5 PERCENT CARBON MONOXIDE ATMOSPHERE TO 281 MPa, 3637°K



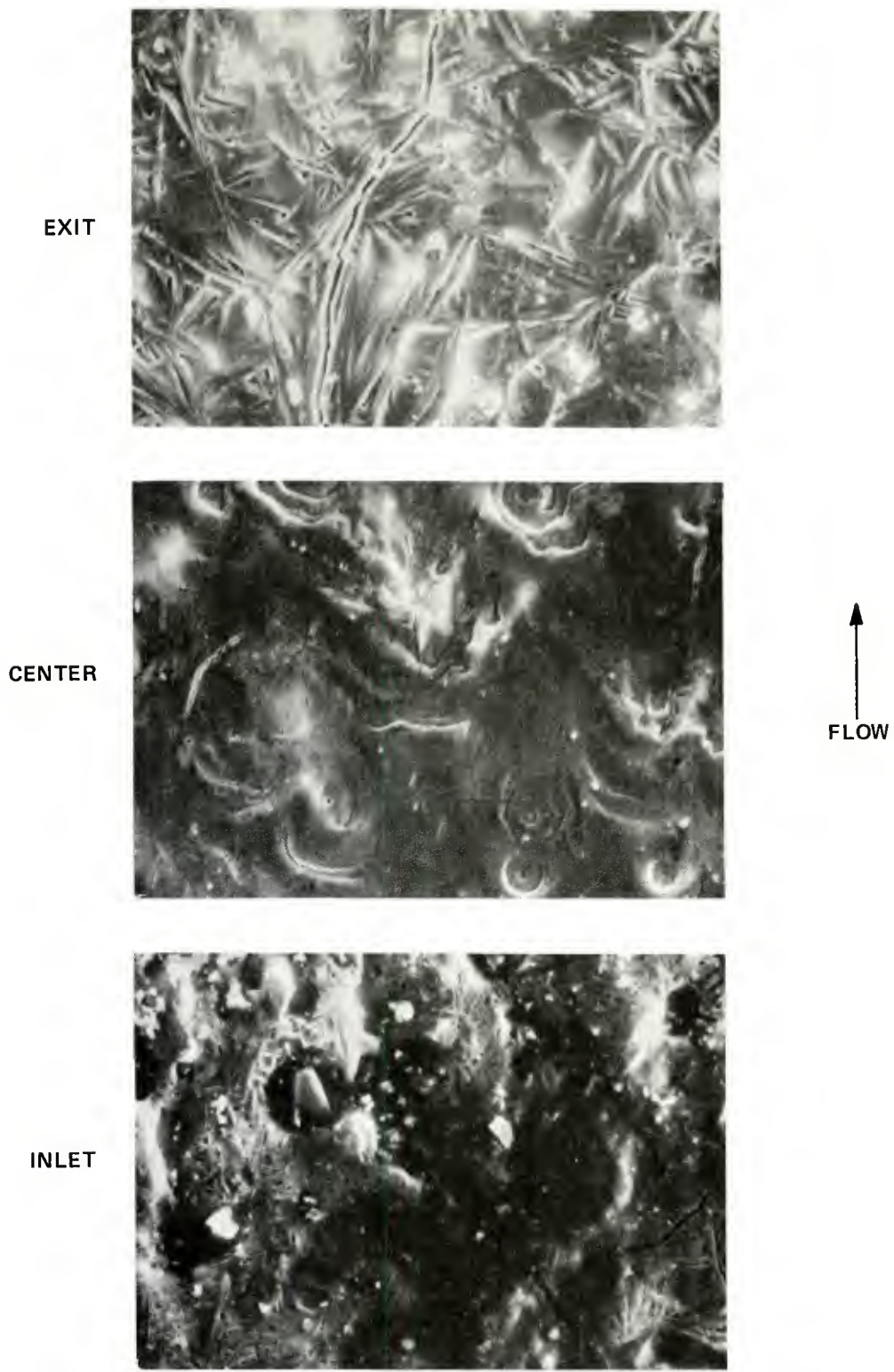
SAMPLE 50, RUN 87, 1000 MAGNIFICATION

Figure 22 4340 STEEL SAMPLE SURFACE TESTED IN A 20.5 PERCENT CARBON MONOXIDE ATMOSPHERE TO 287 MPa, 3665°K



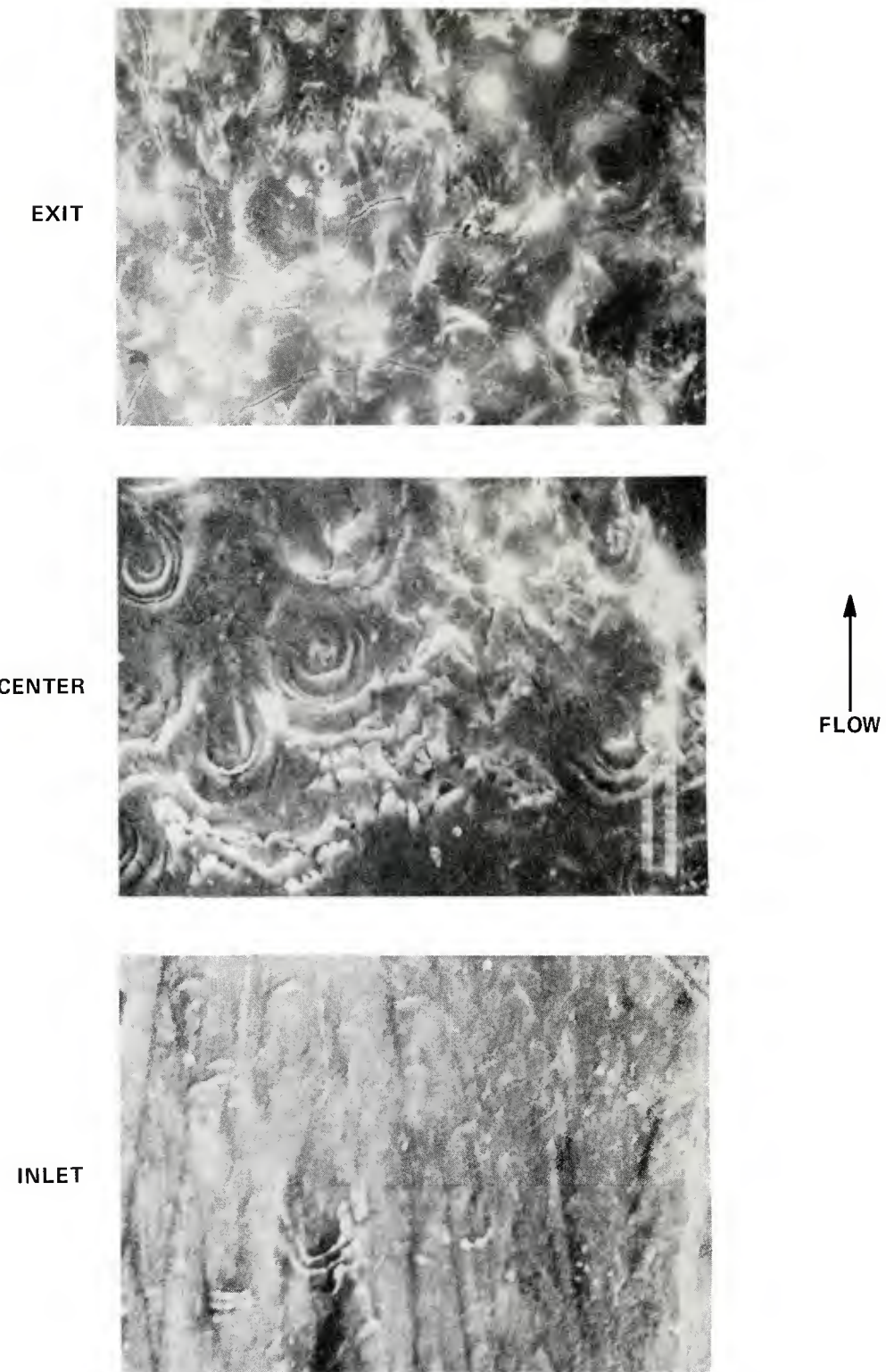
SAMPLE 51, RUN 88, 1000 MAGNIFICATION

Figure 23 4340 STEEL SAMPLE SURFACE TESTED IN A 15.5 PERCENT CARBON MONOXIDE ATMOSPHERE TO 288 MPa, 3673°K



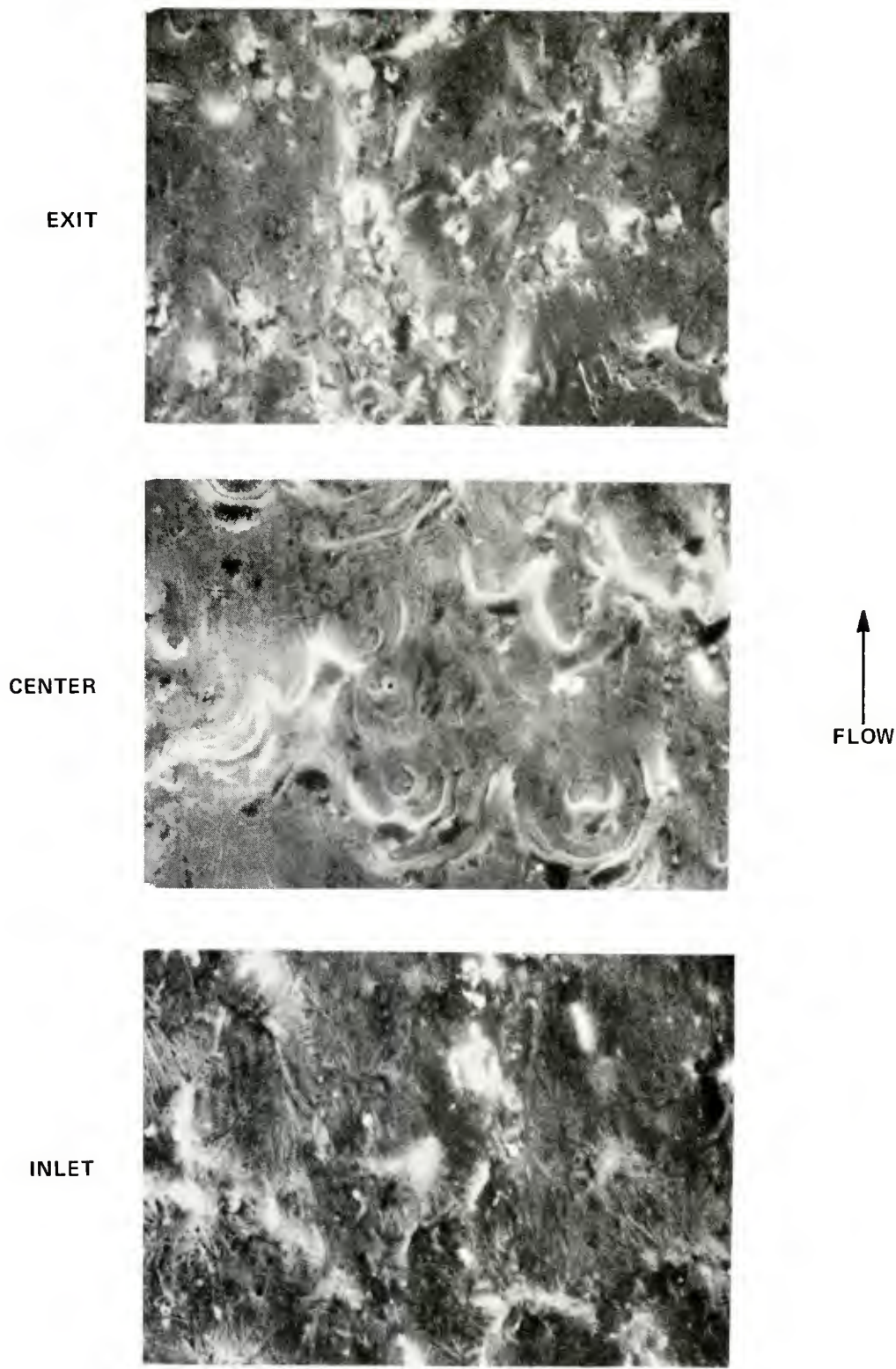
SAMPLE 52, RUN 89, 1000 MAGNIFICATION

Figure 24 4340 STEEL SAMPLE SURFACE TESTED IN A 45.5 PERCENT CARBON MONOXIDE ATMOSPHERE TO 250 MPa, 3479°K



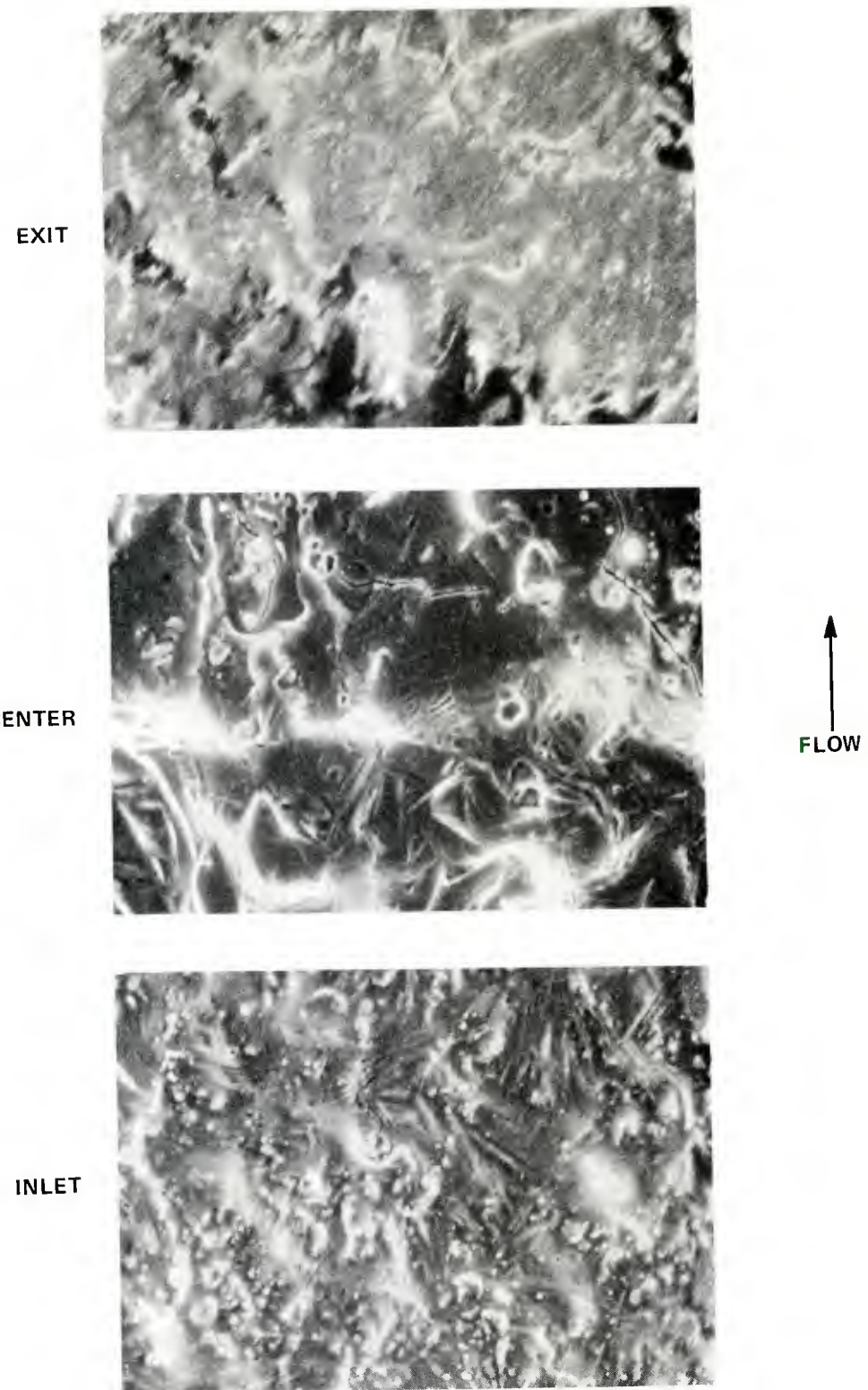
SAMPLE 54, RUN 91, 1000 MAGNIFICATION

Figure 25 4340 STEEL SAMPLE SURFACE TESTED IN A 45.5 PERCENT CARBON MONOXIDE ATMOSPHERE TO 236 MPa, 3422°K



SAMPLE 55, RUN 92, 1000 MAGNIFICATION

Figure 26 4340 STEEL SAMPLE SURFACE TESTED IN A 45.5 PERCENT CARBON MONOXIDE ATMOSPHERE TO 219 MPa, 3351°K



SAMPLE 57, RUN 94, 1000 MAGNIFICATION

Figure 27 4340 STEEL SAMPLE SURFACE TESTED IN A 45.5 PERCENT CARBON MONOXIDE ATMOSPHERE TO 201 MPa, 3268°K

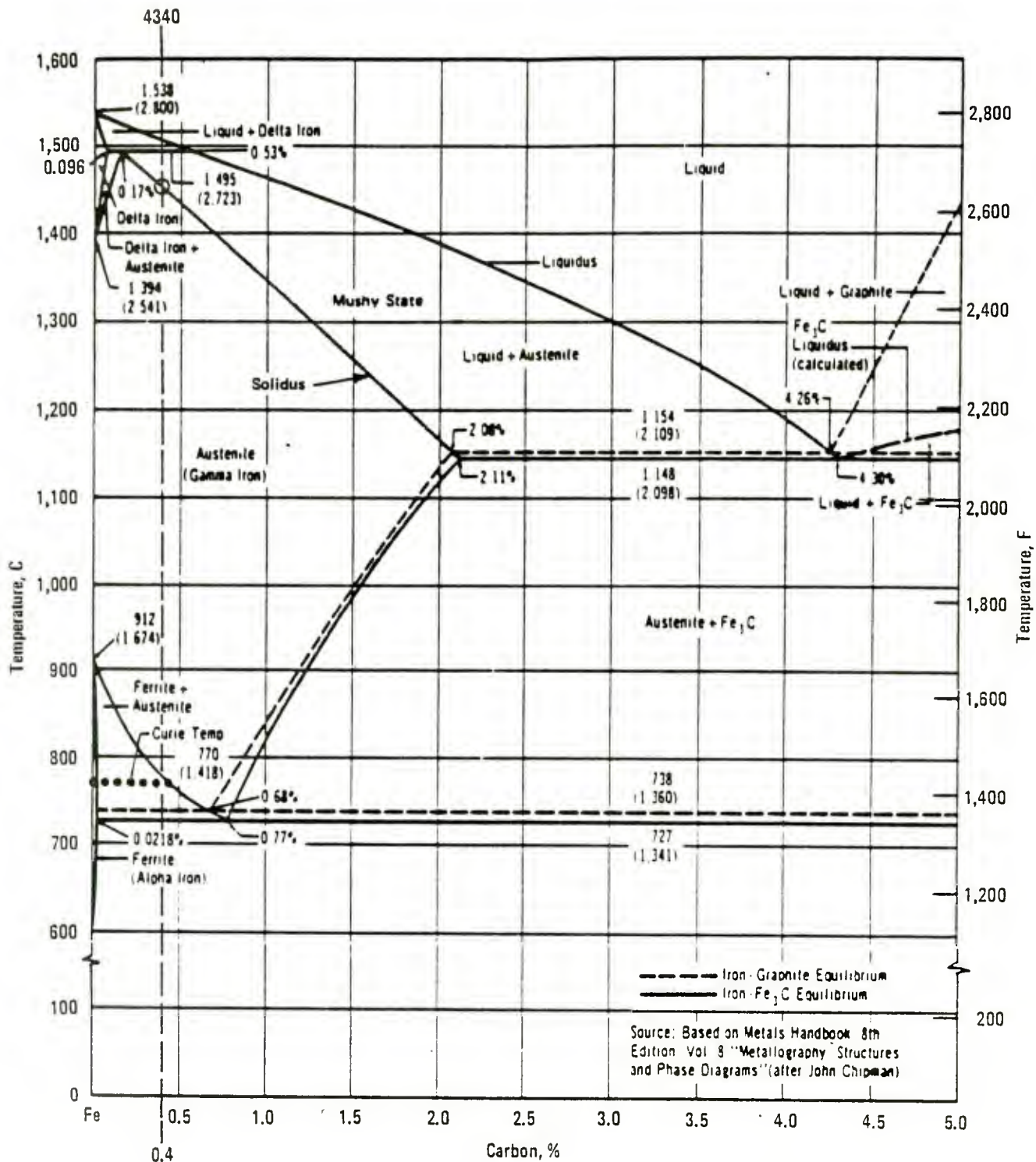


Figure 28 IRON-CARBON EQUILIBRIUM DIAGRAM

VI. CONCLUSIONS

This program is part of an ongoing effort to isolate the various phenomena that contribute to gun barrel erosion. Research dealing with erosion of 4340 steel in a carburizing atmosphere, the primary topic of investigation, led to the following conclusions:

1. Addition of carbon monoxide to the test gas mixture was shown to increase the erosion of 4340 steel.
2. The increase in erosion was nearly independent of carbon monoxide content which is indicative of reaction rate controlled carburization.
3. The addition of carbon monoxide shifted the erosion threshold to less severe flow conditions.
4. An inert gas mixture (45.5% N₂) produced no indication of surface melting at conditions comparable to the erosion threshold for a gas mixture containing 45.5 percent carbon monoxide. This indicates that carburization takes the form of a surface reaction.

VII. REFERENCES

1. F.A. Vassallo, "Mathematical Models and Computer Routines Used in Evaluation of Caseless Ammunition Heat Transfer," Calspan Report No. GM-2948-Z-1, June 1971.
2. E.B. Fisher, C.C. Morphy, "The Role of Oxygen in Gun Barrel Erosion and Cracking--A Shock Tube Gun Investigation," U.S. Army Ballistic Research Laboratory, ARRADCOM, Contract Report No. ARBRL-CR-00427, April 1980.
3. F.A. Vassallo, W.R. Brown, "Shock Tube Gun Melting Erosion Study," USA Ballistic Research Laboratory, ARRADCOM, Contract Report No. ARBRL-CR-00406, January 1979. (AD #A076219)
4. D.J. Taylor, J. Morris, "Gun Erosion and Methods of Control," Proceedings of the "Gun Tube Erosion and Control" Meeting, Watervliet Arsenal, Watervliet, N.Y., 25-26 February, 1970.

APPENDIX I

SHOCK TUBE GUN COMPUTER SIMULATION

Overview

The mathematical model described in this Appendix simulates the operation of the Shock Tube Gun. The simulation provides a complete description of the entire cycle of the Shock Tube Gun, beginning with release and subsequent acceleration of the piston by the high pressure driver gas. As the piston is accelerated through the driven tube, the simulation computes the increase in pressure and temperature of the test gas. In addition, the simulation evaluates the total temperature, pressure and density in the plenum chamber and computes the flow through the test specimen. The heat flux to the specimen, the resulting temperature history at a location on the surface of the specimen and the temperature distribution normal to the surface are also calculated. Finally, the simulation calculates the travel of a projectile through the barrel.

The objective of this code is to provide a means for calculating test conditions for the purpose of establishing the initial driver pressure and gas mixture. Differences in the ballistic cycle of the Shock Tube Gun due to gas composition are reflected through differences in pressure and total heat input. A primary use of the code is to help distinguish between erosion due to melting and that due to chemical effects. This is done through computation of the convective heating to the sample without chemistry which provides a means for comparing tests within a test matrix on an equal basis as far as the inherent flow heating of the test gas. Thus, excess material removal from one gas mixture in comparison to another is likely due to chemical effects. This further allows estimates to be made of the effective heat input due to chemical effects. This can be done by comparing the heat input at the onset of erosion, or at points of equal erosion between inert and chemically active gases. The code enables the facility user to quantify levels of heating experienced.

The major assumption applied with formulating the code was that of quasi-steady operation. That is, pressure waves and other unsteady aspects of the event are not calculated. The pressure is assumed to be constant throughout the driver system and throughout the driven tube at any instant of time during the compression cycle.

The other limiting assumption that is currently employed in this code is that of a frozen gas composition whereby the initial gas composition is assumed to be maintained throughout the ballistic cycle. This assumption influences the resulting temperature and pressures to some extent in cases where chemical reactions and dissociation become important.

The individual gas constituents are assumed to be mixed uniformly. Furthermore, the parameters used by the van der Waals equation of state for an imperfect gas and the temperature dependency of specific heat are assumed to be satisfied through a linear averaging according to mole fraction.

The assumption of frozen gas constituency is an interim assumption that will be relieved when a chemical equilibrium gas code, also discussed in this appendix, can be combined with the STG model. At that time, the gas constituency will be assumed to be in thermal and chemical equilibrium at all times. At present, the discrepancy between STG code calculations and actual STG test results, as illustrated in the figure below, can be attributed to both the quasi-steady limitations of the code and the inherent accuracy limitations of the test instrumentation.

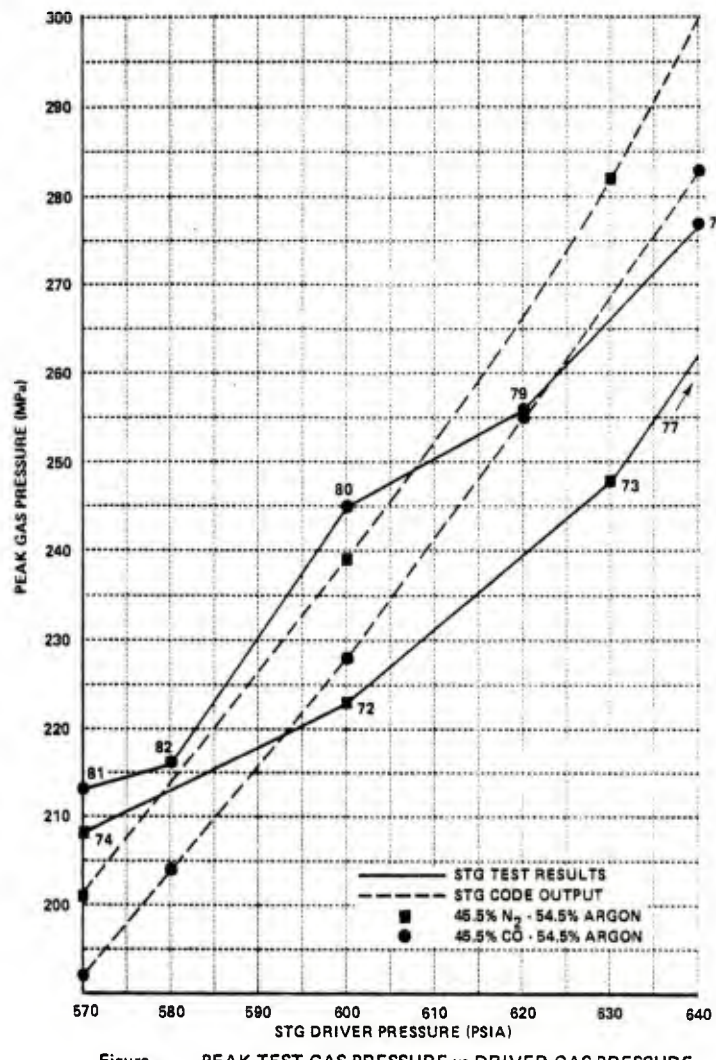


Figure 8 PEAK TEST GAS PRESSURE vs DRIVER GAS PRESSURE

Model Description

Piston Motion

The piston motion is evaluated by applying a force balance on the piston. The accelerating force is applied by the high-pressure nitrogen driver, 500 to 700 psi, on the upstream side of the piston. The driven gas on the downstream side of the piston is initially at atmospheric pressure. It is assumed that no gas leaks past the piston. This is essentially verified, at least initially, by the maintenance of a perfect seal and the ability to evacuate the driven gas chamber. The nitrogen gas is represented by the ideal gas equation of state. The driver conditions are calculated from conservation of energy principles which are used to continually evaluate the amount of energy that is being transferred from the gas to the piston. As cited previously, this calculation is quasi-steady in that the unsteady expansion aspects are not considered and the pressure is assumed to be constant throughout the driver system.

The driver gas (nitrogen) properties are assumed to be constant over the range of temperature and pressure encountered during the compression cycle and are specified by:

Equation of state gas constant, $R = 55.0 \text{ ft-lbf/lbm}^{\circ}\text{R}$

Specific heat at constant volume, $c_v = 0.177 \text{ Btu/lbm-}^{\circ}\text{R}$

Specific heat at constant pressure, $c_p = 0.248$, and

Ratio of specific heats, $\gamma = 1.4$

The assumption of a perfect seal at the piston infers the existence of constant gas mass in the driver system during the cycle so that

$$p_D = \frac{m_D RT}{V},$$

where R and m are constants, the driver volume, V, is expressed in terms of piston travel and the initial volume by

$$V = V_0 + A_T x_p,$$

where A_T is the driver tube area.

Gas temperature is expressed in terms of internal energy where

$$E = c_V m_D T$$

and the energy change resulting from work expended through piston motion is:

$$\Delta E = p_D A_T \Delta x_p / 778. = c_V m_D \Delta T$$

The driver gas is initially at room temperature and it is assumed that the small temperature decrease during the cycle is not influenced by heat transfer.

Piston motion is evaluated by applying a force balance across the piston, taking into account the frictional drag,

$$F = A_t (p_D - p_T) - D$$

where p_D and p_T are the respective pressures of the driver and test gases, and D is the frictional drag of the piston which is expressed in terms of piston velocity by:

$$D = k V_p$$

Piston acceleration, velocity and travel follow:

$$a_p = \frac{F}{m}$$

$$\Delta V_p = a_p \Delta t$$

$$\Delta x_p = \frac{a_p}{2} \Delta t^2 + v_0 \Delta t$$

Test Gas Compression

The compression of the test gas occurs as a result of piston motion. Energy that is added by virtue of the compression is calculated from the conservation of energy equation. The work done by the piston on the test gas during this compression is one term in this conservation of energy equation. Other terms include heat loss to the wall of the tube, which becomes important as the gas temperature rises. The other important equation is conservation of mass. The test chamber is not a closed chamber but contains

an exhaust port at the downstream end where the test sample is located. Thus, test gas is allowed to flow from the test chamber through the test sample. Therefore, the mass in the system is not constant by virtue of mass and energy flow from the driven tube and plenum chamber through the test sample. Terms in the conservation of energy and mass equations reflect this mass and energy loss.

The equation of state that applies to the test gas is the van der Waals equation which includes terms to express the nonlinear relationship between pressure density and temperature. The terms for this equation are determined, as mentioned previously, by a linear averaging of the mole fraction of the test gas constituents.

The test gas specific heat is also assumed to be for non-perfect gas and is expressed in terms of a linear function of the gas temperature. The coefficients in this expression are also linear averages of the mole fraction of the test gas compositions. The test gas specific heat is expressed in terms of a secant function in which the product of the specific heat and the temperature yield the internal energy. This is contrary to a normal expression of specific heat whereby it is a tangent function so that the integral of the product of specific heat and temperature yield the internal energy. The technique used here provides rather simple yet effective means for evaluating the internal energy in a finite difference scheme with many time steps.

The van der Waals equation of state used for the test gas is

$$p = \frac{RT}{v - \beta} + \frac{\alpha}{v^2}$$

where $\frac{\alpha_i}{\beta_1} = \frac{27}{8} RT_{ci}$, $\frac{\alpha_i}{\beta_1^2} = 27 p_{ci}$,

v is the specific volume, and T_{ci} and p_{ci} are the critical temperature and pressure for the i th gas constituent. α and β are the average quantities based on the mole fraction of the i th constituent.

The specific heat at constant volume is defined by

$$c_v = ((c_{vo} + \sum_i X_{gi} c_{vTi} (T - 460)^{e_i})T - \frac{\alpha_0}{778}) \frac{1}{T_i}$$

where c_{vo} and c_{vTi} are the intercept and slope of the temperature-dependent specific heat and X_{gi} is the mole fraction of the i th constituent.

which includes temperature and high density effects.

The test chamber mass balance is given by

$$m_T = m_{To} - \Delta m$$

where Δm is the mass flow through the test sample. Initially this flow is assumed to be negligible and the test chamber and barrel volumes are lumped together. When the projectile velocity exceeds 100 ft/sec, the calculation of flow through the test sample is initiated. This computation involves determination whether sonic or subsonic flow conditions exist within the test sample. The sonic static pressure is given by:

$$p^* = p_1 \left(1 + \frac{\gamma - 1}{2}\right)^{-\gamma/\gamma - 1}$$

where p_1 is the test chamber pressure.

If p^* is greater than the barrel pressure, p_2 , (downstream from the test sample) then sonic conditions exist and

$$\Delta m = p^* A_{12} \left(\frac{\gamma g}{RT^*}\right)^{1/2} \Delta t,$$

where A_{12} is the test sample flow area, T^* is the sonic static temperature, and Δt is the computation time interval.

If subsonic conditions exist,

$$\Delta m = 8.02 A_{12} \left((p_1 - p_2) \frac{\rho_1}{RT_1}\right)^{1/2} \Delta t,$$

where is the equation for flow through a venturi in terms of the upstream and downstream line pressures.

The change in internal energy in the chamber over the calculation time interval is given by

$$\Delta E_1 = \frac{p_1 A_T \Delta x_p}{778} - c_V \Delta m T_1 \gamma$$

which represents the compression work due to the piston and the loss in enthalpy due to flow through the test sample. Heat transfer losses in the driven tube and chamber are not included in this analysis at present. The gas chamber temperature is defined by

$$T_1 = E_1 / c_V m_1$$

where E_1 is the current value of internal energy.

The Test Sample

The test sample is a straight channel with a radiused entrance. The flow through the channel is computed by either sonic or subconic conditions depending on the pressure at the inlet and outlet to the sample. The calculations provide the static flow conditions of pressure, temperature, and density in addition to the flow velocity over the surface of the sample. These conditions are in turn used in the equation that expresses turbulent heat flux to a flat plate. The heat flux is computed and then summed to yield a current level of total heat input. The heat flux to the surface is also applied to an unsteady heat conduction routine by which the surface temperature and the temperature distribution in the test sample are evaluated. These calculations are all performed within the same time step of the overall finite difference calculation.

The technique used to calculate heat flux to the test sample surface requires the flow velocity, density, and viscosity. The density and viscosity are evaluated on the basis of a reference temperature to take the temperature profile resulting from the boundary layer velocity distribution and sample surface temperature into account.

Mach number of flow through the test sample:

$$M = \left[\left(\frac{p_1}{p_s} \right)^{\frac{\gamma - 1}{\gamma}} - 1 \right] \frac{2}{\gamma - 1}^{1/2}$$

where p_s is the sonic static pressure if $M = 1$ or the downstream pressure, p_2 if the flow is subsonic.

Free stream static temperature:

$$T_e = T_1 \left(1 + \left(\frac{\gamma - 1}{2} \right) M^2 \right)^{-1}$$

Free stream velocity:

$$U_e = [5 \times 10^4 \gamma C_V (T_1 - T_e)]^{1/2}$$

Reference temperature:

$$T_{ref} = (T_e + T_{SAMP})/2 + 4.4 \times 10^{-6} \frac{U_e^2}{C_V \gamma}$$

where T_{SAMP} is the test sample surface temperature.

Viscosity:

$$\mu = 7.0 \times 10^{-7} T_{ref}^{1.5} (T_{ref} + 198)^{-1}$$

Density:

$$\rho_{ref} = P_S (\beta P_S + RT_{ref})^{-1}$$

Turbulent flat plate heat flux at the location of the in-wall thermocouple:

$$Q = 0.052 (\rho_{ref} U_e)^{0.8} \mu^{0.2} c_v \gamma (T_1 - T_{SAMP})$$

The sample surface temperature is determined from the one-dimensional unsteady state heat conduction equation,

$$\frac{\partial T}{\partial t} = \alpha \frac{\partial^2 T}{\partial x^2}$$

with the surface boundary condition,

$$Q = K \frac{dT}{dx}$$

for $x = 0$, where Q is the heat flux to the sample surface. This equation does not consider the effects of cylindrical geometry.

A finite difference technique using a geometrical node grid spacing was incorporated into the Calspan code to solve the unsteady heat conduction equation. The general finite difference relationship is given by

$$\frac{\Delta T_i}{\Delta t} = \frac{2\alpha}{(F+1)\Delta x_{i-1}^2} (T_{i-1} - \frac{F+1}{F} T_i + \frac{1}{F} T_{i+1})$$

where α is the thermal diffusivity

T is the temperature rise

t is the time interval

Δx_{i-1} is the thickness of the $i-1$ st grid

F is the geometrical multiplier with the thickness of the i th grid being F times that of the $i-1$ st grid.

The exposed surface boundary condition is satisfied by first determining a fictitious temperature in free space,

$$T_o = 2q \frac{\Delta x_1}{K} + T_2$$

This temperature is then used to establish the surface temperature rise by

$$\frac{\Delta T_1}{\Delta t} = \frac{\alpha}{\Delta x_1^2} (T_o - 2T_1 + T_2)$$

Barrel Flow

The flow through the barrel is expressed as an input of mass and energy to the volume between the test sample and the projectile. As mass and energy are accumulated, this is expressed in terms of pressure and temperature, which in turn provides the accelerating force for the projectile. In this calculation, the quasi-steady assumption of the previous calculation is relaxed by allowing pressure acting on the base of the projectile to be modified according to the Mach number of the flow at the base of the projectile. In this way, the unsteady expansion effects of the flow through the barrel is taken into account. The equation of state and the basic energy and mass conservation equations are the same as for the test gas in the driven tube. These equations are used to define "2" conditions in the barrel.

Projectile motion is calculated by an approximate technique that involves determination of the flow Mach number at the projectile base.

Specific enthalpy:

$$H_2 = \frac{E_2 \gamma}{M_g}$$

where M_g is the mass of gas contained in the barrel.

Static enthalpy at the projectile base:

$$H_{2_\infty} = 2.5 \times 10^4 H_2 - \frac{V_p^2}{2}$$

where V_p is the projectile velocity

Mach number:

$$M = V_p \{(\gamma - 1) H_{2_\infty}\}^{-1/2}$$

The assumption is made that the pressure, p_2 , is not the total pressure, but is a static pressure at the barrel origin.

It is further assumed that the difference in pressure between this location and the projectile base is equal to the difference between the pressure and the total pressure. This is expressed as a Mach number function:

$$\frac{p_{2_\infty}}{p_2} = \frac{\frac{p}{2} - \Delta p}{\frac{p}{2} + \Delta p} = \left(1 + \frac{\gamma-1}{2} M^2\right)^{-\gamma/\gamma-1}$$

This allows the static pressure at the projectile base to be expressed in terms of the barrel origin pressure, p_2 .

From this the projectile acceleration:

$$a_{pr} = 32.2 (p_{2_\infty} - p_r) / W_p$$

where p_r is the projectile resistance to motion, and W_p is the projectile weight, with $p_r = p_{r_o} + p_{r_x} x_{pr}$.

Projectile velocity change:

$$\Delta V_{pr} = a_{pr} \Delta t$$

Projectile displacement:

$$\Delta X_{pr} = V_{pr} \Delta t + a_{pr} \frac{\Delta t^2}{2}$$

```

C
C
C LIST OF CONSTANTS AND VARIABLES USED IN THIS SHOCK TUBE GUN PROGRAM
C
C DRIVER GAS PARAMETERS
C PCH      INITIAL DRIVER GAS PRESSURE - MPA
C T0       INITIAL DRIVER GAS TEMPERATURE - K
C VOL0     INITIAL DRIVER GAS VOLUME - M**3
C RDVR    DRIVER GAS CONSTANT - J/KG-K
C CVDVR   DRIVER GAS SPECIFIC HEAT - J/KG-K
C
C PISTON PARAMETERS
C AT       PISTON FACE AREA - M**2
C KP1      PISTON DRAG RATE CONSTANT - N/M
C VELP     INITIAL PISTON VELOCITY - M/SEC
C WSHELL   PISTON MASS - KG
C SHELRV   PISTON MASS DURING RETURN - KG
C XPMAX    MAXIMUM PISTON DISPLACEMENT - M
C
C TEST GAS PARAMETERS
C P20      INITIAL TEST GAS PRESSURE - MPA
C T20      INITIAL TEST GAS TEMPERATURE - K
C R2       TEST GAS CONSTANT - J/KG-K
C CV2      STANDARD TEST GAS SPECIFIC HEAT - J/KG-K
C CVT2     COMPUTED TEST GAS SPECIFIC HEAT - J/KG-K
C CVEXP    EXPONENT FOR COMPUTING SPECIFIC HEAT OF TEST GAS AT T1
C ALFA2    VAN DER WAALS CONSTANT - MPA-M**3/(KG-MOL)**2
C BETA2    VAN DER WAALS CONSTANT - M**3/KG-MOL
C GAM2     TEST GAS RATIO OF SPECIFIC HEATS
C
C TEST VOLUME PARAMETERS
C A2       TEST VOLUME AREA - M**2
C CD2      TEST VOLUME EXIT FLOW COEFFICIENT
C DOR12    TEST SAMPLE FLOW CHANNEL DIAMETER - M
C VOL1F    TEST GAS COLLECTION CHAMBER VOLUME - M**3
C VOL20    INITIAL TEST GAS VOLUME - M**3
C VOL2F    FINAL TEST GAS VOLUME - M**3
C
C PROJECTILE PARAMETERS
C BARL    BARREL LENGTH - M
C BORED   BORE DIAMETER - M
C PSTART  PRESSURE ABOVE WHICH PROJECTILE IS ALLOWED TO MOVE - MPA
C RES0    Y-INTERCEPT OF PROJECTILE RESISTANCE FUNCTION - N
C RESS    SLOPE OF PROJECTILE RESISTANCE FUNCTION - N/M
C RESC    STEADY-STATE PROJECTILE RESISTANCE - N
C VPROJ   INITIAL PROJECTILE VELOCITY - M/SEC
C XPROJ   INITIAL PROJECTILE DISPLACEMENT - M
C WPROJ   PROJECTILE MASS - KG
C
C TIME PARAMETERS
C DELT    TIME INCREMENT - SEC
C PRCI    DELT MULTIPLIER FOR PRINT INTERVAL
C TFO     LIMITING TIME - SEC
C
C
C

```

```

100 FORMAT (8F10.5)
101 FORMAT (I1)
102 FORMAT (F5.2,5A3,6E10.3)
103 FORMAT (12H1 INPUT DATA,T48,'TEST NO.',T57,I1)
104 FORMAT (///T6,'TEST GAS MIXTURE BY MOLE FRACTION'//)
105 FORMAT (/T6,F6.3,T17,5A3)
110 FORMAT (///T6,'INITIAL CONDITIONS FOR TEST')
120 FORMAT (///T7,'PCH =',T16,F12.5,T29,'PSF',T48,'P20 =',T57,F12.5,
+T70,'PSF',T90,'AT =',T99,F12.5,T112,'FT**2'//T7,'T0 =',T16,F12.5,
+T29,'R',T48,'T20 =',T57,F12.5,T70,'R',T90,'KP1 =',T99,F12.5,T112,
+'LBF/FT'//T7,'VOLO =',T16,F12.5,T29,'FT**3',T48,'R2 =',T57,F12.5,
+T70,'FT-LBF/LBM-R',T90,'VELP =',T99,F12.5,T112,'FT/SEC'//T7,
+'RDVR =',T16,F12.5,T29,'FT-LBF/LBM-R',T48,'CV2 =',T57,F12.5,T70,
+'BTU/LBM-R',T90,'WSHELL =',T99,F12.5,T112,'LBM'//T7,'CVDVR =',T16,
+F12.5,T29,'BTU/LBM-R',T48,'CVT2 =',T57,F12.5,T70,'BTU/LBM-R',T90,
+'SHELRV =',T99,F12.5,T112,'LBM'//T48,'CVEXP =',T57,F12.5,T90,
+'XPMAX =',T99,F12.5,T112,'FT'//T7,'BARL =',T16,F12.5,T29,'FT',T48,
+'ALFA2 =',T57,F12.5,T70,'PSF-FT**3/(LB-MOL)**2'//T7,'BORED =',T16,
+F12.5,T29,'FT',T48,'BETA2 =',T57,F12.5,T70,'FT**3/LB-MOL',T90,
+'A2 =',T99,F12.5,T112,'FT**2'//T7,'PSTART =',T16,F12.5,T29,'PSF',
+T48,'GAM2 =',T57,F12.5,T90,'CD2 =',T99,F12.5//T7,'RESO =',T16,
+F12.5,T29,'LBF',T90,'DOR12 =',T99,F12.5,T112,'FT'//T7,'RESS =',
+T16,F12.5,T29,'LBF/FT',T48,'DELT =',T57,F12.5,T70,'SEC',T90,
+'VOL1F =',T99,F12.5,T112,'FT**3'//T7,'RESC =',T16,F12.5,T29,'LBF',
+T48,'PRCI =',T57,F12.5,T90,'VOL20 =',T99,F12.5,T112,'FT**3'//T7,
+'WPROJ =',T16,F12.5,T29,'LBM',T48,'TFO =',T57,F12.5,T70,'SEC',T90,
+'VOL2F =',T99,F12.5,T112,'FT**3'//T7)
130 FORMAT (//T7,'PCH =',T16,F12.5,T29,'MPA',T48,'P20 =',T57,F12.5,
+T70,'MPA',T90,'AT =',T99,F12.5,T112,'M**3'//T7,'T0 =',T16,F12.5,
+T29,'K',T48,'T20 =',T57,F12.5,T70,'K',T90,'KP1 =',T99,F12.5,T112,
+'N/M'//T7,'VOLO =',T16,F12.5,T29,'M**3',T48,'R2 =',T57,F12.5,T70,
+'J/KG-K',T90,'VELP =',T99,F12.5,T112,'M/SEC'//T7,'RDVR =',T16,
+F12.5,T29,'J/KG-K',T48,'CV2 =',T57,F12.5,T70,'J/KG-K',T90,
+'WSHELL =',T99,F12.5,T112,'KG'//T7,'CVDVR =',T16,F12.5,T29,
+'J/KG-K',T48,'CVT2 =',T57,F12.5,T70,'J/KG-K',T90,'SHELRV =',T99,
+F12.5,T112,'KG'//T48,'CVEXP =',T57,F12.5,T90,'XPMAX =',T99,F12.5,
+T112,'M'//T7,'BARL =',T16,F12.5,T29,'M',T48,'ALFA2 =',T57,F12.5,
+T70,'MPA-M**3/(KG-MOL)**2'//T7,'BORED =',T16,F12.5,T29,'M',T48,
+'BETA2 =',T57,F12.5,T70,'M**3/KG-MOL',T90,'A2 =',T99,F12.5,T112,
+'M**2'//T7,'PSTART =',T16,F12.5,T29,'MPA',T48,'GAM2 =',T57,F12.5,
+T90,'CD2 =',T99,F12.5//T7,'RESO =',T16,F12.5,T29,'N',T90,
+'DOR12 =',T99,F12.5,T112,'M'//T7,'RESS =',T16,F12.5,T29,'N/M',T48,
+'DELT =',T57,F12.5,T70,'SEC',T90,'VOL1F =',T99,F12.5,T112,'M**3'//
+T7,'RESC =',T16,F12.5,T29,'N',T48,'PRCI =',T57,F12.5,T90,
+'VOL20 =',T99,F12.5,T112,'M**3'//T7,'WPROJ =',T16,F12.5,T29,'KG',
+T48,'TFO =',T57,F12.5,T70,'SEC',T90,'VOL2F =',T99,F12.5,T112,
+'M**3'//T7)
187 FORMAT (18H1 TABULATED OUTPUT)
188 FORMAT(///T6,'TIME',T20,'P1',T34,'T1',T48,'M1',T62,'VOL1',T76,'VEL
+P',T90,'VPROJ',T104,'WORK',T118,'QFLUX'/T6,'PCH',T20,'P2',T34,'T2'
+,T48,'M2',T62,'VOL2',T76,'XP',T90,'XPROJ',T104,'UE',T118,'QTOT'/
+T4,'TSAMP(1)',T18,'TSAMP(2)',T32,'TSAMP(3)',T46,'TSAMP(4)',
+T60,'TSAMP(5)',T74,'TSAMP(6)',T88,'TSAMP(7)',T102,'TSAMP(8)',
+T116,'TSAMP(9)'//)
190 FORMAT(9E14.6/9E14.6/9E14.6//)

```

C
C
C

```

READ (5,101) NUMBER
DO 99 NM=1,NUMBER
DIMENSION RG(9),CVG(9),CVTG(9),CVEXP(9),ALFAG(9),BETAG(9),XG(9)
DIMENSION G1(9),G2(9),G3(9),G4(9),G5(9)
DIMENSION TNEW(40),TSAMP(40),DELX(40),DXNEW(40),DTEMP(40)
DIMENSION TSAMPM(40)
REAL*4 KP1,M1,M2,M20
REAL*4 KP1M,M1M,M2M,M20
DATA VOL0/31.5/,CVDVR/0.176/,RDVR/55.2/
DATA AT/0.3068/,WSHELL/150.0/,SHELRV/150.0/,XPMAX/81.0/
DATA A2/0.3068/,CD2/0.75/,DOR12/0.5/,VOL1F/0.082/,VOL2F/0.00223/
DATA BARL/15.0/,BORED/0.0984/,RES0/7200./,RESS/4320./,RESC/7200./
DATA WPROJ/0.25/
JJ=1
KK=1
NN=0
QFLUX=0.0
UE=0.0
R2=0.0
CV2=0.0
CVT2=0.0
CVEXP=0.0
ALFA2=0.0
BETA2=0.0
GAM2=1.0
P20=14.7
T20=530.0
XPROJ=0.0
VELP=0.0
VPROJ=0.0
VOL20=0.0
DOR12=0.5
READ (5,100) PCH,T0,KP1,PSTART,DELT,PRCI,TFO,FACTOR
READ (5,100) SIUIN,SIUOUT
IF (SIUIN.EQ.0.) GO TO 1
PCH = PCH * 145.04
1 READ (5,101) NG
WRITE (6,103) NM
WRITE (6,104)
DO 3 ID=1,NG
READ (5,102) XG(ID),G1(ID),G2(ID),G3(ID),G4(ID),G5(ID),RG(ID),CVG(
+ID),CVTG(ID),CVEXP(ID),ALFAG(ID),BETAG(ID)
IF (SIUIN.EQ.0.) GO TO 2
RG(ID) = RG(ID) * 0.186
CVG(ID) = CVG(ID) * 0.000239
CVTG(ID) = CVTG(ID) * 0.000239
ALFAG(ID) = ALFAG(ID) * 153746.04
BETAG(ID) = BETAG(ID) * 16.214285
2 WRITE (6,105) XG(ID),G1(ID),G2(ID),G3(ID),G4(ID),G5(ID)
R2 = R2 + XG(ID)*RG(ID)
CV2 = CV2 + XG(ID)*CVG(ID)
GAM2 = GAM2 + XG(ID)*(RG(ID)/(778.*CVG(ID)))
ALFA2 = ALFA2 + XG(ID)*ALFAG(ID)
BETA2 = BETA2 + XG(ID)*BETAG(ID)
3 CONTINUE
ABORE = 0.785* BORED**2
CV=CVDVR
DELT0=DELT

```

```

DOR12=DOR12/12.0
A12=0.7854*DOR12**2
IPRC=IFIX(PRCI)
IPRINT=0
PCH=PCH*144.
PCHP=PCH/144.
P20=P20*144.0
PARTIM = 0.
PSTART=PSTART*144.
QTOT=0.0
RGAS=RDVR
CP=RGAS/778.+CV
GAM=CP/CV
GM = PCH/(RGAS*T0)*VOLO
E=GM*(CP-RGAS/778.)*T0
TIME = 0.
VMAX=XPMAX*AT
XP=XPMAX
C INITIAL CONDITIONS - UPSTREAM - FROM PISTON FACE TO TEST SAMPLE
P1=P20
VOL1=VOL1F+XP*A2
T1=T20
M1=P1*VOL1/R2/T1
CVT2=0.0
DO 4 J=1,NG
  CVT2=CVT2+XG(J)**CVTG(J)*(T1-460.0)**CVEXP(G(J))
4 CONTINUE
E1=M1*(CV2+CVT2)*T1
RHO1=M1/VOL1
VV1=1.0/RHO1
C INITIAL CONDITIONS - DOWNSTREAM - FROM TEST SAMPLE TO PROJECTILE BASE
P2=P20
VOL2=VOL2F+XPROJ*ABORE
T2=T20
M2=P2*VOL2/R2/T2
CVT2=0.0
DO 5 J=1,NC
  CVT2=CVT2+XG(J)**CVTG(J)*(T2-460.0)**CVEXP(G(J))
5 CONTINUE
E2=M2*(CV2+CVT2)*T2
RHO2=M2/VOL2
VV2=1./RHO2
WRITE (6,110)
IF (SIROUT.EQ.0.) GO TO 6
PCHM = PCH * 0.00004792
P20M = P20 * 0.00004792
ATH = AT * 0.093
TCM = T0 * 5./9.
T20M = T20 * 5./9.
KP1M = KP1 * 14.596
VOL0M = VOLO * 0.020
RCM = R2 * 5.376
VELPM = VELP * 0.305
RDVRM = RDVR * 5.376
CV2M = CV2 * 4184.1
WSHELM = WSHELL * 0.454
CVDVRM = CVDVR * 4184.1
CVT2M = CVT2 * 4184.1

```

```

SHELRM = SHELRV * 0.454
XPMAXM = XPMAX * 0.305
BARLM = BARL * 0.305
ALFA2M = ALFA2 * 0.0000065
BOREDM = BORED * 0.305
BETA2M = BETA2 * 0.061674
A2M = A2 * 0.093
PSTARTM = PSTART * 0.00004788
RESOM = RESO * 4.45
DOR12M = DOR12 * 0.305
RESSM = RESS * 14.596
VOL1FM = VOL1F * 0.028
RESCM = RESC * 4.45
VOL20M = VOL20 * 0.028
WPROJM = WPROJ * 0.454
VOL2FM = VOL2F * 0.028
WRITE (6,130) PCHM,P20M,ATM,T0M,T20M,KP1M,VOLOM,R2M,VELPM,RDVRM,
+CV2M,WSHELM,CVDVRM,CVT2M,SHELRM,CVEXP,XPMAXM,BARLM,ALFA2M,BOREDM,
+BETA2M,A2M,PSTARTM,GAM2,CD2,RES0M,DOR12M,RESSM,DELT,VOL1FM,RESCM,
+PRCI,VOL20M,WPROJM,TFO,VOL2FM
GO TO 7
6 WRITE (6,120) PCH,P20,AT,T0,T20,KP1,VOLO,R2,VELP,RDVR,CV2,WSHELL,
+CVDVR,CVT2,SHELRV,CVEXP,XPMAX,BARL,ALFA2,BORED,BETA2,A2,PSTART,
+GAM2,CD2,RES0,DOR12,RESS,DELT,VOL1F,RESC,PRCI,VOL20,WPROJ,TFO,
+VOL2F
7 DEPTH = 0.5/12.0
XK = 19.3/3600.
ALPHA = XK/57.6
F=1.3
DELX0=SQRT(ALPHA*DELT/0.25)
SUMX=DELX0
DELX(1)=DELX0
DO 8 I=1,40
TSAMP(I)=T0
TNEW(I)=T0
8 CONTINUE
DO 9 I=1,39
DELX(I+1)=DELX(I)*F
IF(SUMX.GE.DEPTH) GO TO 9
SUMX=SUMX+DELX(I)
KTEMP = I
9 CONTINUE
CONST1=ALPHA*2.0/(1.0+F)
CONST2=(1.0+F)/F
CONST3=1.0/F
TZIP=QFLUX*2.0*DELX(1)/XK+TSAMP(2)
10 CONTINUE
T=T0
RGAS=57.4+.333E-5*PCH
CV=0.175+.183E-4*T
CP=RGAS/778.+CV
GAM=CP/CV
IF(VELP.LT.-0.1) WSHELL=SHELRV
C COMPUTE THE DYNAMICS AND THERMODYNAMICS OF PISTON MOTION.
24 XD=XPMAX-XP
DRAG=KP1*ABS(VELP)
FOVM=((PCH*AT-P1*A2)-DRAG)/WSHELL*32.17
26 DVLP = FOVM * DELT

```

```

28 VELP =VELP +DVELP
  IF(XP.LE.0.00001.AND.VELP.GT.0.0) VELP=0.0
  DXP=DELT*(VELP+FOVM*DELT/2.)
  XP=XP-DXP
  IF(XP.LE..00001) GO TO 99
  WORK = PCH * AT * DXP/778.
  E = E - WORK
30 VOL=VOL0+AT*XD
  RHOCH = GM/VOL
  T = E/((CP-RGAS/778.)*GM)
  PCH = RHOCH*RGAS*T
C COMPUTE TEST GAS PROPERTIES.
  CVTX=0.0
  CVTY=0.0
  DO 31 J=1,NG
    CVTX=CVTX+XG(J)*CVTG(J)*(T2-460.0)**CVEXPG(J)
    CVTY=CVTY+XG(J)*CVTG(J)*(T1-460.0)**CVEXPG(J)
31 CONTINUE
  CVY=((CV2+CVTY)*T1-ALFA2*RHO1/778.0)/T1
  CVX=((CV2+CVTX)*T2-ALFA2*RHO2/778.0)/T2
  RESIST = RES0 + RESS * XPROJ
32 IF(RESIST.LT.RESC) RESIST=RESC
  H2=E2*GAM2/M2
  H2INF=25000.*H2-VPROJ**2/2.
  XM2INF=VPROJ/SQRT((GAM2-1.0)*H2INF)
  FM=(1.0+(GAM2-1.0)/2.0*XM2INF**2)**(-GAM2/(GAM2-1.0))
  DELP=P2*(1.0-FM)/(1.0+FM)
33 P20=P2+DELP
  P2INF=P2-DELP
  PFORCE = ABORE *(P2INF-RESIST)
  IF(PFORCE.LT.0.0) PFORCE=0.0
  IF(P2.LT.PSTART) PFORCE=0.0
  APROJ = PFORCE/WPROJ*32.17
  DXPROJ = VPROJ * DELT + APROJ * DELT**2/2.
35 XPROJ = XPROJ + DXPROJ
  IF(XPROJ.GE.BARL) GO TO 99
  VPROJ = VPROJ + APROJ* DELT
  VOL1=VOL1F+XP*A2
  VOL2=VOL2F+XPROJ*ABORE
36 P1AVE=P1
  XN1=I1
  XN2=M2
  IPASS=0
  P1SAV=P1
  P2SAV=P2
37 CONTINUE
  IPASS=IPASS+1
  PSTAR=P1*(1.0+(GAM2-1.0)/2.0)**(-GAM2/(GAM2-1.0))
  TTOT=T1
  PS=PSTAR
  PTOT=P1
  IF(P20.GT.P1) GO TO 47
  IF(PSTAR.GE.P20) GO TO 38
  PS=P20
  DELTM1=8.02*A12*SQRT((P1-P20)*P1/R2/T1)*DELT
  GO TO 49
38 TSTAR=T1*2.0/(GAM2+1.0)
  DELTM1=PSTAR*A12*SQRT(GAM2*32.2/R2/TSTAR)*DELT

```

```

GO TO 49
47 CONTINUE
PSTAR=PSTAR*P20/P1
TTOT=T2
PS=PSTAR
PTOT=P20
IF(PSTAR.GE.P1) GO TO 48
PS=P1
DELTMI=-8.02*A12*SQRT((P20-P1)*P20/R2/T2)*DELT
GO TO 49
48 TSTAR=T2*2.0/(GAM2+1.0)
DELTMI=-PSTAR*A12*SQRT(GAM2*32.2/R2/TSTAR)*DELT
49 CONTINUE
XM1=M1-DELTMI
XM2=M2+DELTMI
RHO1=XM1/VOL1
RHO2=XM2/VOL2
VV1=1.0/RHO1
VV2=1./RHO2
WORK=-ABORE*DXPROJ*P2INF/778.0-P2/288.*XPROJ*3.1416*BORED*DELT
IF(VPROJ.LT.100.) GO TO 58
DELH=CVY*DELTMI*T1*GAM2
50 IF(DELTMI.LT.0.0) DELH= CVX*DELTMI*T2*GAM2
EX=E2+WORK+DELH
T2=EX/CVX/XM2
PX=(R2*T2)/(VV2-BETA2)+ALFA2/VV2**2
P2=(PX+P2SAV)/2.0
EY=E1-DELH+P1AVE/778.0*A2*DXP
T1=EY/CVY/XM1
PY=(R2*T1)/(VV1-BETA2)+ALFA2/VV1**2
P1=(PY+P1SAV)/2.0
54 DELP1=PY-P1
P1AVE=P1+DELP1/2.0
P20=P2+DELP
55 IF(IPASS.LT.3) GO TO 37
E1=EY
E2=EX
P1=PY
P2=PX
M1=XM1
M2=XM2
XMOR=SQRT(((PTOT/PS)**((GAM2-1.0)/GAM2)-1.0)*2.0/(GAM2-1.0))
TE=TTOT/(1.0+(GAM2-1.0)/2.0*XMOR**2)
UE=SQRT(5.0E4*CVY*GAM2*(TTOT-TE))
TREF=(TE+TSAMP(1))/2.0+4.4E-6*UE**2/CVY/GAM2
VIS=7.0E-7*TREF**1.5/(TREF+198.0)
RHOREF=PS/(BETA2*PS+R2*TREF)
QFLUX=0.052*(RHOREF*UE)**0.8*VIS**0.2*CVY*GAM2*(TTOT-TSAMP(1))
IF(TSAMP(1).GT.3100.0) QFLUX=QFLUX*(TTOT-3100.0)/(TTOT-TSAMP(1))
QFLUX = QFLUX*FACTOR
TZIP=QFLUX*2.0*DELX(1)/KK+TSAMP(2)
DTEMP(1)=ALPHA/(DELX(1)**2)*(TZIP-2.0*TSAMP(1)+TSAMP(2))
DO 56 K=2,KTEMP
DTEMP(K)=CONST1/(DELX(K-1)**2)*(TSAMP(K-1)-CONST2*TSAMP(K)+*
CONST3*TSAMP(K+1))
56 CONTINUE
DO 57 K=1,KTEMP
TSAMP(K)=TSAMP(K)+DTEMP(K)*DELT

```

```

57 CONTINUE
  TSAMP(KTEMP+1)=TSAMP(KTEMP-1)
  QTOT=QTOT+QFLUX*DELT
  IF(P20.GT.P1) UE=-UE.
  GO TO 60
58 CONTINUE
  VOL=VOL1+VOL2
  XMTOT=M1+M2
  ESUM=E1+E2+P1*A2*DXP/778.0 +WORK
  M1=XMTOT*VOL1/VOL
  M2=XMTOT*VOL2/VOL
  E1=ESUM*VOL1/VOL
  E2=ESUM*VOL2/VOL
  T1=ESUM/CVX/XMTOT
  T2=T1
  VVT=VOL/XMTOT
  P1=(R2*T1)/(VVT-BETA2)+ALFA2/VVT**2
  P2=P1
  RHO1=M1/VOL1
  RHO2=M2/VOL2
  VV1=1.0/RHO1
  VV2=1.0/RHO2
60 CONTINUE
  IF (VOL1.GT.0.2*VMAX) GO TO 80
  IF(VOL1.LE.0.2*VMAX)DELT=0.1*DELTO
  IF(VOL1.LE.0.2*VMAX.AND.KK.EQ.1) GO TO 62
  IF(VOL1.LE.0.02*VMAX)DELT=0.01*DELTO
  IF(VOL1.LE.0.02*VMAX.AND.KK.EQ.2) GO TO 62
  GO TO 80
C   REVISE GRID SIZE DUE TO CHANGE IN TIME STEP.
62 DELX0=SQRT(ALPHA*DELT/0.25)
  SUMX=DELX0
  DXNEW(1)=DELX0
  DO 64 I=2,40
    DXNEW(I)=DXNEW(I-1)*F
    IF(SUMX.GE.DEPTH) GO TO 64
    SUMX=SUMX+DXNEW(I)
    KMAX = I
64 CONTINUE
  XKOLD=DELX(1)
  XKNEW=0.0
  K=1
  KNEW=1
  A=(TZIP-TSAMP(2))/(2.0*DELX(K))
  B=(TSAMP(1)-TSAMP(2)-A*DELX(K))/DELX(K)**2
  TNEW(1)=TSAMP(1)
66 KNEW=KNEW+1
  XKNEW=XKNEW+DXNEW(KNEW-1)
  TNEW(KNEW)=TSAMP(1)-(A*XKNEW+B*XKNEW**2)
  IF(XKNEW.LT.XKOLD)GO TO 66
67 K=K+1
  XKOLD=XKOLD+DELX(K)
  A=(TSAMP(K-1)-TSAMP(K+1))/((F+1.0)*DELX(K-1))
  B=(TSAMP(K)-TSAMP(K+1)-A*DELX(K))/DELX(K)**2
68 KNEW=KNEW+1
  XKNEW=XKNEW+DXNEW(KNEW-1)
  XDEL=XKNEW-XKOLD+DELX(K)
  TNEW(KNEW)=TSAMP(K)-(A*XDEL+B*XDEL**2)

```

```

IF(XKNEW.LT.XKOLD.AND.KNEW+1.LE.KNMAX) GO TO 68
IF(K+1.LE.KTEMP.AND.KNEW+1.LE.KNMAX) GO TO 67
DO 70 I=1,KNMAX
DELX(I)=DXNEW(I)
TSAMP(I)=TNEW(I)
TNEW(I)=TO
70 CONTINUE
KTEMP=KNMAX
KK = KK+1
80 CONTINUE
C PRINT OUT COMPUTED RESULTS.
IF (JJ.EQ.1) GO TO 88
87 NN=1
PARTIM=PARTIM+DELT
IF(TIME.GT.TFO) GO TO 99
IF(IPRINT.LT.IPRC) GO TO 95
GO TO 89
88 WRITE (6,187)
WRITE (6,188)
JJ=JJ+1
89 PCHP=PCH/144.
P1P=P1/144.0
P2P=P2/144.
TIME=TIME+PARTIM
PARTIM = 0.
IF (SIUOUT.EQ.0.) GO TO 92
P1PM = P1P * 0.0068946
T1M = T1 * 5./9.
M1M = M1 * 0.454
VOL1M = VOL1 * 0.028
VELPM = VELP * 0.305
VPROJM = VPROJ * 0.305
WORKM = WORK * 1.356
QFLUXM = QFLUX * 0.0113566
PCHPM = PCHP * 0.0068946
P2PM = P2P * 0.0068946
T2M = T2 * 5./9.
M2M = M2 * 0.454
VOL2M = VOL2 * 0.028
XPM = XP * 0.305
XPROJM = XPROJ * 0.305
UEM = UE * 0.305
QTOTM = QTOT * 0.0113566
DO 90 I=1,9
TSAMPM(I) = TSAMP(I) * 5./9.
90 CONTINUE
WRITE (6,190) TIME,P1PM,T1M,M1M,VOL1M,VELPM,VPROJM,WORKM,QFLUXM,
+PCHPM,P2PM,T2M,M2M,VOL2M,XPM,XPROJM,UEM,QTOTM,(TSAMPM(I),I=1,9)
GO TO 93
92 WRITE(6,190) TIME,P1P,T1,M1,VOL1,VELP,VPROJ,WORK,QFLUX,PCHP,P2P,T2
+,M2,VOL2,XP,XPROJ,UE,QTOT,(TSAMP(I),I=1,9)
93 IF(NN.EQ.0) GO TO 87
IPRINT = 0
95 IPRINT=IPRINT+1
GO TO 10
99 CONTINUE
STOP
END

```

A sample printout of the STG program follows. Definitions of "Initial Condition" variables are given in the preceding program printout. However, some explanation of the "Tabulated Output" variables is required.

TIME	Time after piston release - seconds. Time is initially zero and increases to a maximum value either when the projectile exits the barrel or when it equals a limiting value, i.e., TFO.
PCH	Driver gas pressure - MPa. PCH is a prescribed maximum at TIME zero and decreases as the driver gas displaces the unlatched piston.
VOL1	Test gas volume included from piston face to test specimen inlet - m ³ . VOL1 is initially the entire volume of the driven tube but decreases to the volume of the test gas collection chamber when the piston has been fully displaced.
P1, T1, M1	Test gas pressure, temperature and mass associated with VOL1, measured in MPa, °K and kg, respectively.
VOL2	Test gas volume included from test specimen inlet to projectile base - m ³ . VOL2 has a minimum value of the test specimen bore volume at TIME zero and increases with projectile displacement to include the entire barrel volume.
P2, T2, M2	Test gas pressure, temperature and mass associated with VOL2, measured in MPa, °K and kg, respectively.
VELP, XP	Piston velocity and displacement - m/sec, m.
VPROJ, XPROJ	Projectile velocity and displacement - m/sec, m.
WORK	Work performed by driver gas on the driven piston, and by test gas on the projectile. During piston rebound, the program also computed negative work done on the piston by the test gas - J.
UE	Test gas free stream velocity - m/sec.
QFLUX	Test sample surface heat flux - J/mm ² -sec.
QTOT	Total integrated heat input to test sample surface - J/mm ² .
TSAMP	Test Sample surface temperature - °K. TSAMP(1) is the computed temperature on the test sample surface. TSAMP(2) through TSAMP(9) are subsurface temperatures computed at depths printed in the nonlinear DELX array, which is amended when the time increment DELT is changed.

INPUT DATA

TEST NO. 1

TEST GAS MIXTURE BY MOLE FRACTION

0.455 CARBON MONOXIDE
0.545 ARGON

INITIAL CONDITIONS FOR TEST

PCH =	4.41262 MPA	P20 =	0.10135 MPA	AT =	0.02853 M**3
T0 =	297.22217 K	T20 =	294.44434 K	KPI =	87.57599 N/M
VOL0 =	0.88200 M**3	R2 =	248.25496 J/KG-K	VELP =	0.0 M/SEC
RDVR =	296.75513 J/KG-K	CV2 =	511.26343 J/KG-K	WSHELL =	68.09999 KG
CVDVR =	736.40186 J/KG-K	CVT2 =	2.29213 J/KG-K	SHELRV =	68.09999 KG
		CVEXP =	0.0	XPMAX =	24.70499 M
BARL =	4.57500 M	ALFA2 =	0.00470 MPA-M**3/(KG-MOL)**2		
BORED =	0.03001 M	BETA2 =	0.00107 M**3/KG-MOL	A2 =	0.02853 M**2
PSTART =	0.34474 MPA	GAM2 =	1.48575	CD2 =	0.75000
RES0 =	32039.9961 N			DOR12 =	0.01271 M
RESS =	63054.7187 N/M	DELT =	0.00100 SEC	VOL1F =	0.00230 M**3
RESC =	32039.9961 N	PRCI =	33.00000	VOL20 =	0.0 M**3
WPROJ =	0.11350 KG	TFO =	0.25000 SEC	VOL2F =	0.00006 M**3

TABULATED OUTPUT

TIME TSAMP(1)	P1 TSAMP(2)	T1 TSAMP(3)	M1 TSAMP(4)	VOL1 TSAMP(5)	VELP TSAMP(6)	VPROJ TSAMP(7)	WORK TSAMP(8)	OFLUX QTOT TSAMP(9)
0.0	0.101905E+00	0.294824E+03	0.979020E+00	0.698041E+00	0.180703E+01	0.0	0.0	0.0
0.439334E+01	0.101905E+00	0.294824E+03	0.875736E-04	0.624400E-04	0.247023E+02	0.0	0.0	0.0
0.297222E+03	0.297222E+03	0.297222E+03	0.297222E+03	0.297222E+03	0.297222E+03	0.297222E+03	0.297222E+03	0.297222E+03
0.339999E-01	0.108773E+00	0.301027E+03	0.979020E+00	0.667796E+00	0.589426E+02	0.0	0.0	0.0
0.419681E+01	0.108773E+00	0.301027E+03	0.915380E-04	0.624400E-04	0.236284E+02	0.0	0.0	0.0
0.297222E+03	0.297222E+03	0.297222E+03	0.297222E+03	0.297222E+03	0.297222E+03	0.297222E+03	0.297222E+03	0.297222E+03
0.669999E-01	0.131268E+00	0.319595E+03	0.978970E+00	0.587706E+00	0.108808E+03	0.0	0.0	0.0
0.373213E+01	0.131268E+00	0.319595E+03	0.104009E-03	0.624400E-04	0.207849E+02	0.0	0.0	0.0
0.297222E+03	0.297222E+03	0.297222E+03	0.297222E+03	0.297222E+03	0.297222E+03	0.297222E+03	0.297222E+03	0.297222E+03
0.999998E-01	0.184641E+00	0.356056E+03	0.978927E+00	0.465856E+00	0.149166E+03	0.0	0.0	0.0
0.317230E+01	0.184641E+00	0.356056E+03	0.131208E-03	0.624400E-04	0.164586E+02	0.0	0.0	0.0
0.297222E+03	0.297222E+03	0.297222E+03	0.297222E+03	0.297222E+03	0.297222E+03	0.297222E+03	0.297222E+03	0.297222E+03
0.133000E+00	0.332495E+00	0.428166E+03	0.978840E+00	0.311649E+00	0.179080E+03	0.0	0.0	0.0
0.264352E+01	0.332495E+00	0.428166E+03	0.196114E-03	0.624400E-04	0.109835E+02	0.0	0.0	0.0
0.297222E+03	0.297222E+03	0.297222E+03	0.297222E+03	0.297222E+03	0.297222E+03	0.297222E+03	0.297222E+03	0.297222E+03
0.165100E+00	0.111617E+01	0.621186E+03	0.977005E+00	0.135334E+00	0.196533E+03	0.360942E+02	-0.586573E-01	0.115468E+01
0.220075E+01	0.892996E+00	0.548238E+03	0.201165E-02	0.307221E-03	0.472348E+01	0.350216E+00	0.250353E+03	0.274272E-02
0.302420E+03	0.300681E+03	0.298990E+03	0.297754E+03	0.297139E+03	0.298060E+03	0.297235E+03	0.297217E+03	0.297248E+03
0.168400E+00	0.137587E+01	0.6616177E+03	0.976112E+00	0.117041E+00	0.196998E+03	0.425963E+02	-0.864374E-02	0.167841E+01
0.215467E+01	0.100431E+01	0.553074E+03	0.289911E-02	0.397732E-03	0.407399E+01	0.480513E+00	0.318143E+03	0.746495E-02
0.307564E+03	0.304921E+03	0.302337E+03	0.300109E+03	0.298555E+03	0.297805E+03	0.297421E+03	0.297253E+03	0.297240E+03
0.171700E+00	0.175923E+01	0.712910E+03	0.974884E+00	0.987274E-01	0.196973E+03	0.498896E+02	-0.125515E-01	0.237258E+01
0.211734E+01	0.116593E+01	0.571488E+03	0.412103E-02	0.503991E-03	0.342377E+01	0.632795E+00	0.375707E+03	0.141065E-01
0.314027E+03	0.310262E+03	0.306486E+03	0.303033E+03	0.300281E+03	0.298502E+03	0.297633E+03	0.297312E+03	0.297243E+03
0.174999E+00	0.236330E+01	0.779209E+03	0.973175E+00	0.804491E-01	0.196237E+03	0.588158E+02	-0.186391E-01	0.345834E+01
0.208116E+01	0.139880E+01	0.604298E+03	0.582325E-02	0.623722E-03	0.277491E+01	0.811550E+00	0.441046E+03	0.236371E-01
0.323109E+03	0.317618E+03	0.312093E+03	0.306966E+03	0.302716E+03	0.299729E+03	0.298082E+03	0.297427E+03	0.297258E+03
0.178299E+00	0.341513E+01	0.869704E+03	0.970698E+00	0.622908E-01	0.194361E+03	0.700618E+02	-0.289722E-01	0.532083E+01
0.204626E+01	0.175776E+01	0.657857E+03	0.829244E-02	0.777212E-03	0.213010E+01	0.102135E+01	0.520972E+03	0.379142E-01
0.337152E+03	0.328742E+03	0.320365E+03	0.312639E+03	0.306209E+03	0.301556E+03	0.298035E+03	0.297642E+03	0.297294E+03

0.181599E+00	0.556590E+01	0.100432E+04	0.968004E+00	0.443993E-01	0.190382E+03	0.856786E+02	-0.406301E-01	0.934863E+01
0.201283E+01	0.199408E+01	0.693572E+03	0.109793E-01	0.957321E-03	0.149487E+01	0.128247E+01	0.567632E+03	0.613830E-01
0.362730E+03	0.348155E+03	0.334127E+03	0.321632E+03	0.311525E+03	0.304316E+03	0.300001E+03	0.298006E+03	0.297365E+03
0.104899E+00	0.113794E+02	0.123480E+04	0.963613E+00	0.270813E-01	0.181525E+03	0.104764E+03	-0.672784E-01	0.204437E+02
0.198134E+01	0.268945E+01	0.819127E+03	0.153649E-01	0.117483E-02	0.879995E+00	0.159410E+01	0.636427E+03	0.107582E+00
0.421750E+03	0.390565E+03	0.362249E+03	0.338615E+03	0.320751E+03	0.308751E+03	0.301819E+03	0.298507E+03	0.297492E+03
0.187659E+00	0.324331E+02	0.165340E+04	0.955582E+00	0.132413E-01	0.160878E+03	0.137676E+03	-0.146923E-01	0.509199E+02
0.195621E+01	0.466566E+01	0.111769E+04	0.233902E-01	0.141118E-02	0.380610E+00	0.193290E+01	0.751354E+03	0.208349E+00
0.580349E+03	0.552110E+03	0.517093E+03	0.479058E+03	0.441077E+03	0.405686E+03	0.371777E+03	0.344441E+03	0.329145E+03
0.187989E+00	0.386446E+02	0.173347E+04	0.953980E+00	0.117683E-01	0.156197E+03	0.144133E+03	-0.167247E-01	0.695128E+02
0.195361E+01	0.514406E+01	0.117926E+04	0.249059E-01	0.144361E-02	0.336310E+00	0.197937E+01	0.772131E+03	0.229525E+00
0.621380E+03	0.505093E+03	0.544635E+03	0.501377E+03	0.457532E+03	0.415813E+03	0.378746E+03	0.349194E+03	0.330044E+03
0.108319E+00	0.468820E+02	0.182545E+04	0.952101E+00	0.103435E-01	0.150530E+03	0.151592E+03	-0.193050E-01	0.830021E+02
0.195111E+01	0.573831E+01	0.125160E+04	0.268576E-01	0.147763E-02	0.205723E+00	0.202013E+01	0.795633E+03	0.254661E+00
0.669442E+03	0.626222E+03	0.578356E+03	0.527594E+03	0.476578E+03	0.420542E+03	0.386715E+03	0.353800E+03	0.331530E+03
0.188649E+00	0.580788E+02	0.193205E+04	0.949862E+00	0.897761E-02	0.143542E+03	0.160325E+03	-0.226620E-01	0.100511E+03
0.194871E+01	0.649177E+01	0.133756E+04	0.290905E-01	0.151351E-02	0.237229E+00	0.207955E+01	0.822419E+03	0.284897E+00
0.7299640E+03	0.677448E+03	0.620020E+03	0.559632E+03	0.499585E+03	0.443785E+03	0.395970E+03	0.358902E+03	0.333487E+03
0.188979E+00	0.7756947E+02	0.205648E+04	0.947137E+00	0.765052E-02	0.134732E+03	0.170703E+03	-0.271484E-01	0.123510E+03
0.194644E+01	0.746962E+01	0.144105E+04	0.310808E-01	0.151515E-02	0.191343E+00	0.213412E+01	0.853131E+03	0.321790E+00
0.806107E+03	0.742414E+03	0.672253E+03	0.599408E+03	0.527790E+03	0.462167E+03	0.406868E+03	0.364656E+03	0.335863E+03
0.189309E+00	0.959814E+02	0.220203E+04	0.943749E+00	0.648667E-02	0.123350E+03	0.183261E+03	-0.333340E-01	0.153830E+03
0.194434E+01	0.877133E+01	0.156704E+04	0.351900E-01	0.159228E-02	0.148789E+00	0.219245E+01	0.888385E+03	0.367480E+00
0.904363E+03	0.824901E+03	0.738627E+03	0.649490E+03	0.562855E+03	0.484627E+03	0.419854E+03	0.371312E+03	0.338681E+03
0.189639E+00	0.128126E+03	0.237045E+04	0.939434E+00	0.541109E-02	0.110827E+03	0.198776E+03	-0.421436E-01	0.193106E+03
0.194246E+01	0.105470E+02	0.172132E+04	0.394973E-01	0.163620E-02	0.110601E+00	0.225530E+01	0.928385E+03	0.424661E+00
0.103086E+04	0.931277E+03	0.823650E+03	0.713231E+03	0.607010E+03	0.512454E+03	0.435580F+03	0.379155E+03	0.341990E+03
0.189969E+00	0.173240E+03	0.255703E+04	0.933843E+00	0.450033E-02	0.879066E+02	0.218380E+03	-0.550319E-01	0.240493E+03
0.194086E+01	0.130346E+02	0.190847E+04	0.450815E-01	0.168413E-02	0.702642E-01	0.232400E+01	0.971844E+03	0.496280E+00
0.119011E+04	0.1056601E+04	0.931811E+03	0.794404E+03	0.662997E+03	0.547334E+03	0.4549101E+03	0.388542E+03	0.345903E+03
0.190299E+00	0.228911E+03	0.273935E+04	0.926612E+00	0.381237E-02	0.605035E+02	0.243622E+03	-0.739458E-01	0.286722E+03
0.193965E+01	0.163474E+02	0.212485E+04	0.520362E-01	0.173720E-02	0.539382E-01	0.240012E+01	0.101360E+04	0.583784E+00
0.137537E+04	0.122659E+04	0.106360E+04	0.895226E+03	0.733331E+03	0.591180E+03	0.478094E+03	0.399932E+03	0.350533E+03
0.190629E+00	0.274907E+03	0.286462E+04	0.917713E+00	0.341657E-02	0.256905E+02	0.276225E+03	-0.100221E+00	0.307826E+03
0.193949E+01	0.205029E+02	0.234532E+04	0.611995E-01	0.179689E-02	0.397H55E-01	0.248557E+01	0.104200E+04	0.603090E+00
0.155252E+04	0.139042E+04	0.120693E+04	0.101107E+04	0.817809E+03	0.645299E+03	0.508711E+03	0.413894E+03	0.356083E+03
0.190959E+00	0.276974E+03	0.287052E+04	0.908004E+00	0.336742E-02	0.128464E+02	0.317074E+03	-0.131029E+00	0.280861E+03
0.193803E+01	0.247171E+02	0.252122E+04	0.709019E-01	0.186504E-02	0.380404E-01	0.258334E+01	0.104352E+04	0.781456E+00
0.166374E+04	0.151190E+04	0.133002E+04	0.112402E+04	0.909121E+03	0.708371E+03	0.544962E+03	0.431019E+03	0.362274E+03
0.191289E+00	0.232819E+03	0.275295E+04	0.898999E+00	0.366629E-02	0.482819E+02	0.364929E+03	-0.162803E+00	0.219230E+03
0.193931E+01	0.278545E+02	0.261740E+04	0.979001E-01	0.193454E-02	0.486516E-01	0.269571E+01	0.101712E+04	0.864118E+00
0.168104E+04	0.155864E+04	0.140116E+04	0.120887E+04	0.992140E+03	0.774425E+03	0.566690E+03	0.451665E+03	0.370654E+03
0.191619E+00	0.176176E+03	0.257143E+04	0.891652E+00	0.425990E-02	0.764224E+02	0.416708E+03	-0.187760E+00	0.156819E+03
0.194031E+01	0.294012E+02	0.264139E+04	0.872404E-01	0.203340E-02	0.697280E-01	0.202426E+01	0.975675E+03	0.925528E+00
0.163232E+04	0.154183E+04	0.141724E+04	0.125335E+04	0.105317E+04	0.843457E+03	0.630819E+03	0.475577E+03	0.380559E+03
0.191949E+00	0.129522E+03	0.238177E+04	0.885990E+00	0.507797E-02	0.972693E+02	0.469148E+03	-0.204926E+00	0.109788E+03
0.194170E+01	0.295934E+02	0.261979E+04	0.928963E-01	0.213540E-02	0.907732E-01	0.297080E+01	0.931527E+03	0.968817E+00
0.155757E+04	0.149233E+04	0.139712E+04	0.126369E+04	0.108879E+04	0.882228E+03	0.673177E+03	0.5015724E+03	0.391915F+03
0.192279E+00	0.962606E+02	0.220920E+04	0.881649E+00	0.606111E-02	0.112509E+03	0.519039E+03	-0.214830E+00	0.778743E+02
0.194338E+01	0.200837E+02	0.257387E+04	0.972303E-01	0.224931E-02	0.133679E+00	0.313045E+01	0.890527E+03	0.999262E+00
0.148000E+04	0.143251E+04	0.135980E+04	0.125252E+04	0.110360E+04	0.915638E+03	0.710457E+03	0.528583E+03	0.404777E+03
0.192609E+00	0.733217E+02	0.205970E+04	0.879264E+00	0.716650E-02	0.124047E+03	0.567318E+03	-0.210775E+00	0.566666E+02
0.194528E+01	0.251598E+02	0.100608E+04	0.237455E-02	0.179286E+00	0.331353E+00	0.416923E+01	0.854282E+03	0.102111E+01
0.140046E+04	0.137312E+04	0.131677E+04	0.123013E+04	0.110422E+04	0.936475E+03	0.741075E+03	0.654648E+03	0.418793E+03
0.192293E+00	0.573636E+02	0.193190E+04	0.875567E+00	0.836449E-02	0.132839E+03	0.610822E+03	-0.210161E+00	0.423617E+02
0.194734E+01	0.261439E+02	0.245282E+04	0.103304E+00	0.251027E-02	0.215460E+00	0.350803E+01	0.822691E+03	0.103723E+01
0.134513E+04	0.131816E+04	0.127364E+04	0.120286E+04	0.109611E+04	0.947569E+03	0.764912E+03	0.570775E+03	0.433506E+03
0.193269E+00	0.459461E+02	0.182189E+04	0.872621E+00	0.963445E-02	0.139750E+03	0.650247E+03	-0.215940E+00	0.326524E+02
0.194953E+01	0.247245E+02	0.238919E+04	0.106239E+00	0.265553E-02	0.260550E+00	0.371621E+01	0.687445E+03	0.104950E+01
0.179010E+04	0.126893E+04	0.123296E+04	0.117421E+04	0.108030E+04	0.951629E+03	0.795723E+03	0.619137E+03	0.463176E+03
0.193599E+00	0.376398E+02	0.172745E+04	0.870403E+00	0.109616E-01	0.145309E+03	0.685505E+03	-0.210406E+00	0.246930E+02
0.195183E+01	0.231593E+02	0.232494E+04	0.108369E+00	0.280941E-02	0.307671E+00	0.393673E+01	0.556611E+03	0.105888E+01
0.124070E+04	0.122422E+04	0.119503E+04	0.114593E+04	0.106734E+04	0.950724E+03	0.795723E+03	0.619137E+03	0.463176E+03
0.193929E+00	0.314368E+02	0.164564E+04	0.868972E+00	0.123352E-01	0.149871E+03	0.716794E+03	-0.202691E+00	0.179797E+02
0.195421E+01	0.215613E+02	0.226189E+04	0.109874E+00	0.297094E-02	0.356439E+00	0.416923E+01	0.426653E+03	0.106588E+01
0.119540E+04	0.118285E+04	0.115931E+04	0.105023E+04	0.946666E+03	0.803079E+03	0.635117E+03	0.477384E+03	0.477384E+03
0.194259E+00	0.266939E+02	0.157414E+04	0.867981E+00	0.137473E-01	0.153680E+03	0.744012E+03	-0.193625E+00	0.118285E+02
0.195666E+01	0.199414E+02	0.220098E+04	0.110860E+00	0.313920E-02	0.406576E+00	0.440937E+01	0.205028E+03	0.107074E+01
0.115294E+04	0.114393E+04	0.112532E+04	0.109092E+04	0.103229E+04	0.940121E+03	0.809160E+03	0.648497E+03	0.490829E+03

APPENDIX II
ISENTROPIC EQUILIBRIUM COMBUSTION CODE

Adiabatic Compression Program

An existing equilibrium combustion program has been modified to calculate the properties of a gas mixture at various points on an isentrope. The program uses a list of thermal properties of possible constituents of the mixture. The program writes output containing the composition and thermal properties of the gas mixture at the input pressures.

Input to the program consists of "REACTANT" cards specifying the composition at the initial point on the isentrope and a namelist, "&INPT2," which specifies the temperature and pressure at the initial point and a schedule of other pressures (up to 26 pressures including the initial value). OMIT cards may be used if desired to exclude certain species from consideration as mixture constituents.

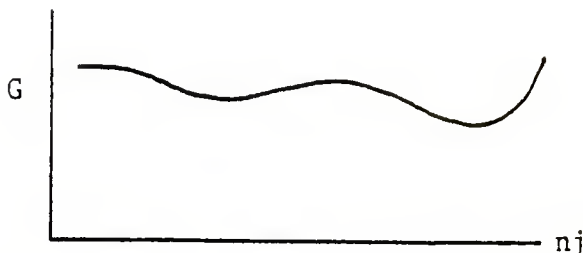
The program operates as follows:

- (1) The initial mixture as specified by the reactant cards and the mixture ratio specified by &INPT2 is analyzed to determine which chemical elements are present. The number of gram-atoms of each element is calculated as well as the mixture molecular weight and mixture total enthalpy (Subroutine REAC).
- (2) The taped thermal data is searched (SEARCH) and the names and thermal properties of possible compounds which could be formed from the available atoms are extracted. This list is then compared to the OMIT cards and the net list of species to be considered is printed.
- (3) Subroutine EQLBRM then varies the composition seeking to minimize the Gibbs free energy of the mixture subject to the constraint that the numbers of atoms of the different elements do not vary.

In this process, species with molefractions of less than 10^{-7} at any iteration are dropped from consideration. Occasionally, the constraint equations

$$\sum_j a_{ij} n_j = b_i$$

where a_{ij} is the number of atoms of type i in species j , become linearly dependent. In this case, the program will print the message "SINGULAR MATRIX" and then calculate the thermal properties of the input mixture at the specified pressure and temperature (Subroutine HCALC). Sometimes the mixture free energy will have a very broad minimum or will possess two minima



as in the sketch. If this is the situation, the program will print the message

"35 ITERATIONS DID NOT SATISFY CONVERGENCE REQUIREMENTS FOR THE POINT "

and then calculate the thermal properties of the input mixture.

- (4) One way or the other, the program will obtain the entropy at point #1. This entropy will then be held constant (SP=.TRUE.), EQLBRM will calculate the equilibrium composition at an estimated temperature and the new pressure, calculate the mixture entropy, and compare it to the entropy at point #1. If the two entropies do not agree, the temperature estimate is changed and a new equilibrium calculated.
- (5) If, at any point, the equilibrium calculation fails, the control program THERMP will call subroutine FRØZEN to obtain the thermal properties corresponding to the fixed entropy, the new pressure and the composition at the previous point.
- (6) After 15 points have been calculated, the program will print the results. Then it will complete and output the remainder of the pressure schedule.
- (7) After completing the pressure schedule, the program will look for a new mixture ratio MIX.

NO INPT2 VALUE GIVEN FOR OF, EORAT, FA, OR FPCT

SPECIES BEING CONSIDERED IN THIS SYSTEM

L 5/66	AR	J 3/61	C	J12/67	CH	J12/72	CH2	J 3/61	CH20
J 6/69	CH3	J 3/61	CH4	J 6/69	CN	J 6/66	CNN	J12/70	CN2
J 9/65	CO	J 9/65	CO2	J12/69	C2	J 3/67	C2II	J 3/61	C2II
J 9/65	C2H4	L 5/72	C2H6	J 3/67	C2N	J 3/61	C2N2	J 9/66	C20
J12/69	C3	J 6/68	C3O2	J12/69	C4	J12/69	C5	J 3/77	H
L12/69	HCN	J12/70	HCO	J12/70	HNCO	J 3/63	HNO	J 6/63	HNO2
J 6/63	HNO3	J 3/64	HQ2	J 3/77	H2	L11/65	H2O(S)	L11/65	H2O(L)
J 3/61	H2O	L 2/69	H2O2	J 3/77	N	J12/70	NCO	J12/71	NH
J12/65	NH2	J 9/65	NH3	J 6/63	NO	J 9/64	NO2	J12/64	NO3
J 3/77	N2	J12/65	N2H4	J12/64	N2O	J 9/64	N2O4	J12/64	N2O5
J12/70	N3	J 3/77	O	J12/70	OH	J 3/77	O2	J 6/61	O3

OF = 0.0

ENTHALPY (KG-MOL)(DEG K)/KG	EFFECTIVE FUEL HPP(2)	EFFECTIVE OXIDANT HPP(1)	MIXTURE HSUB0
	-0.36660385E+02	0.0	-0.36660385E+02

KG-ATOMS/KG	BOP(I,2)	BOP(I,1)	B(O)
C	0.27577896E-02	0.0	0.27577896E-02
O	0.27577896E-02	0.0	0.27577896E-02
H	0.27577879E-02	0.0	0.27577879E-02
N	0.27577879E-02	0.0	0.27577879E-02
AR	0.22062317E-01	0.0	0.22062317E-01

P	T	C	O	H	N	AR
1	44.084	-115.450	-25.642	-12.980	-18.666	15.000
2	-1.293	-31.895	-8.120	-11.726	-15.413	15.000
3	-2.395	-28.827	-8.043	-11.735	-15.181	5.000
4	-3.225	-27.055	-8.046	-11.763	-15.068	4.000
5	-3.915	-25.788	-8.060	-11.790	-14.994	3.000
6	-4.463	-24.841	-8.075	-11.814	-14.930	3.000
7	-4.901	-24.105	-8.091	-11.835	-14.894	3.000
8	-5.260	-23.514	-8.106	-11.854	-14.857	3.000
9	-5.560	-23.027	-8.119	-11.870	-14.825	3.000
10	-5.815	-22.615	-8.132	-11.885	-14.797	3.000
11	-6.036	-22.263	-8.145	-11.899	-14.772	3.000
12	-6.230	-21.956	-8.156	-11.912	-14.750	3.000
13	-6.402	-21.685	-8.168	-11.924	-14.729	3.000

THERMODYNAMIC EQUILIBRIUM PROPERTIES AT ASSIGNED
ENTROPY AND PRESSURE

CASE NO. 70

	CHEMICAL FORMULA			MOLES	ENERGY	STATE	TEMP	DENSITY
FUEL	C	O	1.00000	0.10000	-26416.152	G	298.15	0.0
FUEL	H	2.00000		0.05000	0.0	G	298.15	0.0
FUEL	N	2.00000		0.05000	0.0	G	298.15	0.0
FUEL	AR	1.00000		0.80000	0.0	G	298.15	0.0

O/F = 0.0 PERCENT FUEL=100.0000 EQUIVALENCE RATIO= 2.5000 REACTANT DENSITY= 0.0

THERMODYNAMIC PROPERTIES

P, ATM	1.0000	197.39	394.77	592.16	789.55	986.93	1184.32	1381.71	1579.10	1776.48	1973.87	2171.26	2368.64
T, DEG K	300	1381	1732	1990	2198	2374	2528	2665	2790	2904	3010	3108	3200
RHO, G/CC	1.5758-3	6.3614-2	1.0096-1	1.3167-1	1.5891-1	1.8389-1	2.0722-1	2.2929-1	2.5034-1	2.7055-1	2.9005-1	3.0893-1	3.2728-1
H, CAL/G	-119.2	85.1	143.6	184.9	217.8	245.7	270.2	292.1	312.0	330.4	347.4	363.4	378.4
S, CAL/(G)(K)	1.0280	1.0280	1.0280	1.0280	1.0280	1.0280	1.0280	1.0280	1.0280	1.0280	1.0280	1.0280	1.0280
M, MOL WT	38.793	36.513	36.335	36.304	36.296	36.294	36.293	36.292	36.291	36.290	36.288	36.286	36.283
(DLV/DLP)T	-1.00094	-1.00540	-1.00187	-1.00103	-1.00075	-1.00066	-1.00065	-1.00067	-1.00071	-1.00077	-1.00084	-1.00091	-1.00100
(DLV/DLT)P	1.0219	1.0575	1.0151	1.0064	1.0034	1.0024	1.0022	1.0024	1.0029	1.0034	1.0041	1.0049	1.0054
CP, CAL/(G)(K)	0.1660	0.1884	0.1633	0.1597	0.1589	0.1590	0.1595	0.1602	0.1609	0.1617	0.1625	0.1634	0.1643
GAMMA (S)	1.4734	1.4657	1.5226	1.5294	1.5295	1.5274	1.5247	1.5217	1.5186	1.5155	1.5125	1.5095	1.5066
SON VEL,M/SEC	307.8	678.8	776.7	834.8	877.5	911.4	939.7	963.9	985.2	1004.2	1021.2	1036.8	1051.1

MOLE FRACTIONS

AR	0.85587	0.80556	0.80163	0.80095	0.80078	0.80073	0.80071	0.80069	0.80067	0.80064	0.80060	0.80055	0.80049
CH2O	0.0	0.00000	0.00000	0.00000	0.00000	0.00000	0.00000	0.00000	0.00000	0.00000	0.00001	0.00001	0.00001
CH3	0.0	0.00000	0.00000	0.00000	0.00000	0.00000	0.00000	0.00001	0.00001	0.00001	0.00001	0.00001	0.00001
CH4	0.00229	0.00343	0.00068	0.00035	0.00017	0.00010	0.00007	0.00005	0.00004	0.00003	0.00003	0.00002	0.00002
CO	0.03703	0.09539	0.09866	0.09905	0.09908	0.09905	0.09900	0.09894	0.09888	0.09882	0.09875	0.09869	0.09862
CO2	0.03497	0.00182	0.00042	0.00025	0.00022	0.00021	0.00021	0.00022	0.00022	0.00023	0.00024	0.00024	0.00025
C2H2	0.0	0.00000	0.00001	0.00002	0.00002	0.00002	0.00003	0.00003	0.00003	0.00003	0.00003	0.00003	0.00004
C2H4	0.00012	0.00000	0.00000	0.00000	0.00000	0.00000	0.00000	0.00000	0.00000	0.00000	0.00000	0.00000	0.00000
C2HG	0.01623	0.00000	0.00000	0.00000	0.00000	0.00000	0.00000	0.00000	0.00000	0.00000	0.00000	0.00000	0.00000
H	0.0	0.00000	0.00000	0.00001	0.00004	0.00010	0.00018	0.00029	0.00043	0.00060	0.00080	0.00102	0.00125
HCN	0.0	0.00004	0.00022	0.00043	0.00057	0.00066	0.00074	0.00080	0.00086	0.00091	0.00096	0.00100	0.00105
HCO	0.0	0.0	0.00000	0.00000	0.00000	0.00000	0.00000	0.00000	0.00001	0.00001	0.00002	0.00002	0.00002
H2	0.0	0.04175	0.04746	0.04851	0.04876	0.04878	0.04871	0.04861	0.04847	0.04832	0.04816	0.04798	0.04789
H2O	0.0	0.00166	0.00071	0.00056	0.00057	0.00060	0.00065	0.00070	0.00074	0.00079	0.00083	0.00087	0.00091
NH2	0.0	0.0	0.00000	0.00000	0.00000	0.00000	0.00000	0.00000	0.00000	0.00000	0.00000	0.00001	0.00001
NH3	0.0	0.00003	0.00003	0.00003	0.00003	0.00003	0.00003	0.00003	0.00003	0.00003	0.00003	0.00003	0.00003
N2	0.05349	0.05031	0.04997	0.04983	0.04975	0.04970	0.04966	0.04963	0.04959	0.04957	0.04954	0.04951	0.04948
OH	0.0	0.0	0.0	0.00000	0.00000	0.00000	0.00000	0.00000	0.00000	0.00000	0.00000	0.00001	0.00001

ADDITIONAL PRODUCTS WHICH WERE CONSIDERED BUT WHOSE MOLE FRACTIONS WERE LESS THAN 0.50000E-05 FOR ALL ASSIGNED CONDITIONS

C	CH	CH2	CN	CNN	CN2	C2	C7H	C2N	C2N2
C2O	C3	C3O2	C4	C5	HNCO	HNO	HNO2	HN03	H02
H2O(S)	H2O(L)	H2O2	N	NCO	NH	NO	NO2	NO3	N2II4
N2O	N2O4	N2O5	N3	O	O2	O3			

PT	C	O	H	N	AR	
1	-6.556	-21.444	-8.170	-11.934	-14.710	9.000
2	-6.695	-21.227	-8.188	-11.944	-14.692	3.000
3	-6.821	-21.031	-8.198	-11.954	-14.675	3.000
4	-6.937	-20.052	-8.207	-11.963	-14.659	3.000
5	-7.043	-20.689	-8.216	-11.971	-14.645	3.000
6	-7.142	-20.530	-8.225	-11.979	-14.631	3.000
7	-7.233	-20.399	-8.234	-11.986	-14.617	3.000
8	-7.318	-20.269	-8.242	-11.993	-14.605	3.000
9	-7.397	-20.149	-8.250	-11.999	-14.592	3.000
10	-7.471	-20.036	-8.258	-12.006	-14.581	3.000
11	-7.541	-19.930	-8.265	-12.012	-14.570	3.000
12	-7.607	-19.031	-8.273	-12.017	-14.559	3.000
13	-7.669	-19.737	-8.280	-12.023	-14.540	3.000

THERMODYNAMIC EQUILIBRIUM PROPERTIES AT ASSIGNED
ENTROPY AND PRESSURE

CASE NO. 70

CHEMICAL FORMULA		MOLES	ENERGY CAL/MOL	STATE	TEMP DEG K	DENSITY G/CC
FUEL	C 1.00000 O 1.00000	0.10000	-26416.152	G	298.15	0.0
FUEL	H 2.00000	0.05000	0.0	G	298.15	0.0
FUEL	N 2.00000	0.05000	0.0	G	298.15	0.0
FUEL	AR 1.00000	0.80000	0.0	G	298.15	0.0

O/F = 0.0 PERCENT FUEL=100.0000 EQUIVALENCE RATIO= 2.5000 REACTANT DENSITY= 0.0

THERMODYNAMIC PROPERTIES

P, ATM	2566.03	2763.42	2960.80	3158.19	3355.58	3552.97	3750.35	3947.74	4145.12	4342.51	4539.90	4737.29	4934.67
T, DEG K	3287	3369	3447	3522	3593	3660	3726	3788	3849	3907	3964	4018	4071
RHO, G/CC	3.4515-1	3.6261-1	3.7968-1	3.9640-1	4.1291-1	4.2892-1	4.4477-1	4.6036-1	4.7573-1	4.9087-1	5.0581-1	5.2056-1	5.3513-1
H, CAL/G	392.7	406.2	419.0	431.4	443.2	454.5	465.5	476.0	486.3	496.1	505.7	515.1	524.1
S, CAL/(G)(K)	1.0280	1.0280	1.0280	1.0280	1.0280	1.0280	1.0280	1.0280	1.0280	1.0280	1.0280	1.0280	1.0280
M, MOL WT	36.280	36.277	36.273	36.269	36.265	36.261	36.256	36.251	36.247	36.242	36.237	36.232	36.227
(DLV/DLP)T	-1.00108	-1.00117	-1.00127	-1.00137	-1.00147	-1.00157	-1.00167	-1.00178	-1.00188	-1.00199	-1.00209	-1.00220	-1.00231
(DLV/DLT)P	1.0067	1.0076	1.0086	1.0095	1.0105	1.0115	1.0125	1.0135	1.0144	1.0154	1.0164	1.0173	1.0182
CP, CAL/(G)(K)	0.1651	0.1660	0.1669	0.1677	0.1685	0.1694	0.1702	0.1709	0.1717	0.1724	0.1732	0.1739	0.1745
GAMMA (S)	1.5038	1.5011	1.4995	1.4961	1.4937	1.4914	1.4893	1.4872	1.4853	1.4834	1.4816	1.4799	1.4783
SON VEL.M/SEC	1064.3	1076.6	1088.1	1099.0	1109.2	1118.8	1128.0	1136.8	1145.1	1153.1	1160.8	1168.2	1175.3

MOLE FRACTIONS

AR	0.80042	0.80035	0.80027	0.80018	0.80009	0.80000	0.79990	0.79979	0.79969	0.79958	0.79947	0.79936	0.79925
CH2	0.00000	0.00000	0.00000	0.00000	0.00000	0.00000	0.00000	0.00000	0.00000	0.00000	0.00001	0.00001	0.00001
CH2O	0.00001	0.00001	0.00001	0.00001	0.00001	0.00001	0.00001	0.00001	0.00001	0.00001	0.00001	0.00001	0.00001
CH3	0.00001	0.00001	0.00001	0.00002	0.00002	0.00002	0.00002	0.00002	0.00002	0.00002	0.00002	0.00002	0.00002
CH4	0.00002	0.00002	0.00002	0.00001	0.00001	0.00001	0.00001	0.00001	0.00001	0.00001	0.00001	0.00001	0.00001
CN	0.00001	0.00001	0.00001	0.00001	0.00001	0.00002	0.00002	0.00002	0.00003	0.00003	0.00004	0.00004	0.00005
CO	0.09856	0.09849	0.09843	0.09836	0.09830	0.09823	0.09816	0.09810	0.09803	0.09797	0.09790	0.09783	0.09777
CO2	0.00025	0.00026	0.00027	0.00027	0.00028	0.00028	0.00029	0.00029	0.00030	0.00031	0.00031	0.00032	0.00032
C2H	0.00000	0.00000	0.00000	0.00000	0.00000	0.00001	0.00001	0.00001	0.00001	0.00001	0.00001	0.00001	0.00001
C2H2	0.00004	0.00004	0.00004	0.00004	0.00004	0.00004	0.00005	0.00005	0.00005	0.00005	0.00005	0.00005	0.00005
H	0.00151	0.00179	0.00208	0.00238	0.00269	0.00301	0.00334	0.00367	0.00401	0.00435	0.00470	0.00505	0.00540
HCN	0.00109	0.00113	0.00117	0.00120	0.00124	0.00127	0.00130	0.00133	0.00136	0.00139	0.00142	0.00145	0.00148
HCO	0.00002	0.00003	0.00003	0.00004	0.00004	0.00005	0.00005	0.00006	0.00007	0.00008	0.00008	0.00008	0.00008
HNCO	0.00000	0.00000	0.00000	0.00000	0.00001	0.00001	0.00001	0.00001	0.00001	0.00001	0.00001	0.00001	0.00001
H2	0.04760	0.04740	0.04719	0.04697	0.04675	0.04653	0.04631	0.04608	0.04585	0.04562	0.04538	0.04515	0.04492
H2O	0.00094	0.00098	0.00101	0.00104	0.00107	0.00110	0.00112	0.00115	0.00118	0.00120	0.00122	0.00124	0.00127
N	0.00000	0.00000	0.00000	0.00000	0.00000	0.00000	0.00000	0.00000	0.00000	0.00000	0.00001	0.00001	0.00001
NH	0.00000	0.00000	0.00000	0.00000	0.00000	0.00000	0.00000	0.00000	0.00000	0.00000	0.00001	0.00001	0.00001
NH2	0.00001	0.00001	0.00001	0.00001	0.00002	0.00002	0.00002	0.00003	0.00003	0.00003	0.00003	0.00003	0.00004
NH3	0.00003	0.00004	0.00004	0.00004	0.00004	0.00004	0.00004	0.00004	0.00004	0.00004	0.00004	0.00004	0.00004
NO	0.00000	0.00000	0.00000	0.00000	0.00000	0.00001	0.00001	0.00001	0.00001	0.00001	0.00001	0.00002	0.00002
N2	0.04945	0.04943	0.04940	0.04937	0.04935	0.04932	0.04929	0.04926	0.04924	0.04921	0.04918	0.04915	0.04913
O	0.00000	0.00000	0.00000	0.00000	0.00000	0.00000	0.00000	0.00000	0.00000	0.00000	0.00000	0.00001	0.00001
OH	0.00001	0.00002	0.00002	0.00002	0.00003	0.00004	0.00004	0.00005	0.00006	0.00007	0.00008	0.00008	0.00008

ADDITIONAL PRODUCTS WHICH WERE CONSIDERED BUT WHOSE MOLE FRACTIONS WERE LESS THAN 0.50000E-05 FOR ALL ASSIGNED CONDITIONS

C	CH	CNN	CN2	C2	C2H4	C2H6	C2N	C2N2	C20
C3	C302	C4	C5	H2O	HNO2	HN03	H2O2	H2O(S)	H2O(L)
H2O2	NCO	N02	N03	N2H4	N2O	N204	N205	N3	O2

DISTRIBUTION LIST

<u>No. of Copies</u>	<u>Organization</u>	<u>No. of Copies</u>	<u>Organization</u>
12	Commander Defense Technical Info Center ATTN: DDC-DDA Cameron Station Alexandria, VA 22314	6	Commander US Army Armament Research and Development Command ATTN: DRDAR-LC, J. Frasier H. Fair J. Lannon A. Bracuti A. Moss R. Walker Dover, NJ 07801
1	Director of Defense Research and Engineering ATTN: R. Thorkildsen The Pentagon Arlington, VA 20301	3	Commander US Army Armament Research and Development Command ATTN: DRDAR-LC E. Barrieres R. Corn K. Rubin Dover, NJ 07801
1	Director Defense Advanced Research Projects Agency Director, Materials Division 1400 Wilson Boulevard Arlington, VA 22209	2	Commander US Army Armament Research and Development Command ATTN: DRDAR-LC K. Russell D. Downs Dover, NJ 07801
3	HQDA (DAMA-ARZ; DAMA-CSM; DAMA-WSW) Washington, DC 20301	1	Commander US Army Armament Research and Development Command ATTN: DRDAR-QA, J. Rutkowski Dover, NJ 07801
1	Commander US Army Materiel Development and Readiness Command ATTN: DRCDMD-ST 5001 Eisenhower Avenue Alexandria, VA 22333	1	Commander US Army Armament Materiel Readiness Command ATTN: DRSAR-LEP-L, Tech Lib Rock Island, IL 61299
2	Commander US Army Armament Research and Development Command ATTN: DRDAR-TSS Dover, NJ 07801	3	Commander US Army Armament Materiel Readiness Command ATTN: DRSAR-ASR DRSAR-LEA DRSAR-QAL Rock Island, IL 61299
5	Commander US Army Armament Research and Development Command ATTN: DRDAR-SC, D. Gyorog H. Kahn B. Brodman S. Cytron T. Hung Dover, NJ 07801		

DISTRIBUTION LIST

<u>No. of Copies</u>	<u>Organization</u>	<u>No. of Copies</u>	<u>Organization</u>
1	Director US Army ARRADCOM Benet Weapons Laboratory ATTN: DRDAR-LCB-TL Watervliet, NY 12189	1	Commander US Army Communications Rsch and Development Command ATTN: DRDCO-PPA-SA Fort Monmouth, NJ 07703
5	Commander US Army ARRADCOM Benet' Laboratory ATTN: I. Ahmad T. Davidson G. Friar P. Greco M. Kamdar J. Zweig Watervliet, NY 12189	1	Commander US Army Electronics Research and Development Command Technical Support Activity ATTN: DELSD-L Fort Monmouth, NJ 07703
5	Commander US Army ARRADCOM Benet' Laboratory ATTN: J. Busuttil W. Austin R. Montgomery R. Billington J. Santini Watervliet, NY 12189	1	Commander US Army Missile Command ATTN: DRSMI-R Redstone Arsenal, AL 35809
1	Commander US Army Aviation Research and Development Command ATTN: DRDAV-E 4300 Goodfellow Blvd. St. Louis, MO 63120	1	Commander US Army Missile Command ATTN: DRSMI-YDL Redstone Arsenal, AL 35809
1	Director US Army Air Mobility Research and Development Laboratory Ames Research Center Moffett Field, CA 94035	1	Project Manager, M60 Tanks US Army Tank & Automotive Cmd 28150 Dequindre Road Warren, MI 48090
1	Commander US Army Research & Technology Laboratories ATTN: R.A. Langsworth Ft. Eustis, VA 23604	4	Project Manager Cannon Artillery Wpns Systems ATTN: DRCPM-CAWS USA ARRADCOM Dover, NJ 07801
		2	Product Manager - M110E2 ATTN: J. Turkeltaub S. Smith Rock Island, IL 61299

DISTRIBUTION LIST

<u>No. of Copies</u>	<u>Organization</u>	<u>No. of Copies</u>	<u>Organization</u>
1	Project Manager - XM1 Tank US Army Tank Automotive Development Command 28150 Dequindre Road Warren, MI 48090	1	Commander US Army Armor Center ATTN: ATZK-XM1 Fort Knox, KY 40121
1	Project Manager Tank Main Armament ATTN: A. Albright Dover, NJ 07801	1	Commander US Army Field Artillery School Fort Sill, OK 73503
1	Project Manager, ARGADS Dover, NJ 07801	5	Commander Naval Surface Weapons Center ATTN: M. Shamblen J. O'Brasky C. Smith L. Russell T. W. Smith Dahlgren, VA 22448
1	President US Army Armor & Engineer Bd Fort Knox, KY 40121	2	Commander Naval Ordnance Station ATTN: L. Dickinson S. Mitchell Indian Head, MD 20640
1	President US Army Maintenance Mgmt Ctr Lexington, KY 40507	1	Commander Naval Ordnance Station, Louisville ATTN: F. Blume Louisville, KY 40202
2	Director US Army Materials and Mechanics Research Center ATTN: J. W. Johnson K. Shepard Watertown, MA 02172	2	AFATL (D. Uhrig, O. Heiney) Eglin AFB, FL 32542
3	Director US Army Research Office ATTN: P. Parrish E. Saibel D. Squire P. O. Box 12211 Research Triangle Park NC 27709	1	National Bureau of Standards Materials Division ATTN: A. W. Ruff Washington, DC 20234
1	Director US Army TRADOC Systems Analysis Activity ATTN: ATAA-SL, Tech Lib White Sands Missile Range NM 88002	1	National Science Foundation Materials Division Washington, DC 20550
1	Commander US Army Air Defense Center ATTN: ATSA-SM-L Fort Bliss, TX 79916	1	Battelle Columbus Laboratory ATTN: G. Wolken Columbus, OH 43201

DISTRIBUTION LIST

<u>No. of Copies</u>	<u>Organization</u>	<u>No. of Copies</u>	<u>Organization</u>
1	Lawrence Livermore Laboratory ATTN: J. Kury Livermore, CA 94550	1	University of Illinois Dept of Aeronautics and Aerospace Engineering ATTN: H. Krier Urbana, IL 61803
4	Calspan Corporation ATTN: G. Sterbutzel F. Vassallo C. C. Morphy E. B. Fisher P. O. Box 400 Buffalo, NY 14221		<u>Aberdeen Proving Ground</u> Dir, USAMTD ATTN: H. Graves, Bldg. 400 L. Barnhardt, Bldg 400 K. Jones, Bldg 400 R. Moody, Bldg 525
1	Director Chemical Propulsion Info Agency Johns Hopkins University ATTN: T. Christian Johns Hopkins Road Laurel, MD 20810		Cdr, USATECOM ATTN: DRSTE-FA DRSTE-AR DRSTE-AD DRSTE-TO-F
1	Princeton University Forrestal Campus Library ATTN: Tech Lib B. Royce P. O. Box 710 Princeton, NJ 08540		Dir, USAMSAA ATTN: DRXSY-D DRXSY-MP, H. Cohen D. Barnhardt, RAM Div G. Alexander, RAM Div Air Warfare Div Ground Warfare Div RAM Division
1	Purdue University School of Mech Engineering ATTN: J. R. Osborn W. Lafayette, IN 47909		Dir, USACSL, Bldg. E3516, EA ATTN: DRDAR-CLB-PA
1	SRI International Materials Research Center 333 Ravenswood Avenue Menlo Park, CA 94025		

USER EVALUATION OF REPORT

Please take a few minutes to answer the questions below; tear out this sheet, fold as indicated, staple or tape closed, and place in the mail. Your comments will provide us with information for improving future reports.

1. BRL Report Number _____

2. Does this report satisfy a need? (Comment on purpose, related project, or other area of interest for which report will be used.)

3. How, specifically, is the report being used? (Information source, design data or procedure, management procedure, source of ideas, etc.)

4. Has the information in this report led to any quantitative savings as far as man-hours/contract dollars saved, operating costs avoided, efficiencies achieved, etc.? If so, please elaborate.

5. General Comments (Indicate what you think should be changed to make this report and future reports of this type more responsive to your needs, more usable, improve readability, etc.)

6. If you would like to be contacted by the personnel who prepared this report to raise specific questions or discuss the topic, please fill in the following information.

Name: _____

Telephone Number: _____

Organization Address: _____

